IDENTIFICATION OF INERTIA TENSOR OF VEHICLES

A THESIS SUBMITTED TO
THE GRADUATE SCHOOL OF NATURAL AND APPLIED SCIENCES
OF
MIDDLE EAST TECHNICAL UNIVERSITY

BY
EMİR KUTLUAY

IN PARTIAL FULFILLMENT OF THE REQUIREMENTS
FOR
THE DEGREE OF MASTER OF SCIENCE
IN
MECHANICAL ENGINEERING

SEPTEMBER 2007

Approval of the Thesis:

IDENTIFICATION OF INERTIA TENSOR OF VEHICLES

submitted by **EMİR KUTLUAY** in partial fulfillment of the requirements for the degree of **Master of Science in Mechanical Engineering Department, Middle East Technical University** by,

Prof. Dr. Canan ÖZGEN _____
Dean, Graduate School of **Natural and Applied Sciences**

Prof. Dr. Kemal İDER _____
Head of Department, Mechanical Engineering Dept., **METU**

Prof. Dr. Y. Samim ÜNLÜSOY _____
Supervisor, Mechanical Engineering Dept., **METU**

Examining Committee Members:

Prof. Dr. Kemal ÖZGÖREN _____
Mechanical Engineering Dept., METU

Prof. Dr. Y. Samim ÜNLÜSOY _____
Mechanical Engineering Dept., METU

Asst. Prof. Dr. Yiğit YAZICIOĞLU _____
Mechanical Engineering Dept., METU

Asst. Prof. Dr. İlhan KONUKSEVEN _____
Mechanical Engineering Dept., METU

Inst. Kutluk Bilge ARIKAN _____
Mechanical Engineering Dept., Atılım University

Date: 07.09.2007

I hereby declare that all information in this document has been obtained and presented in accordance with academic rules and ethical conduct. I also declare that, as required by these rules and conduct, I have fully cited and referenced all material and results that are not original to this work.

Name, Last name :

Signature :

ABSTRACT

IDENTIFICATION OF INERTIA TENSOR OF VEHICLES

Kutluay, Emir
M.S., Department of Mechanical Engineering
Supervisor: Prof. Dr. Y. Samim ÜNLÜSOY

September 2007, 149 Pages

The aim of this thesis is to develop a methodology for obtaining mass properties of a vehicle using specific test rig. Investigated mass properties are the mass, location of center of gravity and the inertia tensor. Accurate measurement of mass properties of vehicles is crucial for vehicle dynamics research. The test rig consists of a frame on which the vehicle is fixed and which is suspended from the ceiling of the laboratory using steel cables. Mass and location of center of gravity are measured using the data from the test rig in equilibrium position and basic static equations. Inertia tensor is measured using the data from dynamical response of the system. For this purpose an identification routine which employs prediction error method is developed using the built–in functions from the *System Identification Toolbox* of MATLAB®. The experiment was also simulated using *Simmechanics Toolbox* of MATLAB®. Identification code is verified using the results of the experiment simulations for various cases.

Keywords: Identification, Parameter Estimation, Prediction Error, Inertia Tensor, Vehicle Dynamics

ÖZ

ARAÇLARIN ATALET TENSÖRLERİNİN TANILANMASI

Kutluay, Emir
Yüksek Lisans, Makina Mühendisliği Bölümü
Tez Yöneticisi: Prof. Dr. Y. Samim ÜNLÜSOY

Eylül 2007, 149 Sayfa

Bu çalışmanın amacı araçların kütle özelliklerinin özel bir deney düzeneği kullanılarak elde edilebilmesi için bir method geliştirmektir. Araştırılan kütle özellikleri kütle, aüırlık merkezinin konumu ve atalet tensörüdür. Araçların kütle özelliklerinin doğru ölçümü araç dinamiği araştırmaları için çok önemlidir. Deney düzeneği tavandan çelik kablolar vasıtasıyla sarkıtılmış ve üzerine aracın sabitlendiği bir çerçeveden oluşmaktadır. Kütle ve ağırlık merkezi ölçümü deney düzeneği denge konumundayken toplanan veriler ve statik denklemleri vasıtasıyla ölçülmektedir. Atalet tensörü ise sistemin hareketli deneylerinden toplanan veriler kullanılarak bulunmaktadır. Bu amaçla MATLAB® programının *System Identification Toolbox* fonksiyonları aracılığı ile tahmin hatası methodunu kullanan bir tanılama programı yazılmıştır. Deney düzeneği de yine MATLAB® programının *Simmechanics Toolbox* özellikleri kullanılarak simüle edilmiştir. Tanılama kodu farklı durumlar için yapılan deney simülasyonları ile doğrulanmıştır.

Anahtar Kelimeler: Tanılama, Parametre Tahmini, Kestirim Hatası, Atalet Tensörü, Araç Dinamiği

ACKNOWLEDGEMENTS

I would like to express my special thanks to my supervisor Prof. Dr. Y. Samim ÜNLÜSOY for his guidance, tolerance and understanding.

I would like state my gratitude to my colleagues Koray KÜÇÜK for his assistance throughout the thesis in every step in every possible way, Hakan MENCEK for his fruitful discussions on the subject and his patience, Gökhan TEKİN for his company and help at every stage of the study and A. Özgü NURSAL for his software support whenever needed. I would like to extend my gratitude to Kemal ÇALIŞKAN, Murat ŞAHİN and Gökhan KİPER for their advices and aids in the thesis, and TÜBİTAK for their for their financial support.

Finally I would like to thank my family who supported me throughout my life for their trust, never ending love and patience. Without their encouragement, completion of this thesis would not have been possible.

TABLE OF CONTENTS

LIST OF TABLES

TABLES

LIST OF FIGURES

FIGURES

CHAPTER 1

INTRODUCTION

1.1 Introduction

There are many reasons for obtaining inertia measurements in the field of Vehicle Dynamics. Car manufacturers, military organizations, and heavy vehicle manufacturers require inertia properties for use in their vehicle handling, ride, and stability models and simulations of existing vehicles and in the development stages of new vehicle and vehicle subsystem designs.

Accurate values of the dynamic parameters of a car are needed to improve the dynamic control and simulation of a car. Vehicle center-of-gravity height and roll inertia are often used to investigate vehicle's rollover tendency. They also affect response speed of the vehicle to steer inputs. Racing companies rely on these properties for their track time simulations. In order to simulate or identify other parameters of a vehicle [1-4], mass and inertia properties must be known.

Measuring the full inertia tensors of vehicles, or rigid bodies in general has often been considered an involved task. "When classical methods are applied [5,6], the tests require some special effort to position in six different spatial orientations the oscillation axis around which the body under consideration is forced to vibrate in order to

derive the inertia tensor components. Classical methods have been developed many decades ago when numerical identification algorithms were still not properly developed or could not be employed due to the huge amounts of computations required. Presently, computers have sufficient computation speed to obtain the measurement of the full inertia tensor relatively quickly and simply by means of procedures based on parameter identification algorithms" [7].

A number of test rigs have been presented in the literature for the measurement of inertial parameters (mass, center-of-gravity location, inertia tensor) [2,3,4,8-16]. Almost in all of the early or "classical" applications, the body (or vehicle) was either constrained to rotate around one axis and, by measuring the frequency of oscillations, the moment of inertia around that axis was measured or modal analysis techniques were used [5].

1.2 Previous Work

Numerous studies were made on identification, measurement and estimation of inertia tensor. In literature, there are three main approaches to the measurement of inertia properties problem.

The first approach is the most fundamental one; which is simply oscillating the body around the rotating axis for which the relevant inertia property is sought after. In this case the frequency of the oscillations are measured to calculate the inertia terms. However it is hard to obtain the off-diagonal elements of the inertia tensor using these techniques.

The second approach involves using the modal analysis and system identification techniques. In system identification approach, the researcher has the freedom of choosing both the mathematical model which will simulate the response of the system and the parameters of this user defined mathematical model [17]. However, in parameter identification approach, which is the third approach to the problem; the implementer's aim is to identify the free parameters of a predetermined mathematical model.

The main solution of a parameter identification problem is to minimize the differences between the outputs of the mathematical model and the experimental measurements, which will inherently converge the free parameters in the system equations to actual values. In order to achieve this goal, a cost function is defined as the sum of the squares of the differences between the outputs of the mathematical model and the measured values. Minimizing this cost function will lead to the solution of the problem. These definitions actually define a nonlinear least square problem, which can be solved by using unconstrained optimization methods.

A detailed comparison of moment of inertia estimation techniques in the literature can be found in [18]. MacInnis et. al. compared many estimation formulae; which relate dimensional parameters of vehicles to their mass properties and used his findings to simulate vehicle collision dynamics. It must be noted that the methods they employed give moments of inertia estimates but not the actual values.

In 1997 a method was developed by Stebbins et. al. [19] to estimate a rigid body's inertia properties using a prototype six-axis load cell designed to measure all loads and moments applied to the structure. The body was fixed to the experimental set up; excited randomly in

all directions by an impact hammer. Several tri-axial accelerometers were placed on the body (since location of CG was unknown, none of them were placed on the CG). Despite the fact that the basis of the model used in this research was Newton's 2nd Law; the computation process was much more complicated; as the aim of the research was to identify all 10 parameters simultaneously. The method succeeded in estimating all 10 parameters accurately, however because of the prototype six-axis load cell; which was composed of 32 piezoelectric sensing elements; the cost of this technique came out to be rather high.

Metz et. al. [20] measured mass moment of inerta of passenger cars and motorcycle tyres about the tyre spin axis using a torsional pendulum technique, similar to trifilar pendulum method [21]. A pair of linear correlation equations, one for mounted tyres and one for the unmounted tyres, were derived which relate inertia values to tyre diameters and weights.

Venture et. al. [22] developed a robotics approach in 2003. The system was modeled as a multi-body (by using Modified Denavit and Hartenberg notation), which allowed the automatic computation of the dynamic identification model, which was linear with respect to the inertial (mass, center of mass and inertia tensor) and the suspension parameters. Every element of vehicles suspension and chasis were modeled as joints (degrees of freedom). No special experimental setup was required: the experiments were done by performing various predetermined manouvers on test grounds. A total of 34 parameters were identified accurately. The shortcoming of this technique was that the cost of the experimental tools was high due to the number of sensors used. However this research succeeded in

obtaining the inertial parameters and suspension parameters simultaneously.

In 2001 Heydinger et. al. [23] designed a new test rig for measuring center-of-gravity height; roll, pitch, and yaw moments of inertia; and roll/yaw cross product of inertia for a broad range of vehicles and vehicle components (e.g. tank turrets). This facility was capable of handling vehicles up to 3 meters in width, up to 27,000 kg. The mass and horizontal position of the center-of-gravity were measured using a set of four floor scales. The vertical position of center-of-gravity was found by adding an extra weight to a known position and measuring the change in roll angle. The moments of inertia were obtained by measuring the period of oscillations in about each axis. Experiments were made seperately for each element of the inertia tensor. Roll/yaw product of inertia was derived by constraining the roll motion of the vehicle and measuring the force required to keep the vehicle's yaw motion constrained during the yaw moment of inertia test.

Rosenthal et. al. [24] analyzed how vehicle inertial properties relate to typical dimensions (length, width and height) and how these properties affect vehicle dynamics. They reached the conclusion that the vehicle inertial properties were strongly correlated with standard measures of length, width and height. They also correlated accident database analysis with their findings about the handling – inertial properties relations. Note that correlating the typical dimensions of a vehicle with its mass properties resulted in reaching not the actual values but estimates with reasonable error. The values obtained through the techniques described in their work was not suitable for full scale vehicle dynamics modelling and simulation purposes.

Mastinu et. al. [7] focused on the effects of inertia tensor components on ride comfort and handling behaviour of the vehicle. Two multi-body models were used for simulations in different road conditions and to observe the effects on the driver and the handling of the vehicle. Results of this theoretical investigation were used to prescribe the measurement accuracy of the inertia tensor components. Furthermore a new method [6] [25] for measuring the inertia tensor of vehicles, meeting the accuracy determined on the basis of the preliminary theoretical study was proposed.

In 1996 Heydinger et. al. [26] performed a study on determining not only mass properties of a vehicle (mass, center-of-gravity location, diagonal terms of the inertia tensor and roll/yaw coupling term of the inertia tensor), but also those of the sprung and unsprung bodies. The method involved making several experiments and measuring whole vehicle mass properties at different trim heights. Sprung and unsprung mass properties are obtained by comparing and processing the experimental results at different trim heights using numerical algorithms.

A study was made in 1997 by Rizel et. al. [27] which included measurement of human body mass properties (mass, center-of-gravity position, inertia tensor), comparison of these values with numerically estimated data and usage of the results in vehicle crash simulations. The human body was modelled as a multibody of ellipsoids in the computer simulations. Test subjects were secured to the experimental setup (a specially designed chair design). The inertial measurement was done by torsional pendulum technique. Note that only the diagonal elements of the inertia tensor were measured in this study.

In 2002 Mastinu et. al. [6] designed a test rig to measure the mass properties of vehicles and their subsystems. The technique involved suspending the vehicle from a fixed frame and exciting it in order to obtain a motion complicated enough to observe the effects of each component of the inertia tensor. Location of the center-of-gravity is measured when the system is in static equilibrium. The results of the experiment were used in full scale vehicle parameter identification purposes. This test rig was further developed in [25].

Hahn and Niebergall [28,33] designed an experiment robot in order identify ten inertial parameters simultaneously. The designed robot experimentally identified the inertial parameters of a rigid body automatically using the complete information hidden in the nonlinear model equations of the test body. This task was solved in several steps:

- Mathematical modelling of the special motions of a rigid body in space. These model equations were mapped into a form suitable for identification purposes.
- Design of a special measurement robot for performing the identification experiments.
- Identification of the inertia parameters and accuracy tests.

The accuracy of the identified parameters were found to be satisfactory. The designed robot was built for small bodies (i.e. not for vehicles).

1.3 Aim and Scope of the Study

In this study a method to measure the mass properties of vehicles using a specific test rig proposed by Mastinu et. al. [6]. The

measured properties are mass, coordinates of location of center-of-gravity, and inertia tensor. Test rig consists of a frame, on which the body whose properties are to be measured is to be fixed, suspended from the ceiling of the laboratory by steel cables and an unbalanced mass-motor assembly which is fixed to the frame.

A state space model is derived based on Newton's Second Law. Cables are assumed to be inflexible and massless. Also the effects of the inertia and mass of unbalanced mass-motor assembly to the total mass and inertia of the system is neglected.

The mass of the system is simply measured by using a ground scale. The spatial coordinates of the center of gravity is located when the system is in static equilibrium. Two direction cosines are measured; and the resulting geometrical relations and equilibrium equations are solved using non-linear algebraic solvers of MATLAB®.

In order to obtain the inertia tensor, the system is excited via the unbalanced mass-motor assembly; and the resulting force is measured as well as the tensions on the cables, translational accelerations and rotational velocities of the test body. Collected data is preprocessed by a code written in MATLAB® to find the generalized forces on the system. Then using the derived mathematical model and parameter identification toolbox commands of MATLAB®, inertia tensor is identified.

Two graphical user interfaces (GUIs) are developed for two phases of measurement, which can be seen on Figures 2.2, 3.4 and 3.5.

CHAPTER 2

MEASUREMENT OF MASS AND CENTER-OF-GRAVITY (CG)

2.1 Measurement of Mass

The mass of the frame and the test body are measured using a ground scale. Since the frame is a symmetrical structure; the location of its CG is inherently known.

Although the horizontal position of the CG of the test body can be found simply by using four ground scales and writing the static equilibrium equations [23]; they are found simultaneously with the vertical coordinate of the CG in the following section.

2.2 Determination of the Location of CG

According to Baruh [29], “The mass of a rigid body is defined by:

$$m = \int_{body} r dm \tag{2.1}$$

Location of CG is defined as:

$$r_G = \frac{1}{m} \int_{body} r dm \tag{2.2}$$

where r is the vector from the origin to the differential element dm.

Then, one can define any point in the body as:

$$r = r_G + \rho \tag{2.3}$$

Introducing (2.3) to (2.2); following is obtained:

$$r_G = \frac{1}{m}\int_{body} r dm = \frac{1}{m}\int_{body} (r_G + \rho) dm = r_G + \frac{1}{m}\int_{body} \rho dm \tag{2.4}$$

Leading to the conclusion that:

$$\int_{body} \rho dm = 0 \tag{2.5}$$

This equation indicates that the weighted average of the displacement vector about the center of mass is zero. Considering the concepts from statics, one can refer to the definition of the center of mass as the first moment of the mass distribution."

At equilibrium, the position of the body in space is unique, and is a function of mass of body, position of CG, cable lengths, locations of hinge points on body and on frame. Using this information, one can solve static equilibrium equations for coordinates of CG.

In order to determine the location of CG, an experiment is designed. The experiment body and the frame are to be suspended from the ceiling of the laboratory using steel cables. After the system reaches the static equilibrium; the angles between the roll and pitch axes of the body reference frame and the vertical axis of the global frame are

measured using inclinometers. Then using only these two readings, and using the static equilibrium equations, geometric constraint equations and orthonormality equations of the transformation matrix; orientation of the body, cable forces and the location of center of gravity are computed.

Because of the fact that the number of equations are inadequate to compute all the unknowns; two experiments are to be made with the same test body: one with the test body and the carrying frame alone, and one with a dummy mass added to the system.

2.2.1 The Experimental Set-up

In the experiment; the rigid body with unknown CG position is fixed onto a carrying frame, then the carrying frame is swung by four cables which are hinged to four points on carrying frame at one end, and to four points on the ceiling (or a frame fixed to the ceiling) at the other end.

For the sake of simplicity; the points on ceiling frame and carrying frame are taken to be located on rectangles. Moreover the rigid body and the carrying frame are shown as one body on Figure 2.1.

2.2.2 Locating the Body in Space

In order to locate the rigid body in space, one must know the coordinates of body reference frame (which is shown to be located at point A in Figure 2.1) and its Euler angles. However, in this study the angles that x' and y' make with z axis (vertical) are to be measured

using inclinometers. Thus, transformation matrix T will be written in terms of direction cosines instead of Euler angles.

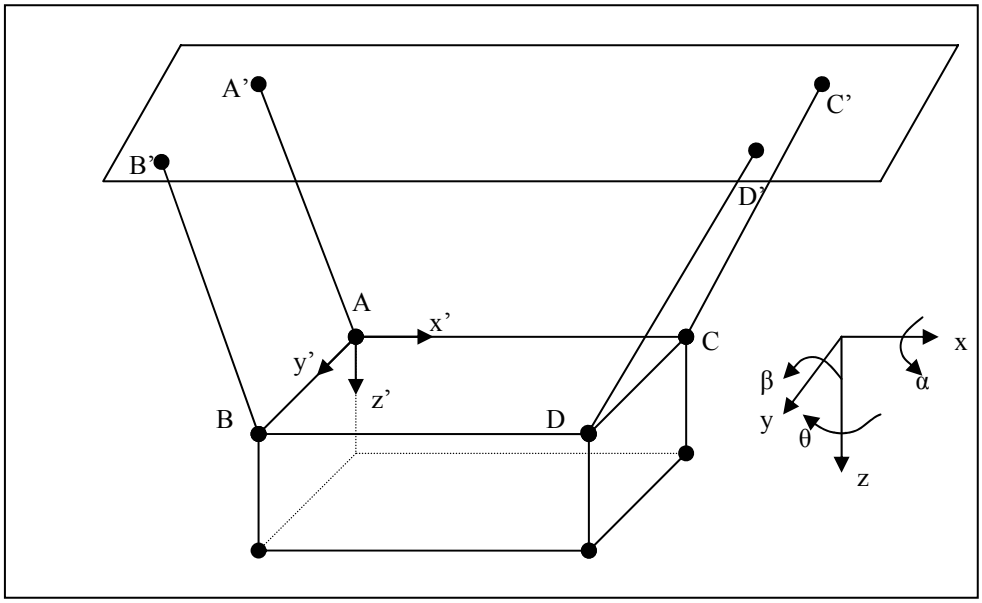

Figure 2.1 Suspended rigid body with known geometry

$$T=\begin{bmatrix} c_{11} & c_{12} & c_{13} \\ c_{21} & c_{22} & c_{23} \\ c_{31} & c_{32} & c_{33} \end{bmatrix} \tag{2.6}$$

Using the orthonormality property of T [29], one can derive six equations as:

$$c_{11}{}^2 + c_{12}{}^2 + c_{13}{}^2 - 1 = 0 \tag{2.7}$$

$$c_{21}{}^2 + c_{22}{}^2 + c_{23}{}^2 - 1 = 0 \tag{2.8}$$

$$c_{31}{}^2 + c_{32}{}^2 + c_{33}{}^2 - 1 = 0 \tag{2.9}$$

$$c_{11}.c_{21} + c_{12}.c_{22} + c_{13}.c_{23} = 0 \tag{2.10}$$

$$c_{11}.c_{31} + c_{12}.c_{32} + c_{13}.c_{33} = 0 \tag{2.11}$$

$$c_{21}.c_{31} + c_{22}.c_{32} + c_{23}.c_{33} = 0 \tag{2.12}$$

where c_{31} and c_{32} are to be obtained from inclinometer measurements (Thus there are six equations and seven unknowns).

Knowing the coordinates of fixed points on the ceiling and the lengths of the cables; four constraint equations can be written for four connection points, A, B, C, D; assuming inextensible cables as:

$$l_A{}^2 - (x_{A'} - x_A)^2 + (y_{A'} - y_A)^2 + (z_{A'} - z_A)^2 = 0 \tag{2.13}$$

$$l_B{}^2 - (x_{B'} - x_B)^2 + (y_{B'} - y_B)^2 + (z_{B'} - z_B)^2 = 0 \tag{2.14}$$

$$l_C{}^2 - (x_{C'} - x_C)^2 + (y_{C'} - y_C)^2 + (z_{C'} - z_C)^2 = 0 \tag{2.15}$$

$$l_D{}^2 - (x_{D'} - x_D)^2 + (y_{D'} - y_D)^2 + (z_{D'} - z_D)^2 = 0 \tag{2.16}$$

Since the frame body is a rigid body with known geometry, the coordinates of points B, C and D can be written in terms of coordinates of point A as:

$$(x_B.\hat{\imath} + y_B.j + z_B.k) = (x_A.\hat{\imath} + y_A.j + z_A.k) + T.(x_B''.\hat{\imath} + y_B''.j + z_B''.k) \quad (2.17)$$

$$(x_C.\hat{\imath} + y_C.j + z_C.k) = (x_A.\hat{\imath} + y_A.j + z_A.k) + T.(x_C''.\hat{\imath} + y_C''.j + z_C''.k) \quad (2.18)$$

$$(x_D.\hat{\imath} + y_D.j + z_D.k) = (x_A.\hat{\imath} + y_A.j + z_A.k) + T.(x_D''.\hat{\imath} + y_D''.j + z_D''.k) \quad (2.19)$$

Note that $(x_B''.\hat{\imath} + y_B''.j + z_B''.k)$ vector stands for position of point B, with respect to the body reference frame, which is located at A.

(2.14), (2.15) and (2.16) can be rewritten in terms of coordinates of point A with respect to the global reference frame only using (2.17), (2.18) and (2.19).

Adding the four constraint equations to the six equations that are obtained from orthonormality relations, a total of ten equations are obtained for ten unknowns (x_A, y_A, z_A, c_{11}, c_{12}, c_{13}, c_{21}, c_{22}, c_{23}, c_{33}).

2.2.3 Computing the Cable Forces and the Location of CG

After finding the location of body reference frame and transformation matrix; one can write force and moment equilibrium equations as follows:

$$\Sigma Fx = 0 \tag{2.20}$$

$$\Sigma Fy = 0 \tag{2.21}$$

$$\Sigma Fz = 0 \tag{2.22}$$

$$\Sigma Mx = 0 \tag{2.23}$$

$$\Sigma My = 0 \tag{2.24}$$

$$\Sigma Mz = 0 \tag{2.25}$$

There are four unknown forces and three unknown coordinates. It is clear that these six equations are not enough to reach a solution.

Moreover, coordinates of the CG (x_{cg}, y_{cg}, z_{cg}) appear neither in equations (2.20), (2.21), (2.22) (force equilibrium equations); nor in (2.25), since weight vector is also in z-direction. It is concluded that one can find four unknown forces using the (2.20), (2.21), (2.22) and (2.25).

To find coordinates of center of gravity, at least one more equation is needed. This equation can be obtained by making a second experiment, in which a known mass with known center of gravity is positioned at a specified point on the carrying frame. In this case, the center of gravity of the system will be:

$$\frac{\{(m_d).(x_{cg}{}^{d}.\hat{i} + y_{cg}{}^{d}.j + z_{cg}{}^{d}.k) + (m + m_{frame}).(x_{cg}.\hat{i} + y_{cg}.j + z_{cg}.k)\}}{(m_d + m + m_{frame})}$$

Where d sub- and superscript denote the relevant properties of the dummy mass and m_{frame} denotes mass of the carying frame.

Rewriting (2.20), (2.21), (2.22) and (2.25) for the new measurements, cable forces for this case can be computed. However it can easily be seen that center of gravity coordinates of this new system with the dummy mass is a function of the coordinates of center of gravity of the system without the dummy mass. Thus; either one of the remaining moment equilibrium equations ((2.23) or (2.24)) can be selected to solve with the two moment equilibrium equations of the system without the dummy mass.

2.3 The Code

In order to solve the stated problem, a computer code is written using MATLAB®. Further, in order to verify the results another code is written to generate the system to be solved, with known center of gravity coordinates.

Case study code calculates the equilibrium position and Euler angles (XYZ sequence) of a given body with user defined shape and experimental set-up parameters.

The aim of the solver code is to calculate the center of gravity; for given mass, dummy mass, coordinates of center of gravity of dummy mass, cable lengths, system geometry and angles between x' – z and y' – z.

The code first computes the position and orientation of the body in space; then calculates the cable forces and finally the coordinates of center of gravity. The code is used through a graphical user interface written in MATLAB, Figure 2.2.

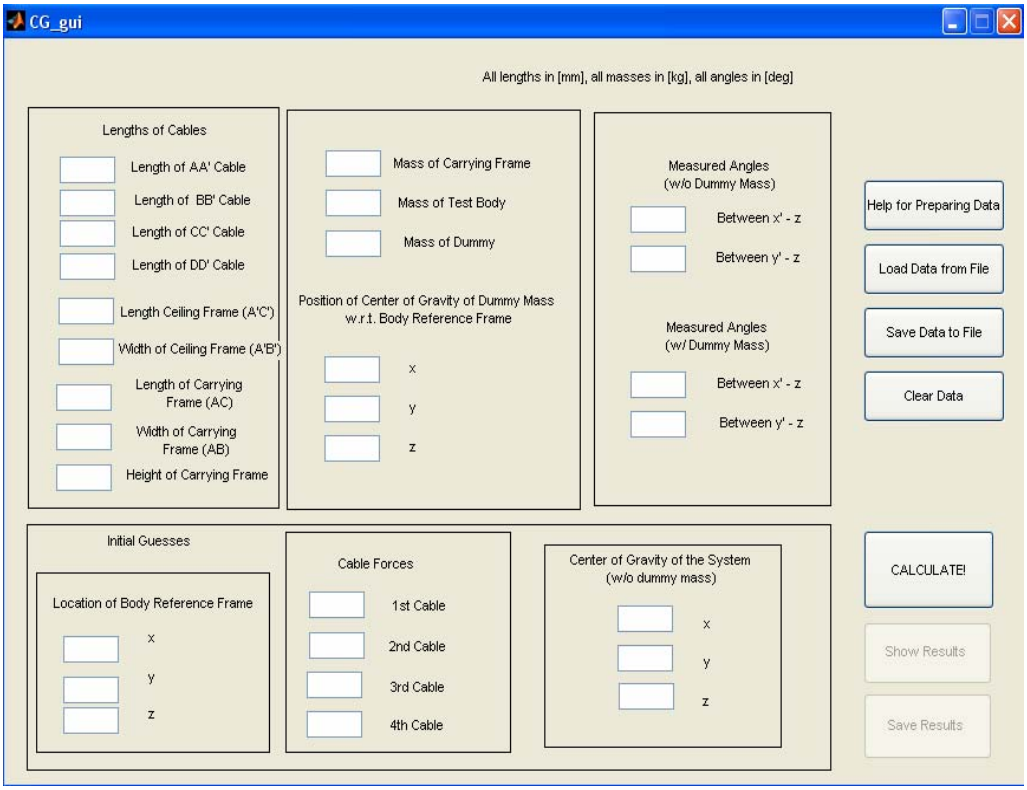

Figure 2.2 Interface of the Solver

2.4 Case Study

In order to verify the developed software a sample case study is solved. In this study a body with known center of gravity is simulated and the location of center of gravity is numerically calculated. The input data is presented in Table 2.1. Calculated coordinates of the center of gravity are:

x = 1771.011 mm

y = 1122.978 mm

z = 609.860 mm

whereas the actual values were:

x = 1771 mm

y = 1123 mm

z = 612 mm

The percentage error between the calculated and actual values are:

$$\%Error = \begin{bmatrix} 0.0006 \\ 0.002 \\ 0.3497 \end{bmatrix}$$

These error values show that the solution technique is satisfactory. The respectively higher error percentage in one of the components is related with the three moments selected for the calculation. Error in this component is always the largest because of the fact that the errors included in the first two terms are involved in the calculation of the third term, resulting in the accumulation of errors.

Maximum absolute error is less than 2.5 milimeters, which is practically zero, since this location will be used to align the ropes for the second experiment, and to fix the accelerometers and gyroscopes if it lies in an accessible and mountable location in the vehicle; and error in experimental set up will most probably be larger than 2.5 milimeters.

Table 2.1 Data for Case Study

Lengths of Cables [mm]:	
1500	
Dimensions of ceiling frame [m]:	
5 x 3	
Dimensions of carrying frame [m]:	
4 x 2 x2	
Mass of carrying frame [kg]:	
262	
Mass of test body [kg]:	
1072	
Center of gravity of test body (w.r.t. b.r.f.) [mm]:	
x	1771
y	1123
z	612
Combined center of gravity of test body + carrying frame (w.r.t. b.r.f.) [mm]:	
x	1816
y	1099
z	688
Mass of dummy mass [kg]:	
50	
Center of gravity of dummy mass (w.r.t. b.r.f.) [mm]:	
x	0
y	0
z	0
Initial guess for Location of body reference frame [mm]:	
x	500
y	500
z	500
Initial guess for Euler angles [rad]:	
0	
0	
0	
Initial guess for Cable forces [N]:	
2000	
Initial guess for center of gravity of whole system (w/o dummy mass) [kg]:	
x	1000
y	1000
z	1000

CHAPTER 3

MEASUREMENT OF INERTIA TENSOR

3.1 Inertia Tensor

Although the knowledge of mass and center of mass provide valuable information for the simulation and analysis of translational motion, it gives no insight of how the mass is distributed throughout the body. Baruh [29] defined mass as “The amount of matter contained in the body and the resistance of the body to translational motion. On the other hand the resistance of the body to a rotational motion is dependent on how the mass is distributed”. Thus, as the first moment of mass distribution defines the center of mass, the second moment of mass distribution defines the moment of inertia of the body. Moment of inertia represents the resistance of the body to rotational motion.

The distribution of mass with respect to an axis is called the mass moment of inertia about that axis. Consider x axis for example. The mass moment of inertia about x axis is defined as:

$$I_{xx} = \int_{body} R_x^2 dm \tag{3.1}$$

Where R_x represents the perpendicular distance between a differential element located at (x_R, y_R, z_R) and the x axis. It is simply:

$$R_x = \sqrt{(y_R^2 + z_R^2)} \tag{3.2}$$

Then one can rewrite (3.1) as:

$$I_{xx} = \int_{body} (y_R^2 + z_R^2) dm \tag{3.3}$$

Similarly mass moment of inertia about y and z axes are defined in the same fashion:

$$I_{yy} = \int_{body} (x_R^2 + z_R^2) dm \tag{3.4}$$

$$I_{zz} = \int_{body} (x_R^2 + y_R^2) dm \tag{3.5}$$

These three terms form the diagonal elements of the so called inertia tensor. As seen from (3.3), (3.4) and (3.5), diagonal elements of the inertia tensor are definitely positive for a rigid body, since the terms inside the integral can not be negative and are non-zero. The diagonal elements of the inertia tensor are measures of the body's resistance to rotation around corresponding axes.

Other than the mass moment of inertia about an axis; one can also define mass moment of inertia with respect to a plane. In this case the resultant quantities are called the products of inertia. Products of inertia are defined as:

$$I_{xy} = \int_{body} (x_R . y_R) dm \tag{3.6}$$

$$I_{xz} = \int_{body} (x_R . z_R) dm \tag{3.7}$$

$$I_{yz} = \int_{body} (y_R . z_R) dm \tag{3.8}$$

It can clearly be seen that $I_{xy} = I_{yx}$, $I_{xz} = I_{zx}$, $I_{yz} = I_{zy}$. These terms can be considered as measures of how asymmetrical the mass is distributed throughout the body and are the off-diagonal elements of the inertia tensor which is defined as:

$$[I] = \begin{bmatrix} I_{xx} & -I_{xy} & -I_{xz} \\ -I_{yx} & I_{yy} & -I_{yz} \\ -I_{zx} & -I_{zy} & I_{zz} \end{bmatrix} \tag{3.9}$$

When the body is symmetrical with respect to any of the planes; the product of inertia terms associated with the axis perpendicular to that plane vanish. As an example to this property, consider an automobile. Usually automobiles have a certain symmetry both in shape and mass distribution with respect to roll/yaw plane (Figure 3.1). Because of this symmetry, I_{xy} and I_{yz} are usually very small in quantity, and the effects of roll/yaw product of inertia I_{xz} to vehicle dynamics problems are much more considerable.

3.2 Experimental Setup

The experimental setup is nearly the same as the one used for the measurement of center of mass. The test body is fixed to the carrying frame, which is suspended from the ceiling of the laboratory using four steel cables. An unbalanced mass-motor assembly is fixed to

one of the corners of the carrying frame. The experiment starts from equilibrium position with initial conditions all zero.

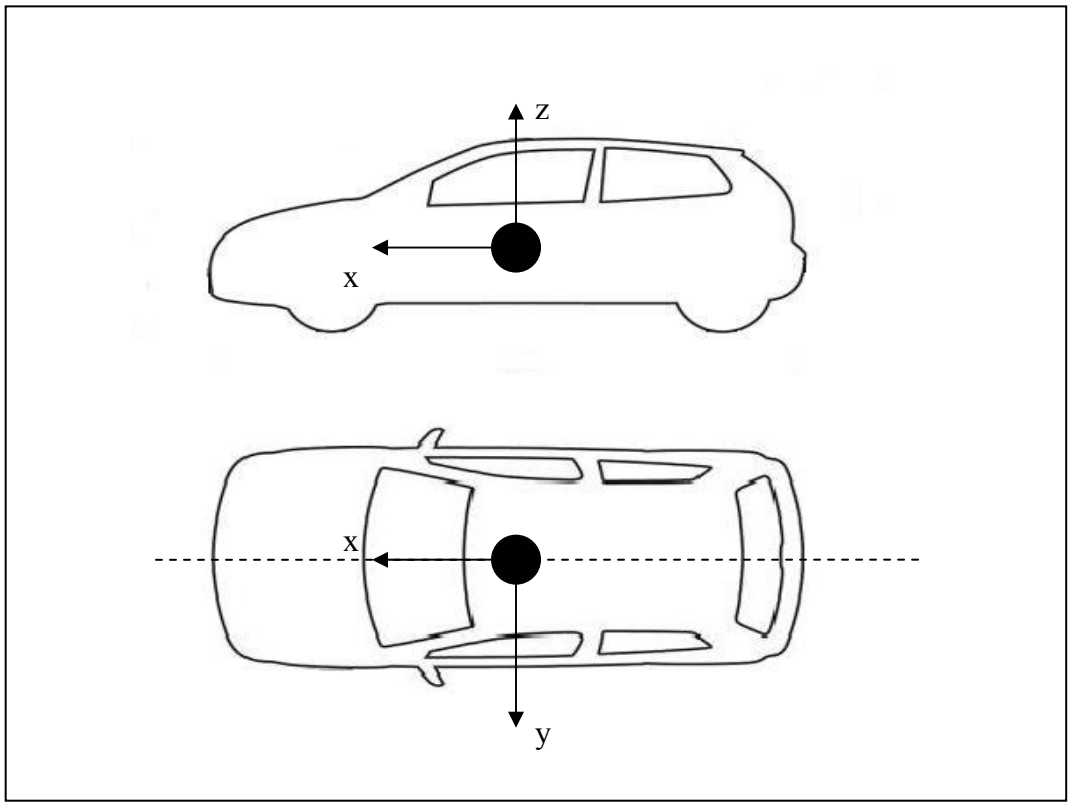

Figure 3.1 Car is symmetrical with respect to roll/yaw axis

Three translational accelerometers and three gyros, measuring the angular velocities are placed at the CG. Cable lengths are so selected that their direction vectors intersect as closely as possible to the CG. Tensions on the cables are also measured as well as the force applied by the unbalanced mass.

When the experiment starts; the unbalanced mass-motor assembly apply a sinusoidal force; which can be resolved into two components with a phase difference of π/2.

In the experiment a total of 3 translational accelerometers, 3 gyroscopes, 6 load cells (4 load cells to measure the load on the cables, 2 for the unbalanced mass-motor assembly) are to be used.

The schematic drawing of the experiment set up can be found in Appendix A.

3.3 Mathematical Model

Newton-Euler Equations can be written for the model neglecting the gyroscopic terms.

$$\begin{pmatrix} F_x \\ F_y \\ F_z \\ M_1 \\ M_2 \\ M_3 \end{pmatrix} = \begin{bmatrix} m & 0 & 0 & 0 & 0 & 0 \\ 0 & m & 0 & 0 & 0 & 0 \\ 0 & 0 & m & 0 & 0 & 0 \\ 0 & 0 & 0 & J_{xx} & -J_{xy} & -J_{xz} \\ 0 & 0 & 0 & -J_{xy} & J_{yy} & -J_{yz} \\ 0 & 0 & 0 & -J_{xz} & -J_{yz} & J_{zz} \end{bmatrix} * \begin{pmatrix} \ddot{x} \\ \ddot{y} \\ \ddot{z} \\ \ddot{\theta}_1 \\ \ddot{\theta}_2 \\ \ddot{\theta}_3 \end{pmatrix} \tag{3.10}$$

Mass inertia coupling terms are taken as zero since body reference frame is located at the center of gravity [30]. If the body reference frame is located in another position on the body, these terms must be calculated accordingly.

In (3.10), F_x , F_y , F_z are components of the total force on the system resolved in body reference frame. M_1, M_2 , M_3 are components of total moment on the system resolved in body reference frame.

This system can be represented in state space as:

$$\begin{pmatrix} \dot{x}_1 \\ \dot{x}_2 \\ \dot{x}_3 \\ \dot{x}_4 \\ \dot{x}_5 \\ \dot{x}_6 \\ \dot{x}_7 \\ \dot{x}_8 \\ \dot{x}_9 \\ \dot{x}_{10} \\ \dot{x}_{11} \\ \dot{x}_{12} \end{pmatrix} = \begin{bmatrix} 0 & 1 & 0 & 0 & 0 & 0 & 0 & 0 & 0 & 0 & 0 & 0 \\ 0 & 0 & 0 & 0 & 0 & 0 & 0 & 0 & 0 & 0 & 0 & 0 \\ 0 & 0 & 0 & 1 & 0 & 0 & 0 & 0 & 0 & 0 & 0 & 0 \\ 0 & 0 & 0 & 0 & 0 & 0 & 0 & 0 & 0 & 0 & 0 & 0 \\ 0 & 0 & 0 & 0 & 0 & 1 & 0 & 0 & 0 & 0 & 0 & 0 \\ 0 & 0 & 0 & 0 & 0 & 0 & 0 & 0 & 0 & 0 & 0 & 0 \\ 0 & 0 & 0 & 0 & 0 & 0 & 0 & 1 & 0 & 0 & 0 & 0 \\ 0 & 0 & 0 & 0 & 0 & 0 & 0 & 0 & 0 & 0 & 0 & 0 \\ 0 & 0 & 0 & 0 & 0 & 0 & 0 & 0 & 0 & 1 & 0 & 0 \\ 0 & 0 & 0 & 0 & 0 & 0 & 0 & 0 & 0 & 0 & 0 & 0 \\ 0 & 0 & 0 & 0 & 0 & 0 & 0 & 0 & 0 & 0 & 0 & 1 \\ 0 & 0 & 0 & 0 & 0 & 0 & 0 & 0 & 0 & 0 & 0 & 0 \end{bmatrix} * \begin{pmatrix} x_1 \\ x_2 \\ x_3 \\ x_4 \\ x_5 \\ x_6 \\ x_7 \\ x_8 \\ x_9 \\ x_{10} \\ x_{11} \\ x_{12} \end{pmatrix} + \begin{bmatrix} 0 & 0 & 0 & 0 & 0 & 0 \\ \frac{1}{m} & 0 & 0 & 0 & 0 & 0 \\ 0 & 0 & 0 & 0 & 0 & 0 \\ 0 & \frac{1}{m} & 0 & 0 & 0 & 0 \\ 0 & 0 & 0 & 0 & 0 & 0 \\ 0 & 0 & \frac{1}{m} & 0 & 0 & 0 \\ 0 & 0 & 0 & 0 & 0 & 0 \\ 0 & 0 & 0 & \frac{A_1}{Den} & \frac{A_2}{Den} & \frac{A_3}{Den} \\ 0 & 0 & 0 & 0 & 0 & 0 \\ 0 & 0 & 0 & \frac{A_3}{Den} & \frac{A_4}{Den} & \frac{A_5}{Den} \\ 0 & 0 & 0 & 0 & 0 & 0 \\ 0 & 0 & 0 & \frac{A_3}{Den} & \frac{A_5}{Den} & \frac{A_6}{Den} \end{bmatrix} * \begin{pmatrix} F_x \\ F_y \\ F_z \\ M_1 \\ M_2 \\ M_3 \end{pmatrix}$$

(3.11)

Where;

$$A_1 = (J_{yy} * J_{zz} - J_{yz}^2)$$
$$A_2 = (J_{xz} * J_{yz} + J_{xy} * J_{zz})$$
$$A_3 = (J_{xy} * J_{yz} + J_{xz} * J_{yy})$$
$$A_4 = (J_{xx} * J_{zz} - J_{xz}^2)$$
$$A_5 = (J_{xy} * J_{xz} + J_{xx} * J_{yz})$$
$$A_6 = (J_{xx} * J_{yy} - J_{xy}^2)$$
$$Den = -J_{xx} * J_{yz}^2 - J_{yy} * J_{xz}^2 - J_{zz} * J_{xy}^2 - 2 * J_{xy} * J_{xz} * J_{xy} + J_{xx} * J_{yy} * J_{zz}$$

and the state variables are:

$$x_1 = x$$
$$x_2 = \dot{x}$$
$$x_3 = y$$
$$x_4 = \dot{y}$$
$$x_5 = z$$
$$x_6 = \dot{z}$$
$$x_7 = \theta_1$$
$$x_8 = \bar{\omega}_1$$
$$x_9 = \theta_2$$
$$x_{10} = \bar{\omega}_2$$
$$x_{11} = \theta_3$$
$$x_{12} = \bar{\omega}_3$$

3.4 MATLAB® Codes

Two codes and a Simulink® model are developed for the identification of inertia tensor part of the thesis.

An experimental model is developed using the SimMechanics® toolbox of Simulink®, which simulates the the experimental model, which is made up of input block, body block, sensors and a tracker block to track the orientation and position of the body with respect to the global frame is provided in Appendix A.

First of the developed MATLAB® codes is a pre-processor which is used to process the data collected from the experiment. Its inputs are the readings of the load cells on the cables and on the unbalanced mass-motor assembly. The load cells measure only the magnitudes of the forces, so in order to calculate the moments one needs to compute the force vectors. The position and orientation history of the test body is computed by the tracker block in the Simulink® model. The output of the code is the generalized force vector which consists of three translational forces and three moments.

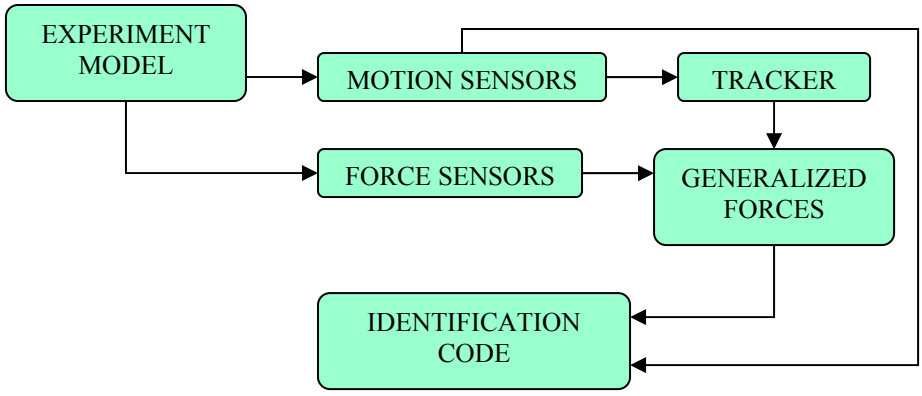

Figure 3.2 Flow Diagram of the System

Second of the developed codes is the identification code. The inputs for this code are the history of the measured outputs of the system (which are selected as the translational and angular accelerations), the history of the generalized force vector and the initial guess vector. The code uses the parameter identification toolbox functions of MATLAB® to identify the elements of the input matrix of the state space representation, and then solves the identified parameters for the elements of the inertia tensor.

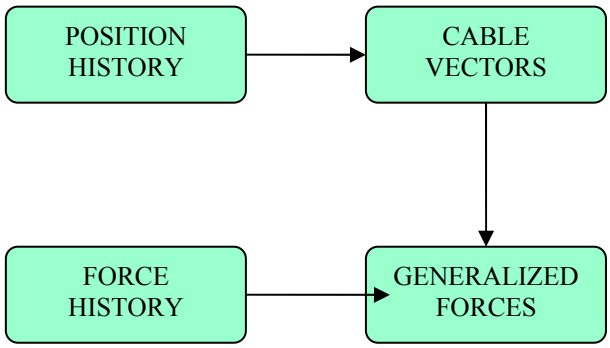

Figure 3.3 Flow Diagram of Pre-processor Code

The used functions are “iddata”, “idgray” and “pem”. The function “iddata” creates a data object from the experimental measurement. The input and measured output and sampling time are the inputs for this function. “idgray” function is used to define the state space model of the system. Although “idss” function can also be used to define the state space models, the models defined by “idss” have uncoupled parameter structure, which is not the case for this study. “idgrey” function is used instead in order to model the state space model with coupled parameters. “pem” is the general parameter identification function of the toolbox. It uses prediction error methods to identify the unknown parameters. The methods used by “pem” are explained in Section 3.5.

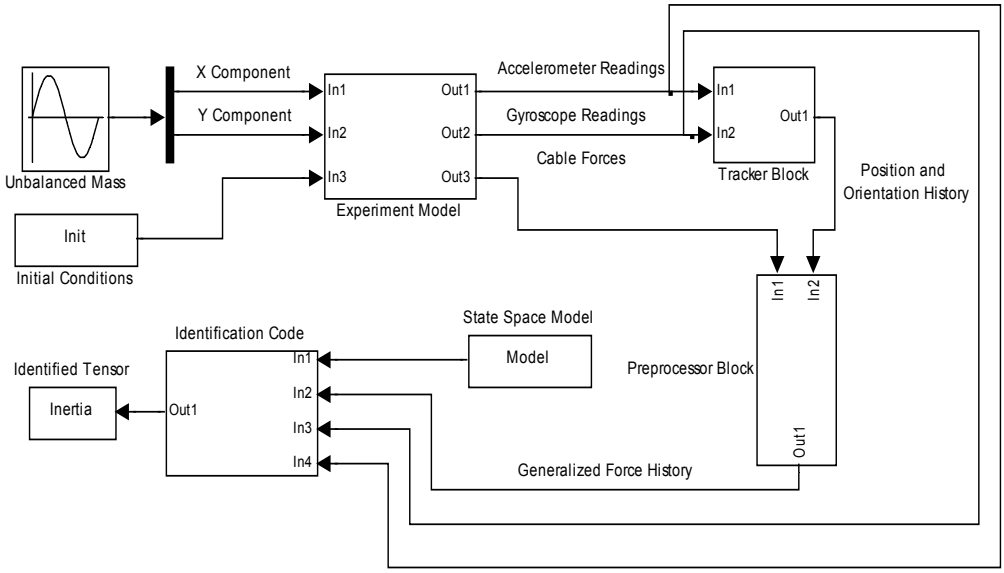

Figure 3.4 Simulink Diagram of the System

3.5 Parameter Estimation

The three main approaches to the measurement of inertia properties problem are mentioned in Chapter 1. These three approaches are oscillating the body around the rotating axis for which the relevant inertia property is sought after and measuring the frequency of the oscillations; using modal analysis and system identification techniques; parameter estimation techniques.

The main difference between the latter two of these three methods is that in system identification approach, the researcher can choose the

mathematical model of the system as well as the parameters of this mathematical model. In parameter identification methods, the mathematical model is predefined and only some of the parameters of this model are unknown.

The solution of a parameter estimation problem is done by minimizing the difference between the outputs of the mathematical model and the experimental measurements. A cost function is defined as the sum of the squares of the difference between the outputs of the mathematical model and the measured values. Minimizing this cost function will lead to the solution of the problem. These definitions actually define a least square problem, which can be solved by using unconstrained optimization methods.

The methods used in this M.Sc. study are commonly known as Prediction Error Methods. Prediction Error Methods constitute a broad family of parameter estimation methods which have a close relationship with Maximum Likelihood method; a statistical method used in system identification and parameter estimation. In both cases the cost function is defined in terms of output error [35].

According to Ljung [34]; “The idea behind the prediction error approach is simple:

- Describe the model as a predictor of the next output:

$$\hat{y}_m(n|n-1) = f(Z^{t-1}) \tag{3.12}$$

Here $\hat{y}_m(n|n-1)$ denotes the one-step ahead prediction of the output, and f is an arbitrary function of past, observed data.

- Parameterize the predictor in terms of a finite dimensional parameter vector θ:

$$\hat{y}(n|\theta) = f(Z^{t-1}, \theta) \tag{3.13}$$

- Determine an estimate of θ (denoted $\hat{\theta}_N$) from the model parameterization and the observed data set Z^N, so that the distance between $\hat{y}(1|\theta), \mathrm{K}\ , \hat{y}(N|\theta)$ and $y(1), \mathrm{K}\ , y(N)$ is minimized in a suitable norm.

In case the above norm is chosen such as to match the assumed probability density functions, the estimate $\hat{\theta}_N$ will coincide with the Maximum Likelihood estimate."

In short, the main idea is to predict the output of the next step using a function, which includes the measured outputs of the current time step and the unknown parameters. Once this function is defined using the derived mathematical model and measurements are made, the problem reduces to minimizing the distance between the predicted outputs, which are functions of unknown parameters, and the measured ones [42].

$$V_N(\theta) = \sum_{n=1}^{N} l(y(n) - f(Z^{t-1}, \theta)) \tag{3.14}$$

Here l is a suitable distance measure, such as $l(\varepsilon) = \|\varepsilon\|^2$, in which case the problem becomes a least squares optimization problem.

The numerical search for the minimum can be carried out using any of the many methods available such as Gauss-Newton Method, or

Lavenberg-Marquardt Method. Note that the first derivative of the difference of outputs has to be derived to use these methods.

In this study prediction error estimator of MATLAB® is used to estimate the unknown parameters, which is also programmed by Ljung.

To implement this method; the first thing to do is to discretize the state space model (Equation 3.11).

The derivative of the states with respect to time is defined as:

$$x'(t) = \lim_{T \to 0} \frac{x(t+T) - x(t)}{T} \tag{3.15}$$

In state space:

$$\lim_{T \to 0} \frac{x(t+T) - x(t)}{T} = Ax(t) + Bu(t) \tag{3.16}$$

The limit in (3.16) equation can be removed in state space system equations since the sampling time (T) is positive and non-negligible. By definition, a discrete system is only defined at certain time points, and not at all time points as the limit would have indicated otherwise.

Rearranging the system equations in state space gives:

$$x(t+T) = x(T) + T \cdot Ax(t) + T \cdot Bu(t) \tag{3.17}$$

Then:

$$x(t+T) = (1 + T \cdot A)x(t) + T \cdot Bu(t) \tag{3.18}$$

In the case of constant sampling time throughout the measurement, time can be expressed as:

$$t = n \cdot T \tag{3.19}$$

Inserting (3.19) into (3.18) gives:

$$x(n \cdot T + T) = (1 + T \cdot A)x(n \cdot T) + T \cdot Bu(n \cdot T) \tag{3.20}$$

Equation (3.20) can further be simplified by removing sampling time terms in state indices.

$$x(n+1) = (1 + T \cdot A)x(n) + T \cdot Bu(n \cdot)$$

So the state space equations are redefined as:

$$\begin{aligned} x(n+1) &= A_d x(n) + B_d u(n) \\ y(n) &= Cx(n) + Du(n) \end{aligned} \tag{3.21}$$

Next an equation which relates the output of the next step to the measurements of the current state is to be derived. Normally:

$$\hat{y}(n+1) = Cx(n+1) + Du(n+1) \tag{3.22}$$

Inserting the x(n+1) equation found in (3.21) into (3.22):

$$\hat{y}(n+1) = C(A_d x(n) + B_d u(n)) + Du(n+1) \tag{3.23}$$

x(n) can also be rewritten using the output part of (3.21) (provided that the output matrix C is invertible) as:

$$x(n) = C^{-1} y(n) - C^{-1} Du(n) \tag{3.24}$$

Inserting (3.24) into (3.23) leads to:

$$\hat{y}(n+1) = CA_d C^{-1} y(n) + (CB_d - CA_d C^{-1} D)u(n) + Du(n+1) \tag{3.25}$$

Equation (3.25) represents the predicted output in terms of the measured output and input data. The coefficient matrices are all nonlinear functions of the unknown parameters. Note that:

$$A_d = (1 + T \cdot A) \tag{3.26}$$

$$B_d = T \cdot B \tag{3.27}$$

Equation (3.25) is actually what is implied by equation (3.13), since it relates the output predictor to previous observed data and unknown parameters.

The next step is defining the cost function simply as the difference between the measured outputs and predicted outputs and minimizing the cost function using a proper optimization algorithm.

The equation defined in (3.14) can easily be turned into a least squares problem by using the definition $1(\varepsilon) = \|\varepsilon\|^2$ or $1(\varepsilon) = \frac{1}{2}\|\varepsilon\|^2$ and then can be minimized using the Gauss-Newton algorithm or Levenberg-Marquardt method.

The Levenberg-Marquardt algorithm provides a numerical solution to the mathematical problem of minimizing a function, generally nonlinear, over a space of parameters of the function.

In this method the parameter vector θ is replaced by a new estimate θ + δ at each iteration step. To determine δ, the predictor equation is approximated by its linearization.

$$\hat{y}(\theta + \delta) \approx \hat{y}(\theta) + J\delta \tag{3.28}$$

where J is the Jacobian of $\hat{y}$ with respect to the vector θ at given step.

Differentiating the square of the right hand side of the equation above and setting to zero leads to:

$$(J^T J)\delta = -J^T \hat{y}(\theta(n)) \tag{3.29}$$

from which δ can be obtained by inverting $J^T J$. Then using (3.28) the predictor function is updated. The key to the Levenberg-Marquardt algorithm is to replace this equation by a 'damped version'.

$$(J^T J - \lambda I)\delta = -J^T \hat{y}(\theta) \tag{3.30}$$

The (non-negative) damping factor λ is adjusted at each iteration.

Similarly the Gauss-Newton algorithm is also an iterative procedure. In Gauss-Newton algorithm, the new guess for the parameter vector is computed using the following relation instead of the linearization of the predctor function as in Levenberg – Marquardt Method:

$$\theta(n+1) = \theta(n) - (J^T J)^{-1} J^T \hat{y}(\theta(n)) \tag{3.31}$$

J denotes the Jacobian of $\hat{y}$ with respect to the parameter vector at n.

However equation (3.31) is usually reduced to (3.32) in order to avoid the inversion.

$$\theta(n+1) = \theta(n) + \delta \tag{3.32}$$

where δ is computed according to the solution of the following equation:

$$J^T J\delta = -J^T \hat{y}(\theta(n)) \tag{3.33}$$

Another implementation of the Gauss-Newton algorithm also employs a line search algorithm in which equation (3.33) is altered as:

$$\theta(n+1) = \theta(n) + \alpha \cdot \delta \tag{3.34}$$

Here α is a scalar, adjusted according to the criterion $V(n+1) < V(n)$.

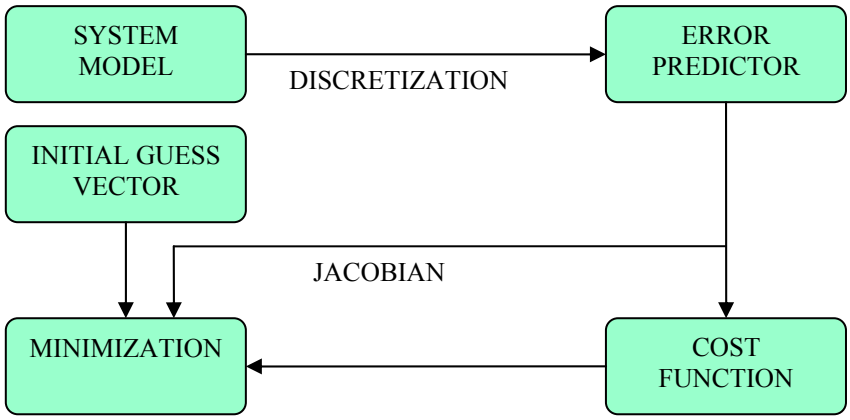

Figure 3.5 Flow Diagram of Identification Code

For the case studied in this thesis, the measured outputs are three linear accelerations and three rotational velocities of the CG. Discretizing the system in (3.11) and rewriting according to (3.25), output predictor is obtained in terms of unknown parameters. Then using either one of the Levenberg-Marquardt method or Gauss-Newton algorithm, the distance between the actual outputs and the predicted outputs is minimized.

The inputs for the developed code are the input and output measurements which are obtained from the simulation of the experimental system, the state space system defined as (3.11) and the initial guess vector for the parameters.

In this study prediction error estimator of MATLAB® is used to estimate the unknown parameters. This estimator allows user to choose between different line search algorithms. Possible choices are Gauss-Newton, a regularized version of the Gauss-Newton direction in which eigenvalues less than a user defined value of the Hessian are neglected and the Levenberg-Marquardt method. [43].

The code first the simulates the motion of the body under user defined forcing and calculates the generalised forces of the system and then identifies the inertia tensor using the prediction error method. The code is used through a graphical user interface written in MATLAB, Figures 3.6

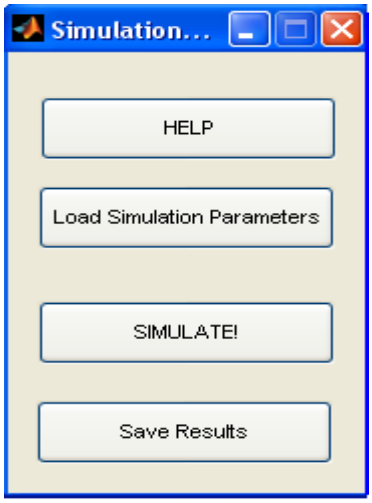

Figure 3.6 Simulator GUI

CHAPTER 4

CASE STUDIES AND RESULTS

Several case studies has been investigated in the development stage of the thesis and several more were inspected to ensure that the procedure is working properly.

The case studies 1-9 are done in the process of development of the thesis. These studies demonstrate various initial condition and forcing techniques, and the results of these studies are analysed in order to determine the most suitable test setup and initial conditions. In most of these cases, theoretical bodies are used. The case studies 10-17 are carried out using measured data from literature [31,32].

4.1 Case Study 1

Table 4.1 Data for Case Study 1

CASE 1		
Cable Lengths [m]	2.5	
Coordinates of CG (initially) [m]	[2; 2.5; -2.5616]	
Mass [kg]	250	
Jxx [N.m^2]	1000	
Jyy [N.m^2]	1000	
Jzz [N.m^2]	1000	
Jxy [N.m^2]	50	
Jxz [N.m^2]	50	
Jyz [N.m^2]	50	
Coordinates of Hinge Points on the Ceiling [m]		
[0;0;0]		
[4;0;0]		
[0;5;0]		
[4;5;0]		
Body Dimensions [m]		
3x2x1 (Rectangular Prism)		
Coordinates of Hinge Points on the Body (wrt to their respective hinge points on the ceiling)		
[1;1;-2.0616]		
[1;-1;-2.0616]		
[-1;1;-2.0616]		
[-1;-1;-2.0616]		
Initial Conditions		
No Initial Displacement		
Applied Forces		
Force Vector [N]	**Point of Action [m]**	**Time interval [s]**
[200;0;0]	[0;-1.5;0]	[0.1,1.1]
[0;200;0]	[0;-1.5;0]	[4.1,5.1]
Initial Guess Vector for Inertia Tensor [N.m2]		
[750;300;300;750;300;750]		
Length of the Experiment [s]	**Sampling [s]**	
10	0.01	

4.1.1 Data Consistency Check for Case Study 1

The simulink model has two sensors both mounted on the CG. First sensor (world sensor) measures the quantities with respect to world coordinates whereas the other one (body sensor) with respect to the. body reference frame; which is the real case. The readings from the world sensor is used for verification purposes only. All the data to be used in identification are either read directly from the body sensor, or derived from its readings.

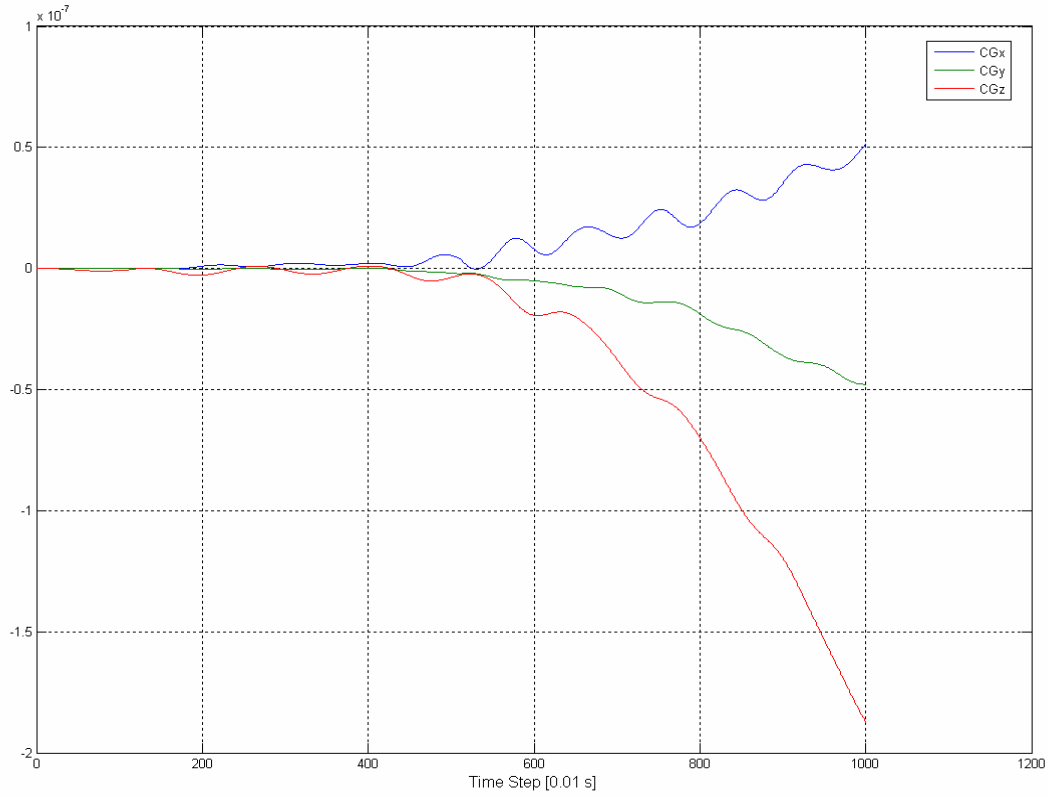

Figure 4.1 Percentage Error of Measured CG Coordinates

The percentage difference between the world sensor and body sensor readings of position of center of gravity (3 components) and the components of the transformation matrix (9 components) can be seen in Figures 4.1 and 4.2 respectively. Note that body sensor readings are processed in the “Tracker” to obtain position data.

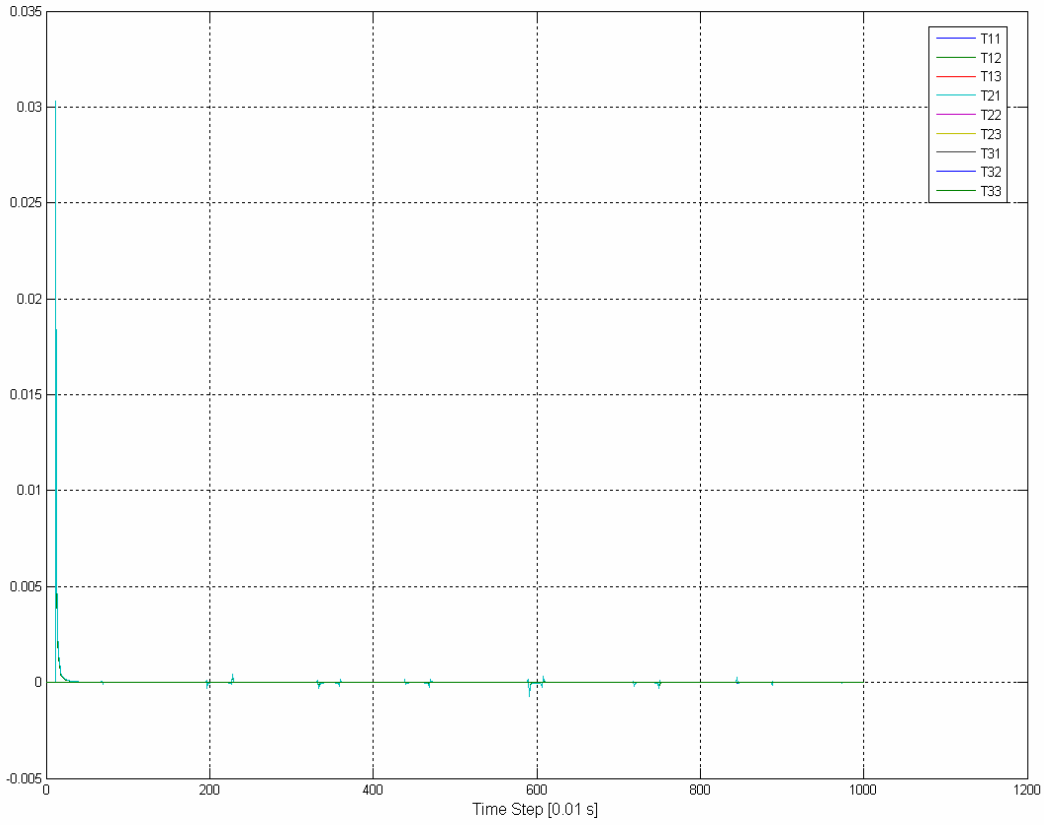

Figure 4.2 Percentage Error of Transformation Matrix Components

As can be seen from the Figures 3.2 and 3.3; percentage error between the real values and the calculated values are extremely low. Collected data are consistent with the readings of world sensor. Thus, the function of the “Tracker” block is validated.

The error caused by the “Tracker” is important because of the fact that the force vectors are found using this position and transformation matrix data and measured force magnitudes. Considerable error in position data at this stage will lead to inadequate accuracy in force vectors and identification results.

4.1.2 The Results of the Experiment of Case Study 1

The resulting motion of the experiment can be observed in Figures 4.3, 4.4 and 4.5.

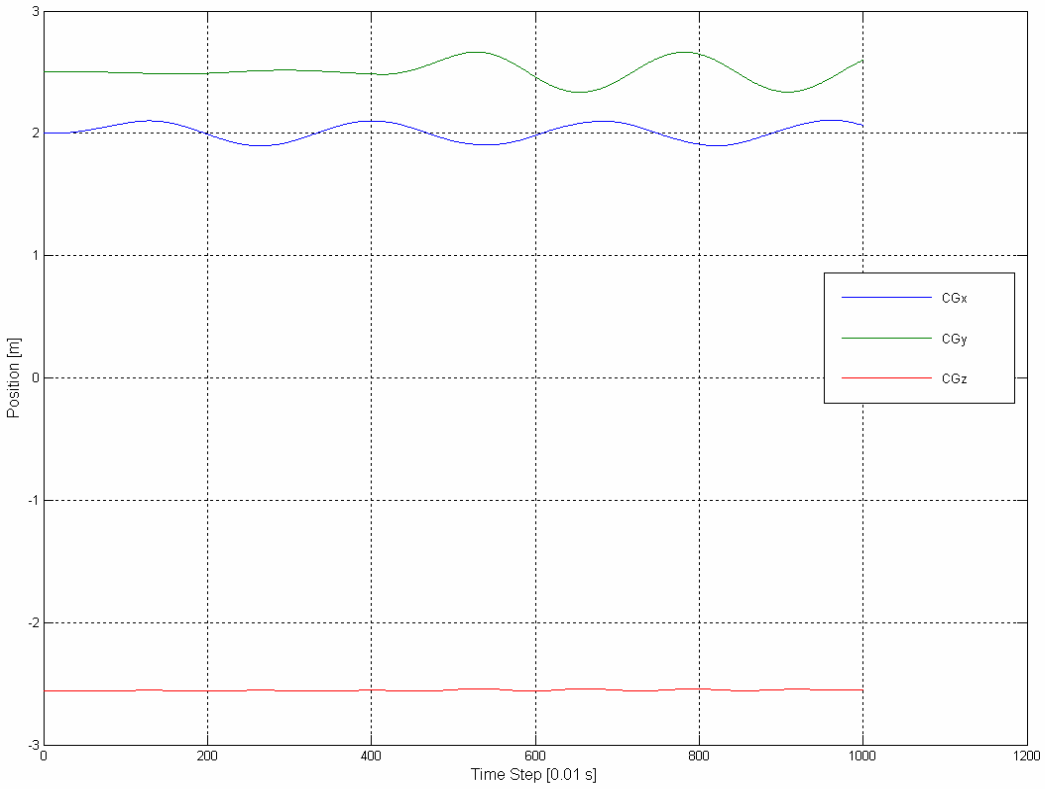

Figure 4.3 Position of CG

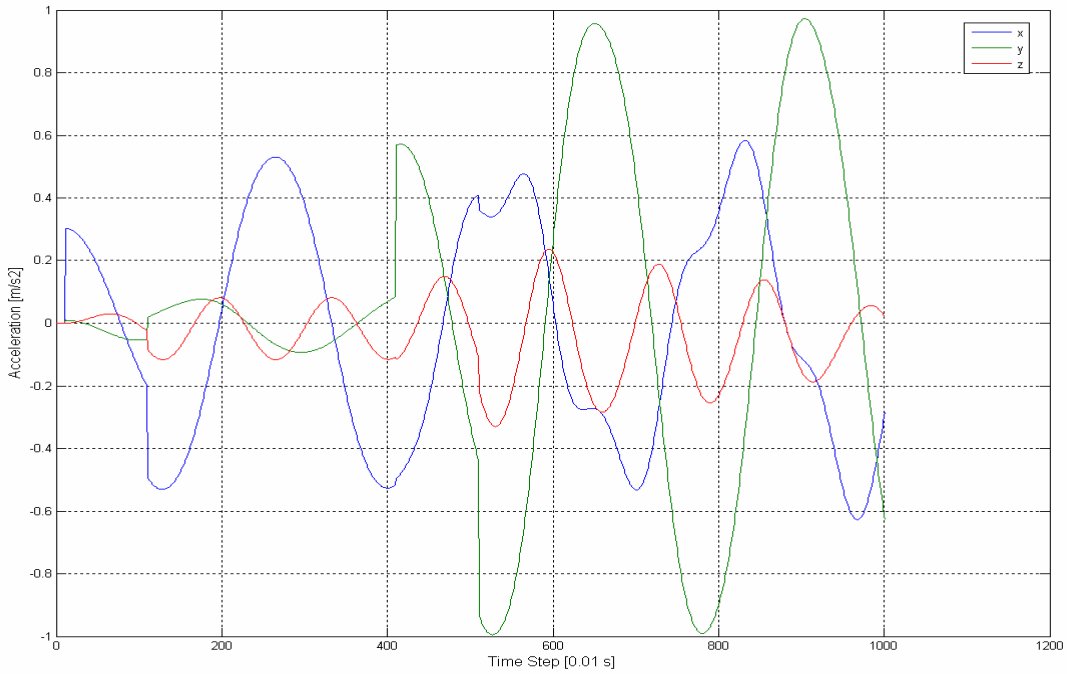

Figure 4.4 Acceleration of CG

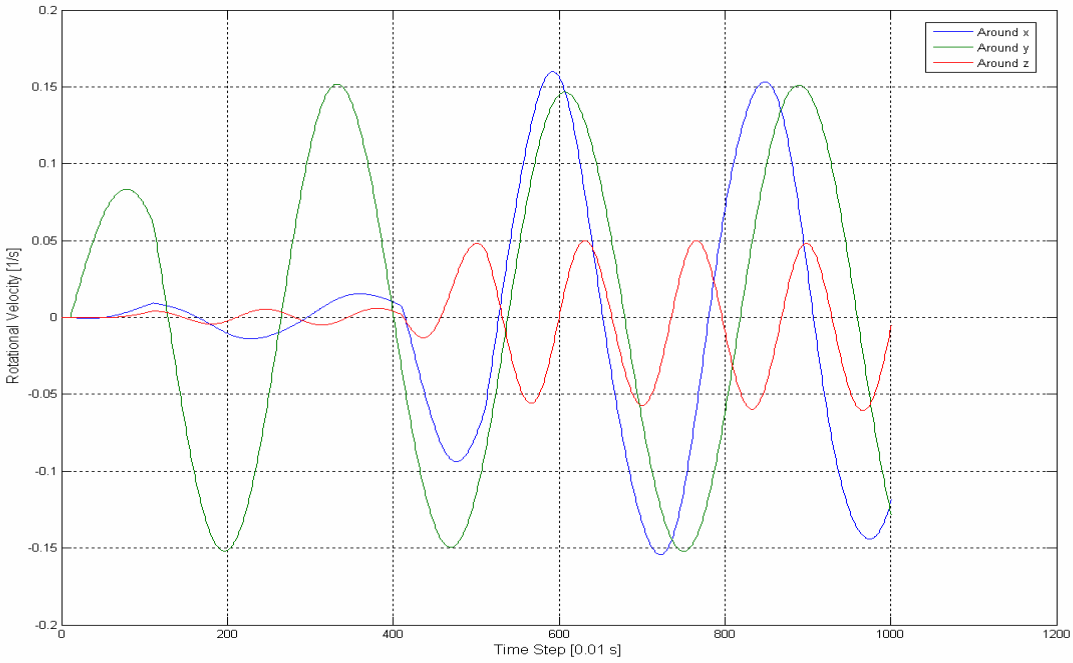

Figure 4.5 Rotational Velocity of the Body with respect to CG

Since the input force has started to act on the system at t= 0.1 s; all graphs stay at initial conditions until 0.1s. The effects of the exciting force can be seen clearly in Figure 4.4; as discontinuities in accelerations.

4.1.3 The Results of the Identification Run for Case Study 1

After the experiment run; collected data are processed to compute the generalized force vector. Then the acceleration history, rotational velocity history and the generalized force vector history are fed to the identification code.

Identification code calculated the following inertia tensor:

$$J = \begin{bmatrix} 1005.4 & 48.6 & 53.4 \\ 48.6 & 1004.2 & 46.0 \\ 53.4 & 46.0 & 1004.0 \end{bmatrix}$$

Whereas the original tensor was:

$$J = \begin{bmatrix} 1000 & 50 & 50 \\ 50 & 1000 & 50 \\ 50 & 50 & 1000 \end{bmatrix}$$

Percentage error of the components are:

$$\%Error = \begin{bmatrix} 0.54 & 2.8 & 6.8 \\ 2.8 & 0.42 & 8 \\ 6.8 & 8 & 0.40 \end{bmatrix}$$

With a maximum error of 8 percent for off diagonal elements and 0.54 percent for diagonal elements, the results are found to be satisfactory for most vehicle dynamics studies.

Figure 4.6 shows the comparison of the identified system and the measured system's output measurements.

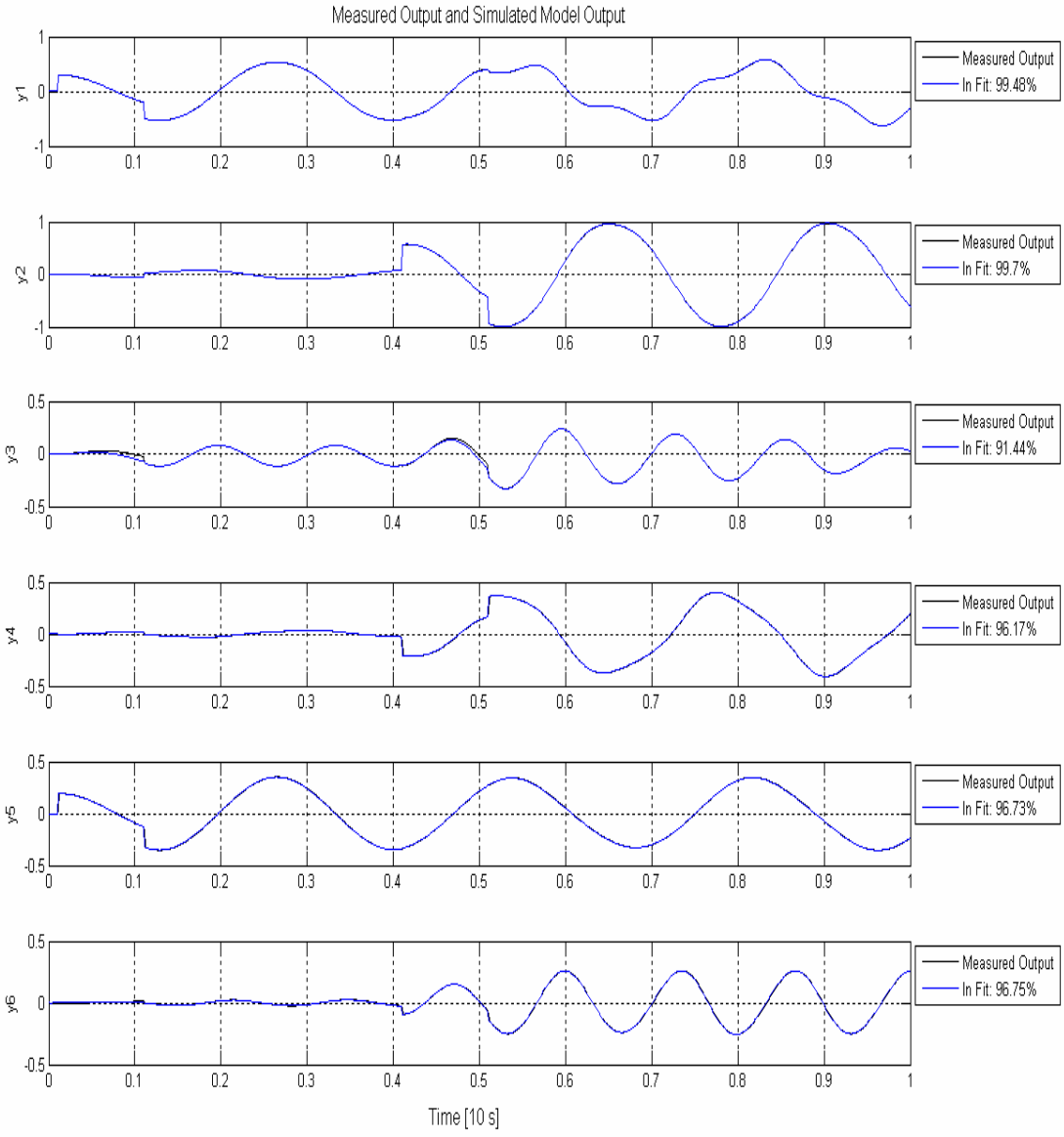

Figure 4.6 Comparison of the Identified System and the Measured System

4.2 Case Study 2

Table 4.2 Data for Case Study 2

CASE 2		
Cable Lengths [m]	2.5	
Coordinates of CG (initially) [m]	[2; 2.5; -2.5616]	
Mass [kg]	200	
Jxx [N.m^2]	160.2	
Jyy [N.m^2]	826.3	
Jzz [N.m^2]	756.7	
Jxy [N.m^2]	0	
Jxz [N.m^2]	92.4	
Jyz [N.m^2]	0	
Coordinates of Hinge Points on the Ceiling [m]		
[0;0;0]		
[4;0;0]		
[0;5;0]		
[4;5;0]		
Body Dimensions [m]		
3x2x1 (Rectangular Prism)		
Coordinates of Hinge Points on the Body (wrt to their respective hinge points on the ceiling)		
[1;1;-2.0616]		
[1;-1;-2.0616]		
[-1;1;-2.0616]		
[-1;-1;-2.0616]		
Initial Conditions		
No Initial Displacement		
Applied Forces		
Force Vector [N]	**Point of Action [m]**	**Time interval [s]**
[200;0;0]	[0;-1.5;0]	[0.1,1.1]
[0;200;0]	[0;-1.5;0]	[4.1,5.1]
Initial Guess Vector for Inertia Tensor [N.m2]		
[250;0;150;750;0;750]		
Length of the Experiment [s]	**Sampling [s]**	
10	0.01	

This data set is based on a real system. The mass and inertia properties are that of a tractor, scaled by 0.1.

4.2.1 The Results of the Experiment of Case Study 2

The resulting motion of the experiment can be observed in Figures 4.7, 4.8 and 4.9.

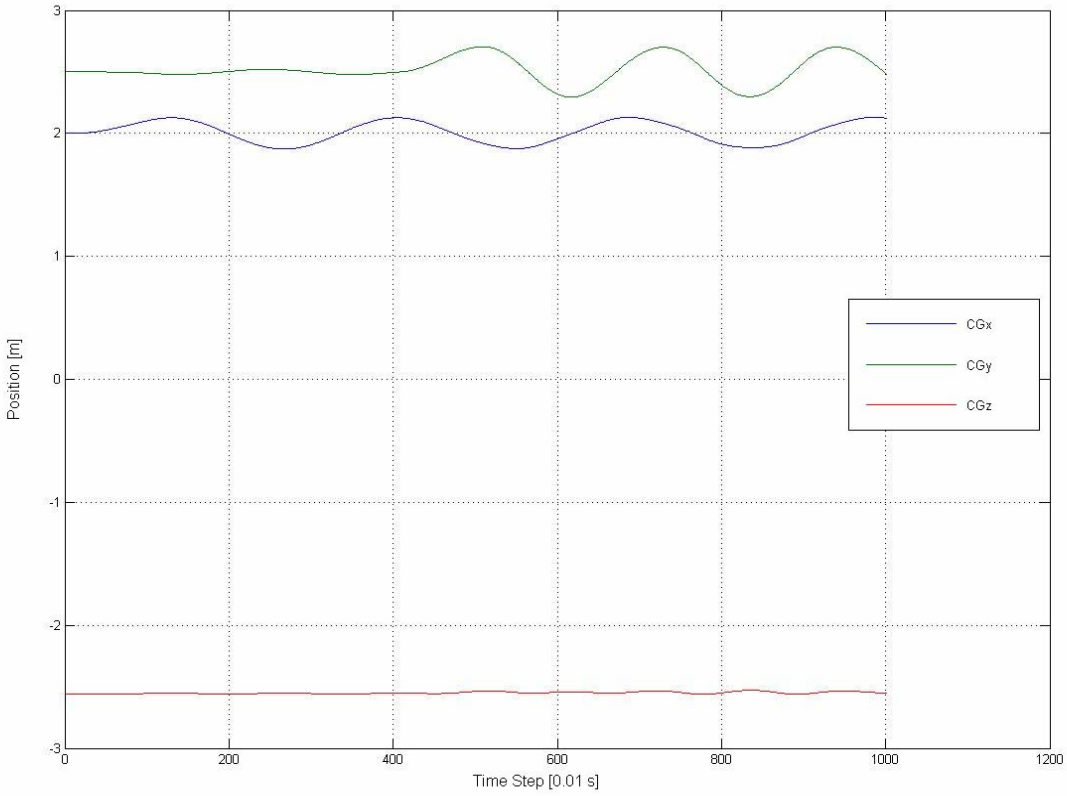

Figure 4.7 Position of CG

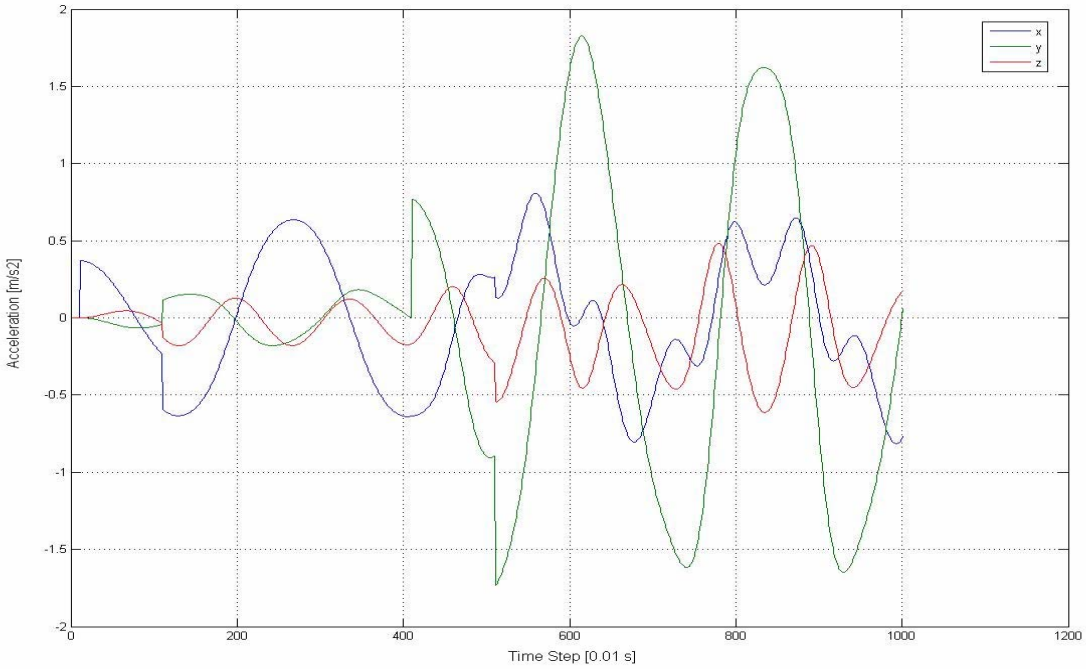

Figure 4.8 Acceleration of CG

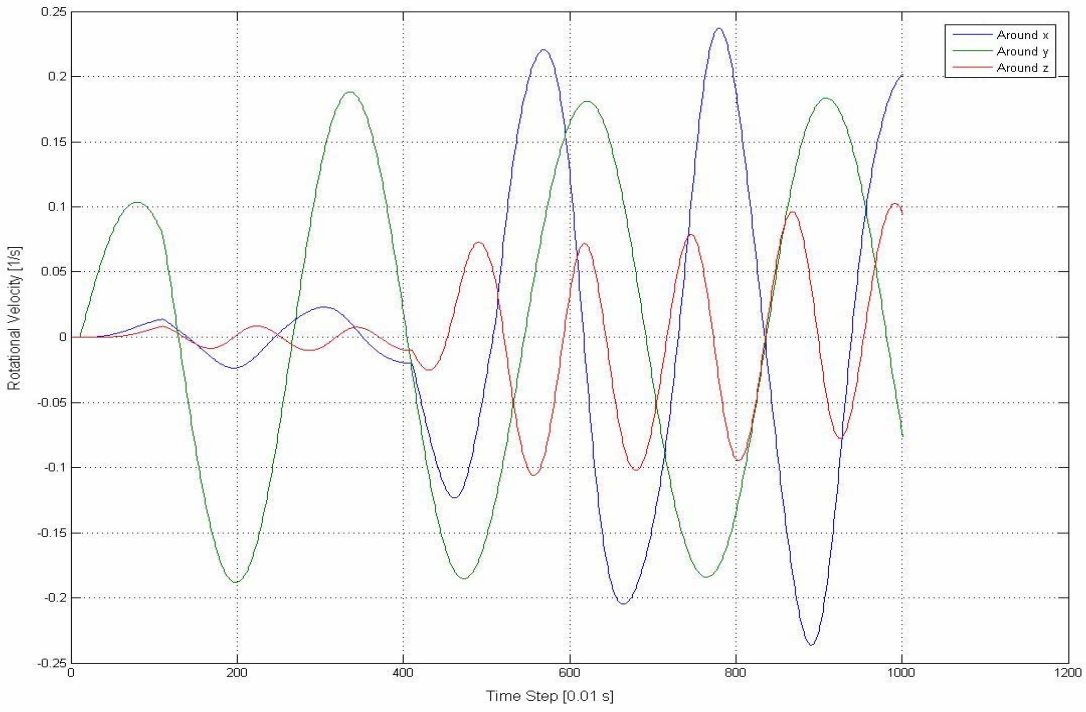

Figure 4.9 Rotational Velocity of the Body with respect to CG

4.2.2 The Results of the Identification Run for Case Study 2

In case study 2; the data of a real system were used. As stated in Section 3.1; pitch/yaw and roll/pitch product of inertia terms are inherently zero.

Identification code calculated the following inertia tensor:

$$J = \begin{bmatrix} 163.56 & -0.44 & 96.24 \\ -0.44 & 836.72 & 1.53 \\ 96.24 & 1.53 & 789.88 \end{bmatrix}$$

Whereas the original tensor was:

$$J = \begin{bmatrix} 160.2 & 0 & 92.4 \\ 0 & 826.3 & 0 \\ 92.4 & 0 & 756.7 \end{bmatrix}$$

Percentage error is:

$$\%Error = \begin{bmatrix} 2.10 & \pm 0.44 & 4.16 \\ \pm 0.44 & 1.26 & \pm 1.53 \\ 4.16 & \pm 1.53 & 4.39 \end{bmatrix}$$

(Note that absolute error is given for zero terms)

In this case, yaw inertia error came out to be more than 4 percent. Although the other identified terms are acceptable in terms of vehicle dynamics studies; better accuracy can be obtained in diagonal elements, namely yaw inertia, using other, simpler methods.

Figure 4.10 shows the comparison of the identified system and the measured system's output measurements.

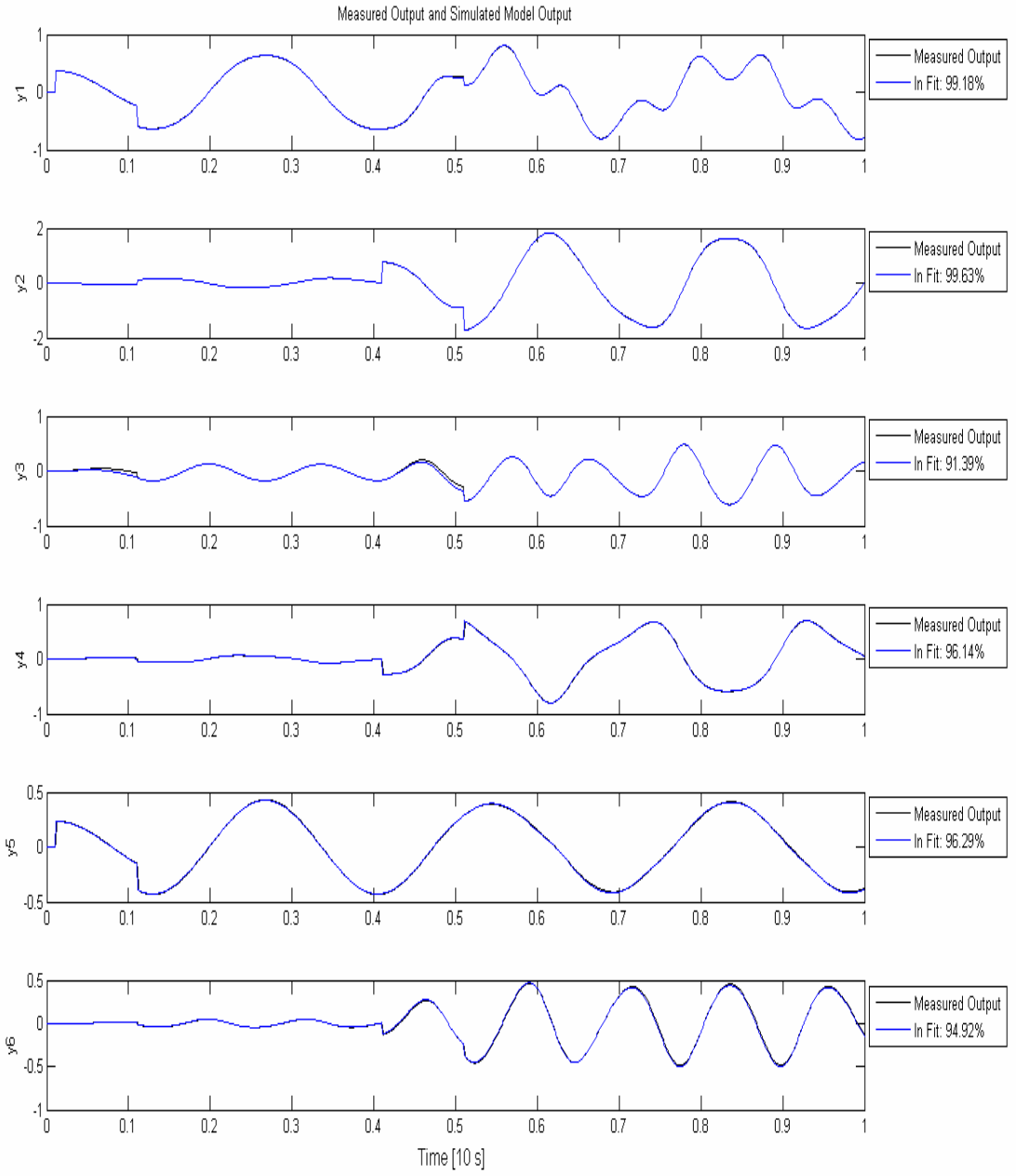

Figure 4.10 Comparison of the Identified System and the Measured System

4.3 Case Study 3

Table 4.3 Data for Case Study 3

CASE 3		
Cable Lengths [m]	2.5	
Coordinates of CG (initially) [m]	[2; 2.5; -2.5616]	
Mass [kg]	250	
Jxx [N.m^2]	1000	
Jyy [N.m^2]	1000	
Jzz [N.m^2]	1000	
Jxy [N.m^2]	50	
Jxz [N.m^2]	50	
Jyz [N.m^2]	50	
Coordinates of Hinge Points on the Ceiling [m]		
[0;0;0]		
[4;0;0]		
[0;5;0]		
[4;5;0]		
Body Dimensions [m]		
3x2x1 (Rectangular Prism)		
Coordinates of Hinge Points on the Body (wrt to their respective hinge points on the ceiling)		
[1;1;-2.0616]		
[1;-1;-2.0616]		
[-1;1;-2.0616]		
[-1;-1;-2.0616]		
Initial Conditions		
No Initial Displacement		
Applied Forces		
Force Vector [N]	**Point of Action [m]**	**Time interval [s]**
[200;0;0]	[0;-1.5;0]	[0.1,1.1]
[0;200;0]	[0;-1.5;0]	[4.1,5.1]
Initial Guess Vector for Inertia Tensor [N.m2]		
[750;200;200;750;200;750]		
Length of the Experiment [s]	**Sampling [s]**	
10	0.01	

In this case; the same data set which was used in case study 1 was used with the same forcing. Thus, the motion of the body is the same as that case. No graph are given to demonstrate the motion of the test body in the experiment of case study 3.

However, in this case; the externally applied forcing is not measured. Because of this, the generalized force vector is composed of only the tension forces in the cables, which are in fact affected by the external loading. This simplification will introduce some error to the identification results. The aim of this experiment is to find out if accuracy of the results will be acceptable or not. If they are found to be acceptable; this experiment method brings considerable ease to the implementation of the test setup.

4.3.1 The Results of the Identification Run for Case Study 3

Identification code calculated the following inertia tensor:

$$J = \begin{bmatrix} 1003.7 & 50.5 & 47.4 \\ 50.5 & 1001.5 & 43.7 \\ 47.4 & 43.7 & 1300.7 \end{bmatrix}$$

Whereas the original tensor was:

$$J = \begin{bmatrix} 1000 & 50 & 50 \\ 50 & 1000 & 50 \\ 50 & 50 & 1000 \end{bmatrix}$$

Percentage error is:

$$\%Error = \begin{bmatrix} 0.37 & 1 & 5.2 \\ 1 & 0.15 & 12.6 \\ 5.2 & 12.6 & 30.07 \end{bmatrix}$$

Four of the six parameters are identified with acceptable accuracy in this case. Although 12.6 percent looks somewhat inaccurate, the contribution of this element to the dynamics of the vehicle is relatively low with respect to the diagonal elements and this amount of error can be consşdered “good enough”. However 30 percent error in yaw inertia shows that the method used in this case is inapplicaple, since yaw inertia plays an important role in rollover research in vehicle dynamics.

Figure 4.11 shows the comparison of the identified system and the measured system’s output measurements.

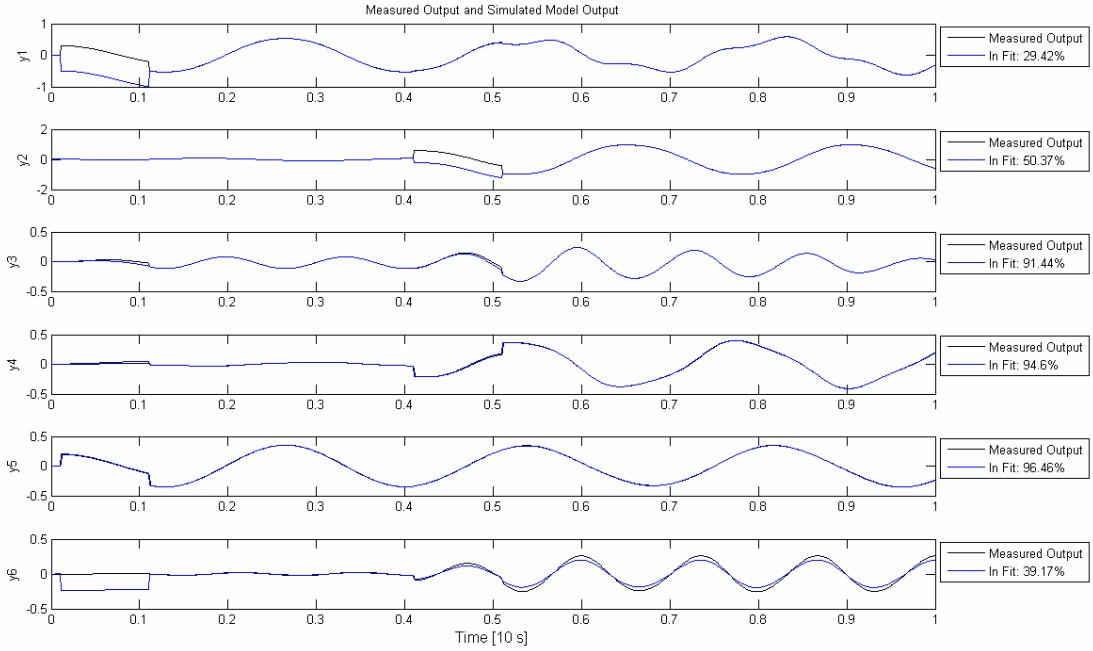

Figure 4.11 Comparison of the Identified System and the Measured System

4.4 Case Study 4

Table 4.4 Data for Case Study 4

CASE 4		
Cable Lengths [m]	2.5	
Coordinates of CG (initially) [m]	[2; 2.5; -2.5616]	
Mass [kg]	250	
Jxx [N.m^2]	1000	
Jyy [N.m^2]	1000	
Jzz [N.m^2]	1000	
Jxy [N.m^2]	50	
Jxz [N.m^2]	50	
Jyz [N.m^2]	50	
Coordinates of Hinge Points on the Ceiling [m]		
[0;0;0]		
[4;0;0]		
[0;5;0]		
[4;5;0]		
Body Dimensions [m]		
3x2x1 (Rectangular Prism)		
Coordinates of Hinge Points on the Body (wrt to their respective hinge points on the ceiling)		
[1;1;-2.0616]		
[1;-1;-2.0616]		
[-1;1;-2.0616]		
[-1;-1;-2.0616]		
Initial Conditions		
No Initial Displacement		
Applied Forces		
Force Vector [N]	**Point of Action [m]**	**Time interval [s]**
[200;0;0]	[0;-1.5;0]	[0.1,1.1]
[0;200;0]	[0;-1.5;0]	[4.1,5.1]
Initial Guess Vector for Inertia Tensor [N.m2]		
[750;200;200;750;200;750]		
Length of the Experiment [s]	**Sampling [s]**	
15	0.01	

4.4.1 The Results of the Experiment of Case Study 4

The resulting motion of the experiment can be observed in Figures 4.12, 4.13 and 4.14.

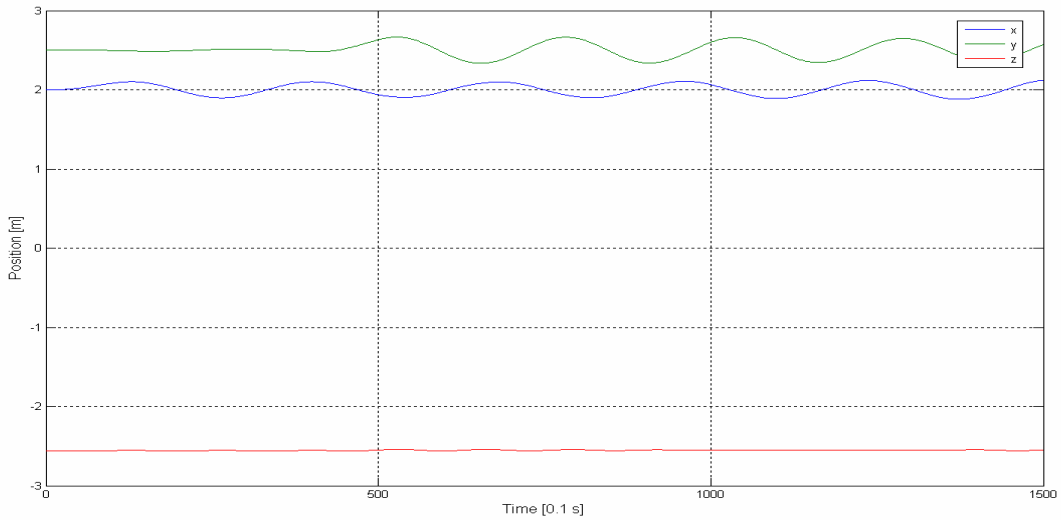

Figure 4.12 Position of CG

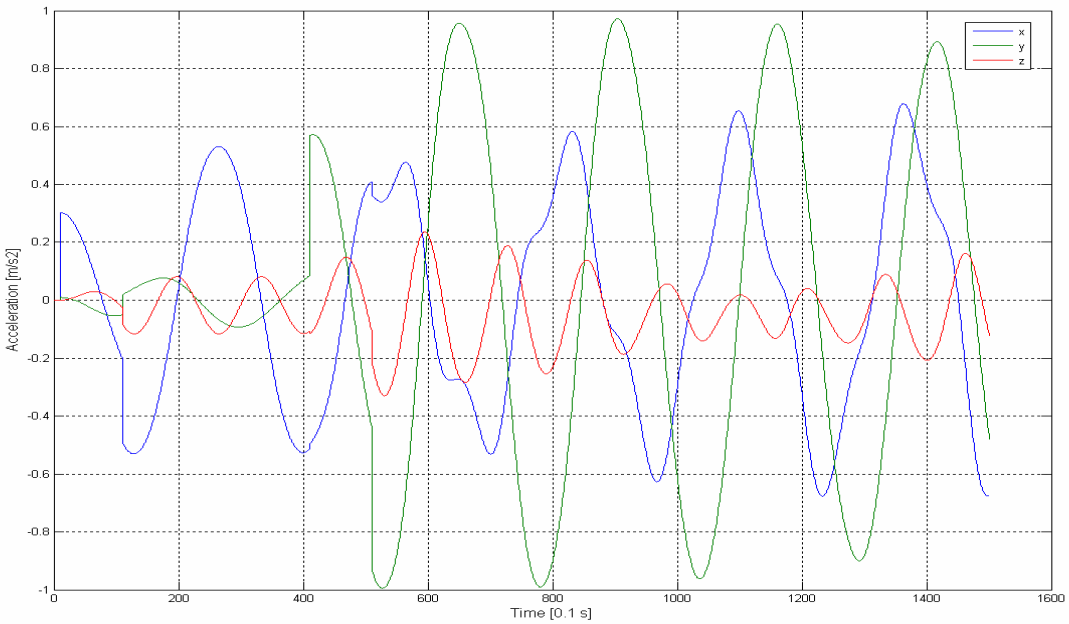

Figure 4.13 Acceleration of CG

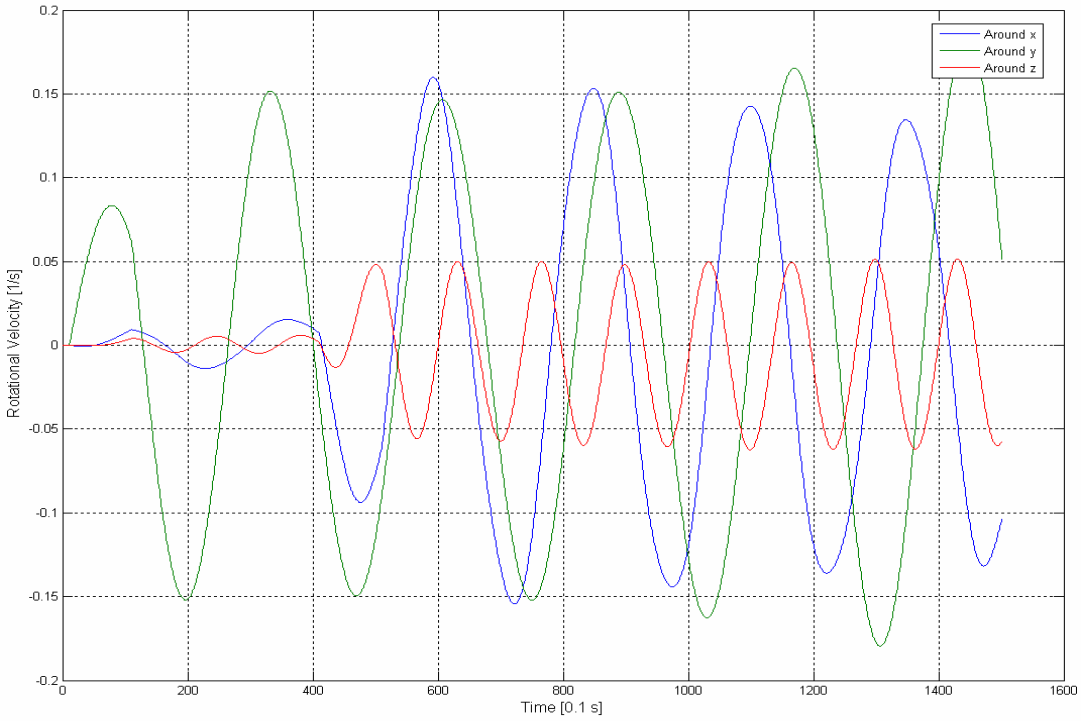

Figure 4.14 Rotational Velocity of the Body with respect to CG

4.4.2 The Results of the Identification Run for Case Study 4

In case study 4, the same data set which was used in case study 1 was used with the same forcing. However on this occasion; the experimental was held for 15 seconds. The aim is to apply the external forces in the first 5.1 seconds of the experiment; and then use the data which is taken during rest of the 15 seconds.

Among the collected experimental data; only those taken between the time interval [5.1s, 15s] are used in the identification run. In the specified interval, there are no external forces on the system. The states of the system at t=5.1 s are given as initial conditions for the

identification run mathematical model. In this experiment it is aimed to see whether it is possible to identify the required parameters with good accuray without measuring the external force applied on the system. If the aim is reached; the implementation cost of the test setup will decrease considerably.

Identification code calculated the following inertia tensor:

$$J = \begin{bmatrix} 870.9 & 244.3 & 58.4 \\ 244.3 & 865.3 & 41.9 \\ 58.4 & 41.9 & 1002.0 \end{bmatrix}$$

Whereas the original tensor was:

$$J = \begin{bmatrix} 1000 & 50 & 50 \\ 50 & 1000 & 50 \\ 50 & 50 & 1000 \end{bmatrix}$$

Percentage error is:

$$\%Error = \begin{bmatrix} 12.91 & 388.6 & 16.8 \\ 388.6 & 13.47 & 16.2 \\ 16.8 & 16.2 & 0.2 \end{bmatrix}$$

In this case, all the elements of the tensor, except for the yaw inertia are unacceptably inaccurate. However error of the yaw inertia is very low. It is concluded that this method can be applied in conjunction with the technique in the previous case.

Figure 4.15 shows the comparison of the identified system and the measured system's output measurements.

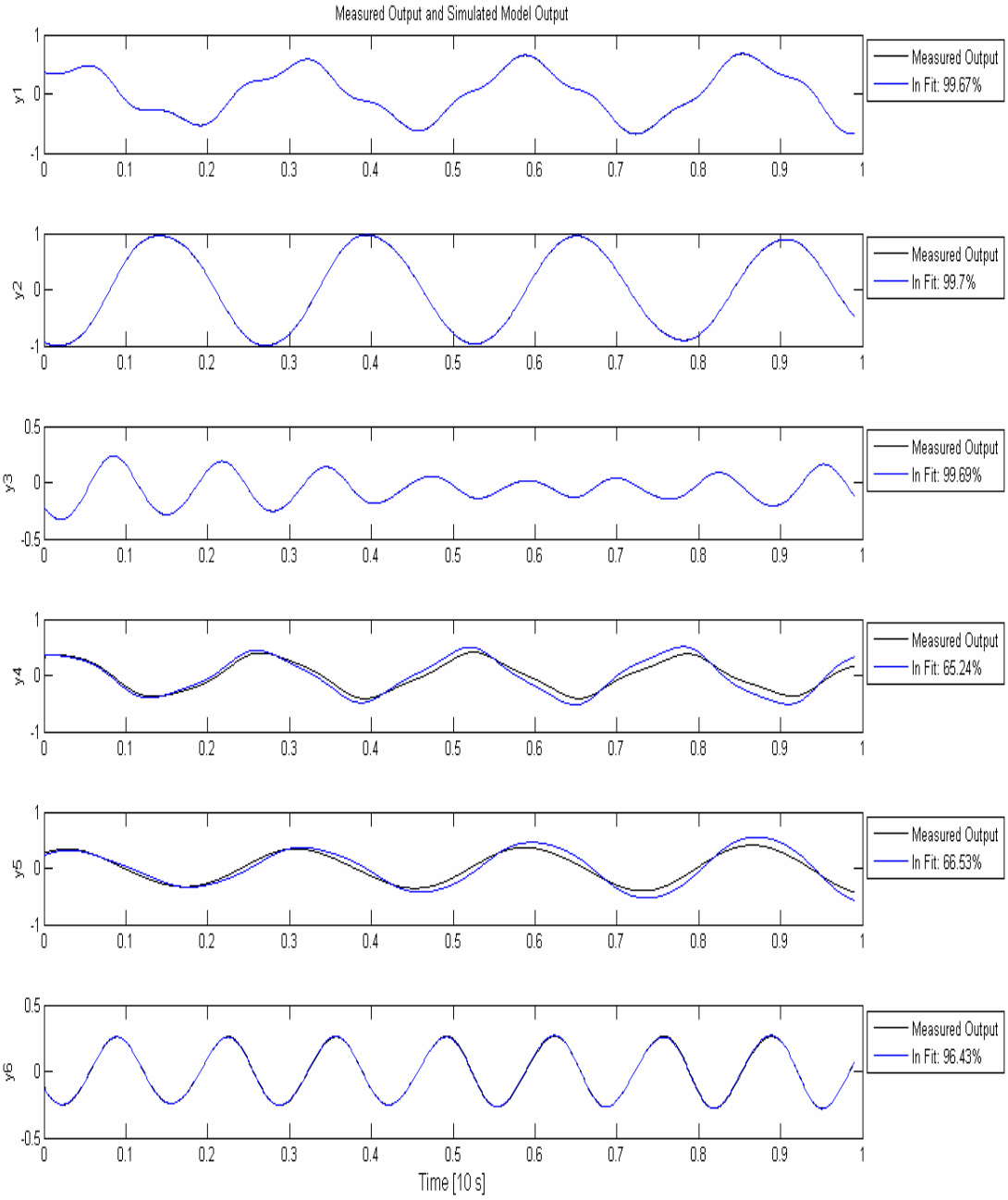

Figure 4.15 Comparison of the Identified System and the Measured System

4.5 Case Study 5

Table 4.5 Data for Case Study 5

CASE 5		
Cable Lengths [m]	2.5	
Coordinates of CG (initially) [m]	[2; 2.5; -2.5616]	
Mass [kg]	250	
Jxx [N.m^2]	1000	
Jyy [N.m^2]	1000	
Jzz [N.m^2]	1000	
Jxy [N.m^2]	50	
Jxz [N.m^2]	50	
Jyz [N.m^2]	50	
Coordinates of Hinge Points on the Ceiling [m]		
[0;0;0]		
[4;0;0]		
[0;5;0]		
[4;5;0]		
Body Dimensions [m]		
3x2x1 (Rectangular Prism)		
Coordinates of Hinge Points on the Body (wrt to their respective hinge points on the ceiling)		
[1;1;-2.0616]		
[1;-1;-2.0616]		
[-1;1;-2.0616]		
[-1;-1;-2.0616]		
Initial Conditions		
No Initial Displacement		
Applied Forces		
Force Vector [N]	**Point of Action [m]**	**Time interval [s]**
[200;0;0]	[0;-1.5;0]	[0.1,1.1]
[0;200;0]	[0;-1.5;0]	[4.1,5.1]
Initial Guess Vector for Inertia Tensor [N.m2]		
[750;200;200;750;200;750]		
Length of the Experiment [s]	**Sampling [s]**	
10	0.01	

In this case; 990 identification runs were made with the same data used for the case study 1. The identification code is put into a “for” loop and the code was run 990 times; every time starting from another data point to start and using the data between that point and the end of data (1000th data point). i.e. starts from [1,1000], [2,1000], [3,1000] ... [989,1000], [990,1000]. The initial conditions for the mathematical model was also changed with the values of the states at that data point.

The results were plotted in the fashion which will reveal the convergence and divergence zones in the solution history. The aim of this experiment and identification run is to obtain a better understanding of the identification routine. The solution history includes the cases in which the forces were measured; and the cases in which the identification started after the external forces were released. Thus the results for both of the situation can be seen on the same graphs which will help with the comparison of the techniques.

Figure 4.16 shows the solution history for all six parameters. Figure 4.17 shows only the diagonal terms and Figure 4.18 shows only the off-diagonal terms.

According to the results, it can be said that the solution is unstable for the runs that start after the application of the seconf force. It is seen that, for the runs that start after 650th data point, the solution run is enden before the convergence is reached.

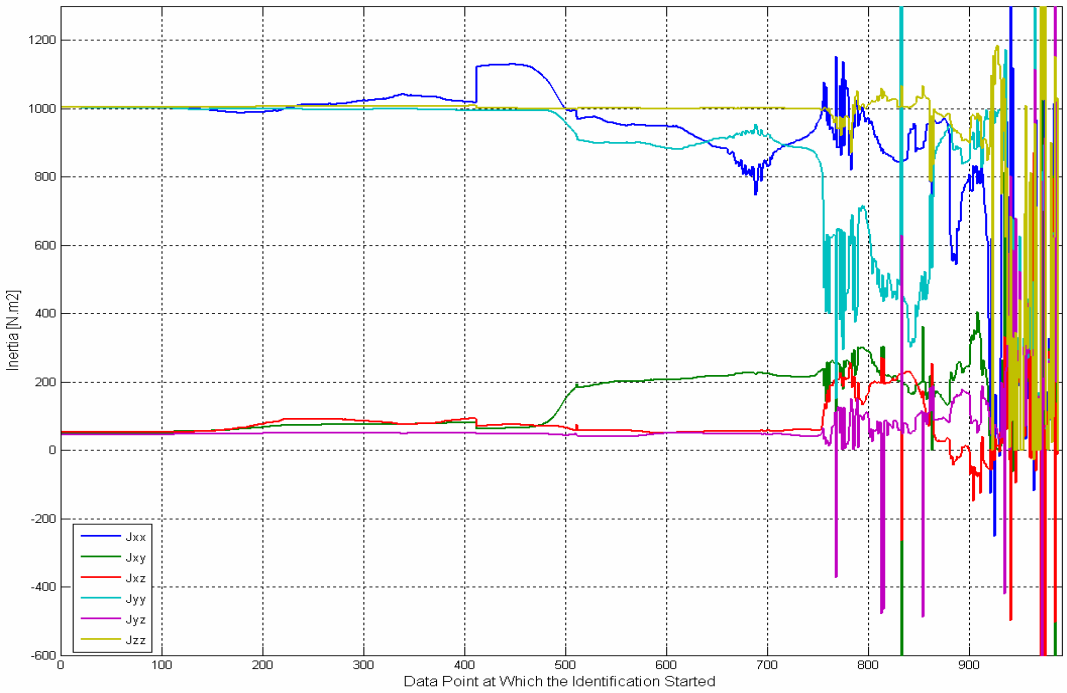

Figure 4.16 Solution History for Case 5

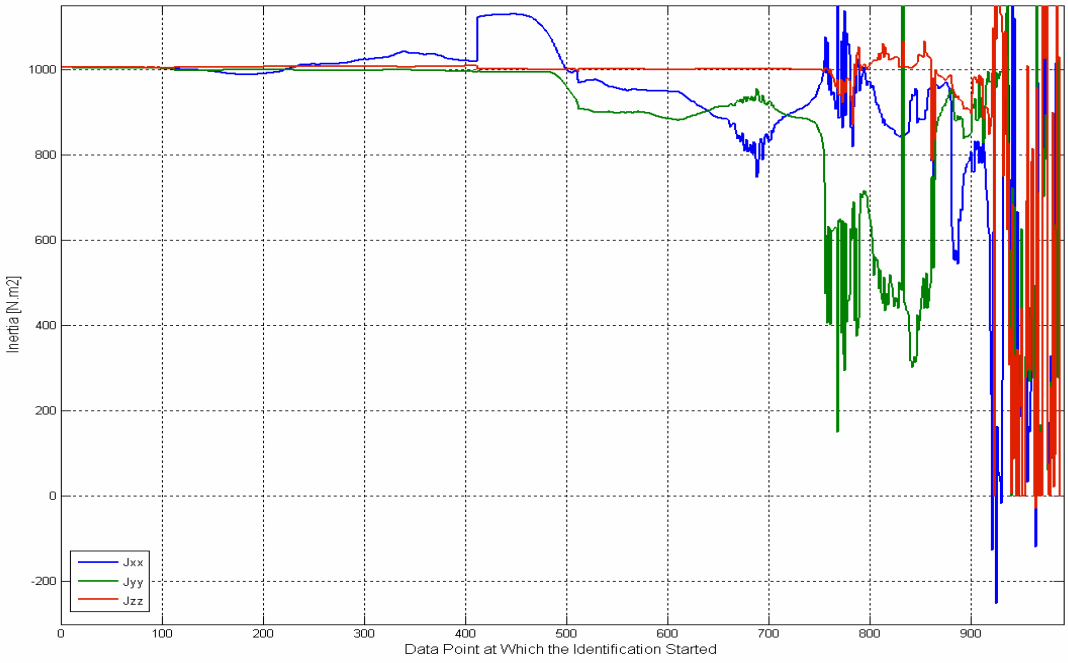

Figure 4.17 Solution History for Case 5 - Diagonal Terms

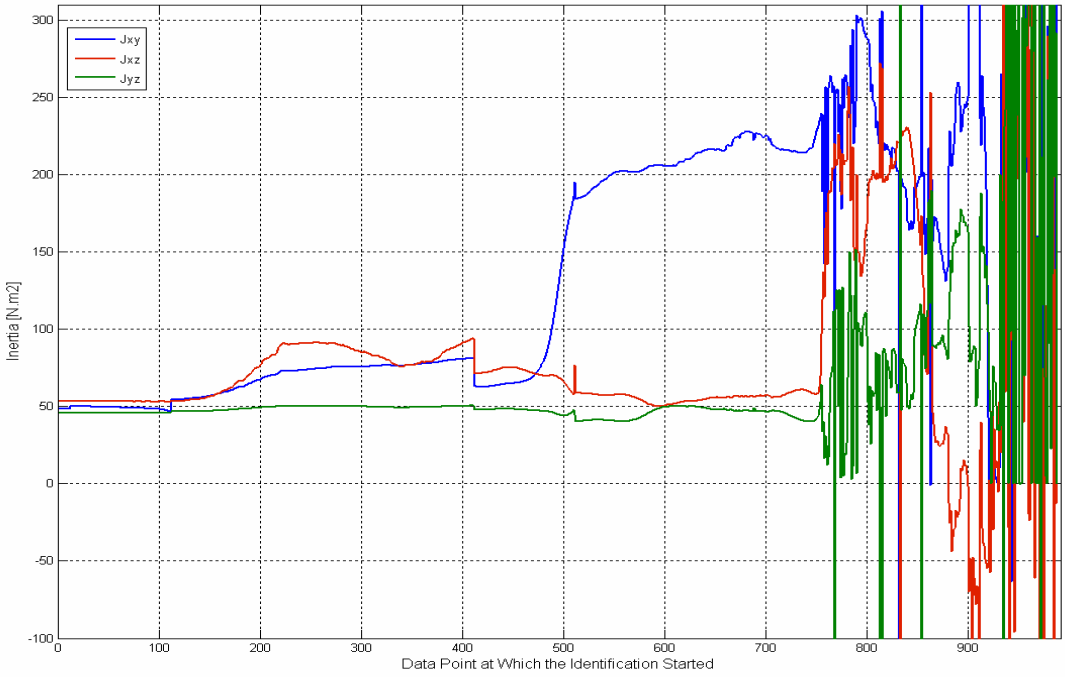

Figure 4.18 Solution History for Case 5 – Off-Diagonal Terms

4.6 Case Study 6

In this case; t=[75.1s,100s] was used for identification (2490 data points).

Thus, no external force was applied on the system in the data used for the identification run. The data set was the same as the data set used for the case study 1.

The expected results of the experiment were:

- The system will reach an equilibrium position where the external forces applied on the system are equal to cable forces and the weight

- After the system is released (t=75.1 s); the system will oscillate freely from this newly reached equilibrium position. Thus; the velocity terms of the initial conditions for the identification run would be zero.

Table 4.6 Data for Case Study 6

CASE 6		
Cable Lengths [m]	2.5	
Coordinates of CG (initially) [m]	[2; 2.5; -2.5616]	
Mass [kg]	250	
Jxx [N.m^2]	1000	
Jyy [N.m^2]	1000	
Jzz [N.m^2]	1000	
Jxy [N.m^2]	50	
Jxz [N.m^2]	50	
Jyz [N.m^2]	50	
Coordinates of Hinge Points on the Ceiling [m]		
[0;0;0]		
[4;0;0]		
[0;5;0]		
[4;5;0]		
Body Dimensions [m]		
3x2x1 (Rectangular Prism)		
Coordinates of Hinge Points on the Body (wrt to their respective hinge points on the ceiling)		
[1;1;-2.0616]		
[1;-1;-2.0616]		
[-1;1;-2.0616]		
[-1;-1;-2.0616]		
Initial Conditions		
No Initial Displacement		
Applied Forces		
Force Vector [N]	**Point of Action [m]**	**Time interval [s]**
[50;0;0]	[0;-1.5;0]	[0.1,75.1]
[0;50;0]	[0;-1.5;0]	[0.1,75.1]
Initial Guess Vector for Inertia Tensor [N.m2]		
[750;200;200;750;200;750]		
Length of the Experiment [s]	**Sampling [s]**	
100	0.01	

However it was observed that, as the force acts on the system, the system oscillates around an equilibrium position; and when the force is zero; the system oscillates around its initial equilibrium position (free equilibrium position), but this time makes larger oscillations.

It is concluded that; this result is obtained due to the fact that the experimental model had no damping. No identification run is made for case study 6.

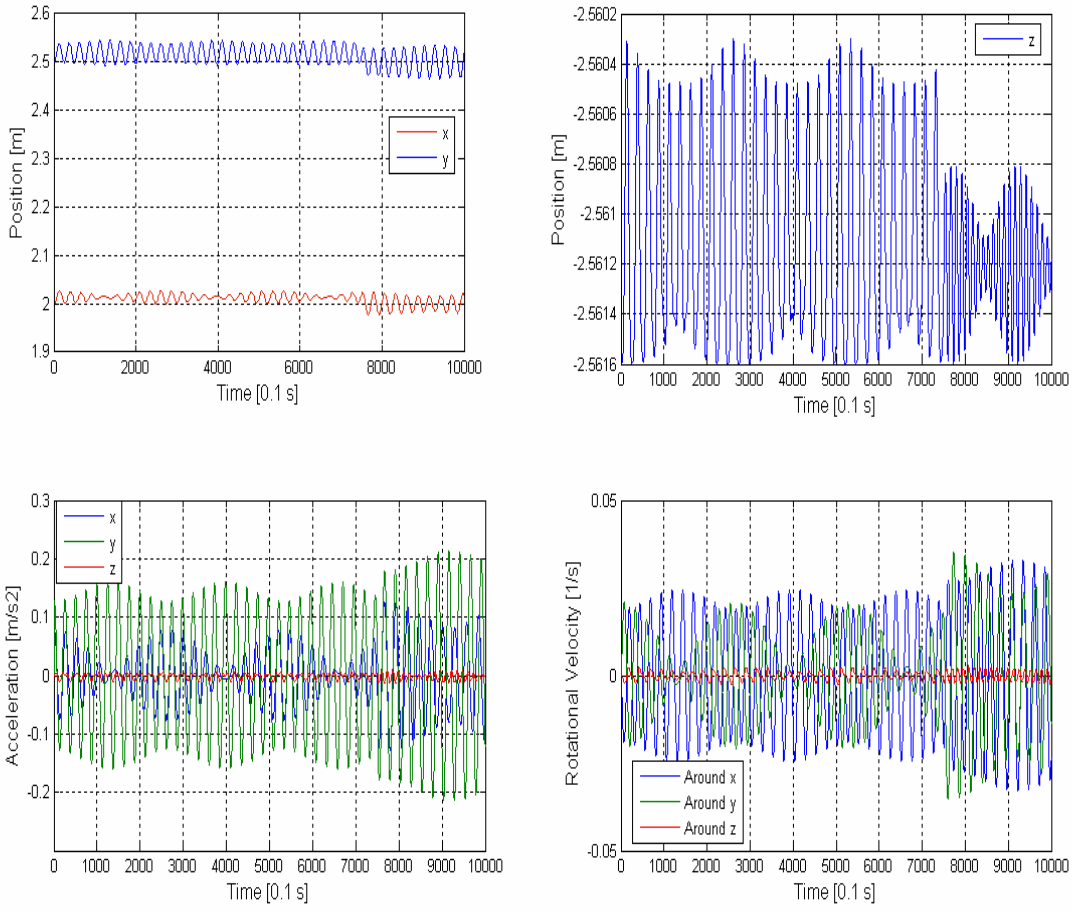

Figure 4.19 The Motion of the Body for Case 6

4.7 Case Study 7

Table 4.7 Data for Case Study 7

CASE 7		
Cable Lengths [m]	2.5	
Coordinates of CG (initially) [m]	[2; 2.5; -2.5616]	
Mass [kg]	250	
Jxx [N.m^2]	1000	
Jyy [N.m^2]	1000	
Jzz [N.m^2]	1000	
Jxy [N.m^2]	50	
Jxz [N.m^2]	50	
Jyz [N.m^2]	50	
Coordinates of Hinge Points on the Ceiling [m]		
[0;0;0]		
[4;0;0]		
[0;5;0]		
[4;5;0]		
Body Dimensions [m]		
3x2x1 (Rectangular Prism)		
Coordinates of Hinge Points on the Body (wrt to their respective hinge points on the ceiling)		
[1;1;-2.0616]		
[1;-1;-2.0616]		
[-1;1;-2.0616]		
[-1;-1;-2.0616]		
Initial Conditions		
No Initial Displacement		
Applied Forces		
Force Vector [N]	**Point of Action [m]**	**Time interval [s]**
[300;0;0]	[0;-1.5;0]	[0.1, 1]
[0;300;0]	[0;-1.5;0]	[0.1, 1]
[0;0;300]	[0;-1.5;0]	[0.1, 0.6]
Initial Guess Vector for Inertia Tensor [N.m2]		
[750;200;200;750;200;750]		
Length of the Experiment [s]	**Sampling [s]**	
10	0.01	

In this case study; a larger force with components in three directions is used to excite the system. The aim of the experiment is to obtain a greater deflection from the equilibrium position; in order to use as the initial condition for the case study 8.

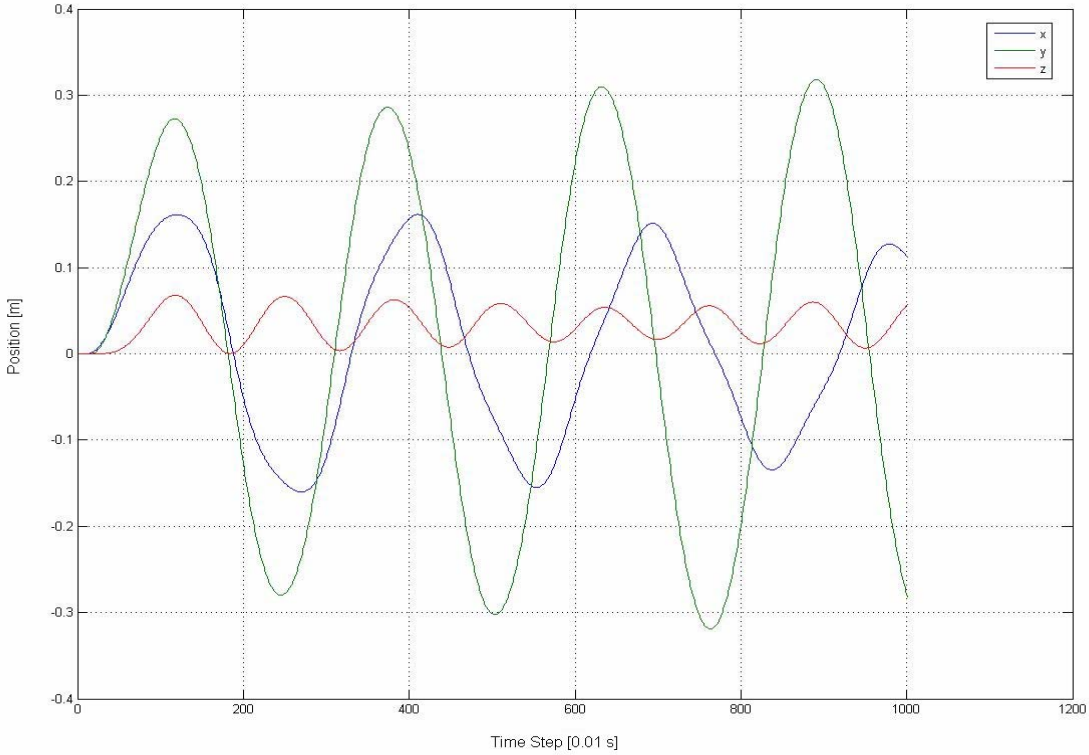

Figure 4.20 The Motion of the Body for Case 7
(with respect to body reference frame)

t=1.2 s is selected; where x=2.1614; y=2.772; z=-2.4937 and

$$T = \begin{bmatrix} 0.989 & -0.0752 & -0.1273 \\ 0.0627 & 0.993 & -0.0997 \\ 0.134 & 0.0906 & 0.9868 \end{bmatrix}$$

Then the Euler Angles are [-0.0759; 0.1276; -0.1007] radians.

4.8 Case Study 8

Table 4.8 Data for Case Study 8

CASE 8	
Cable Lengths [m]	2.5
Coordinates of CG (initially) [m]	[2.1614; 2.772; -2.4937]
Mass [kg]	250
Jxx [N.m^2]	1000
Jyy [N.m^2]	1000
Jzz [N.m^2]	1000
Jxy [N.m^2]	50
Jxz [N.m^2]	50
Jyz [N.m^2]	50
Coordinates of Hinge Points on the Ceiling [m]	
[0;0;0]	
[4;0;0]	
[0;5;0]	
[4;5;0]	
Body Dimensions [m]	
3x2x1 (Rectangular Prism)	
Coordinates of Hinge Points on the Body (wrt to their respective hinge points on the ceiling)	
[1;1;-2.0616]	
[1;-1;-2.0616]	
[-1;1;-2.0616]	
[-1;-1;-2.0616]	
Initial Conditions	
Initial Displacement	**Euler Angles [radians]**
See Coordinates of CG	[-0.0759; 0.1276; -0.1007]
Applied Forces	
No External Force on the System	
Initial Guess Vector for Inertia Tensor [N.m2]	
[750;200;200;750;200;750]	
Length of the Experiment [s]	**Sampling [s]**
10	0.01

4.8.1 The Results of the Experiment of Case Study 8

The resulting motion of the experiment can be observed in Figures 4.21, 4.22 and 4.23.

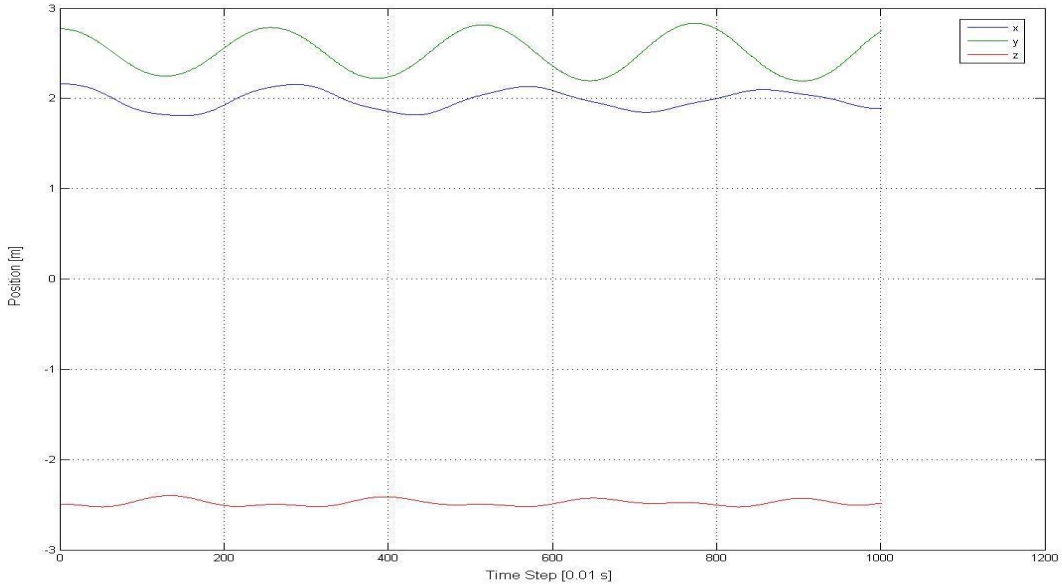

Figure 4.21 Position of CG

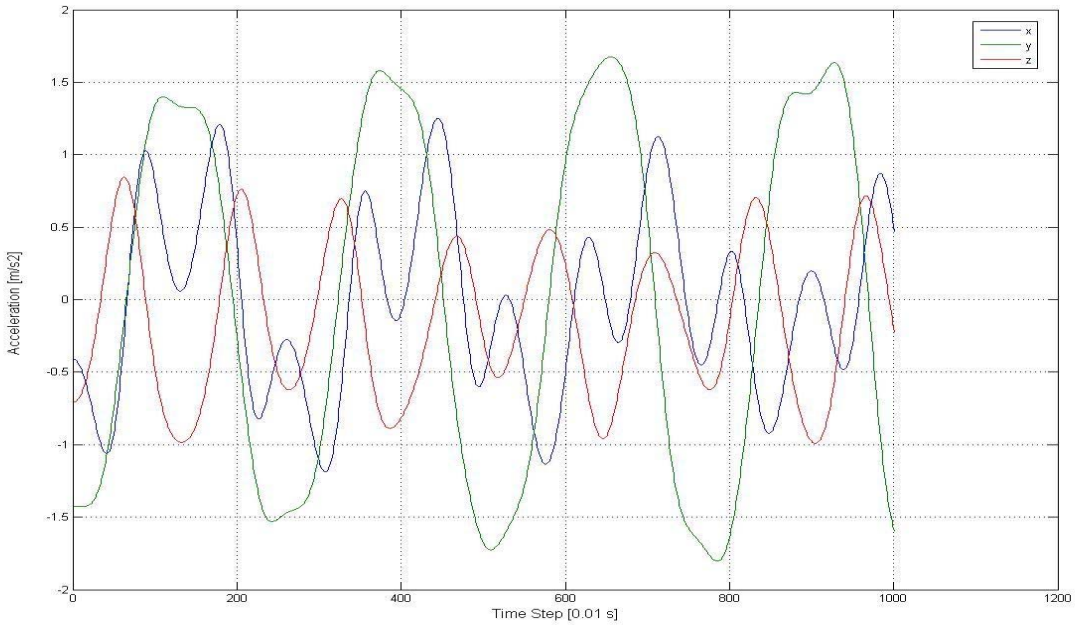

Figure 4.22 Acceleration of CG

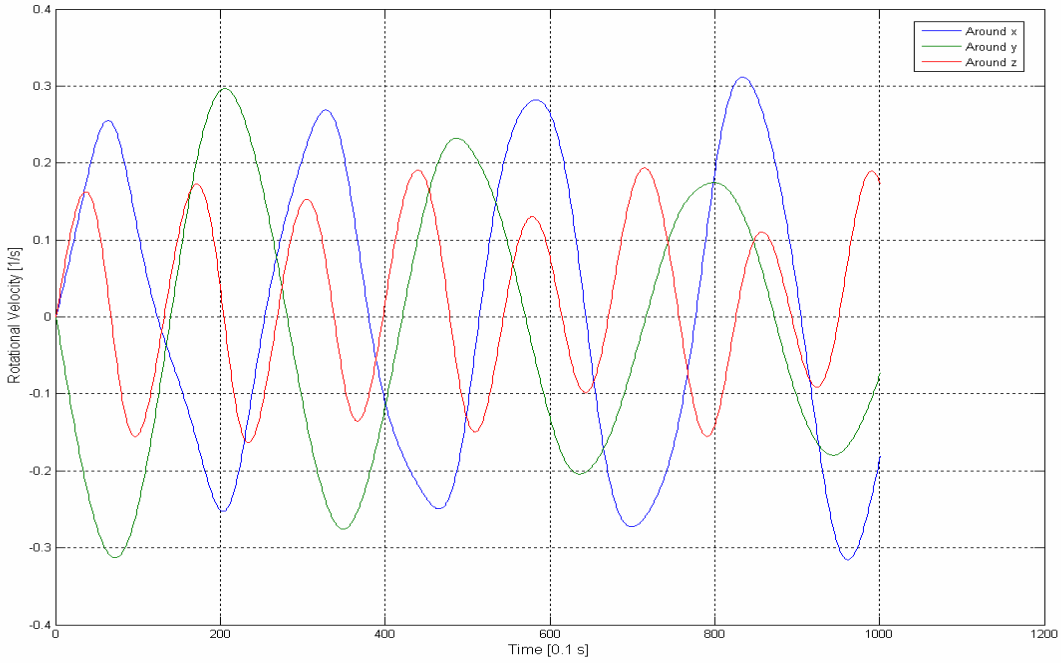

Figure 4.23 Rotational Velocity of the Body with respect to CG

4.8.2 The Results of the Identification Run for Case Study 8

Identification code calculated the following inertia tensor:

$$J = \begin{bmatrix} 1032.0 & 88.6 & -12 \\ 88.6 & 1037.6 & -35.9 \\ -12 & -35.9 & 1006.8 \end{bmatrix}$$

Whereas the original tensor was:

$$J = \begin{bmatrix} 1000 & 50 & 50 \\ 50 & 1000 & 50 \\ 50 & 50 & 1000 \end{bmatrix}$$

Percentage error is:

$$\%Error = \begin{bmatrix} 3.2 & 77.27 & 124.04 \\ 77.27 & 3.76 & 171.89 \\ 124.04 & 171.89 & 0.68 \end{bmatrix}$$

The accuracy of diagonal elements are satisfactory for the vehicle dynamics studies. However error of the off diagonal terms are extremely high. This method can not be used, sşnce there are relatively easier methods to obtain the diagonal elements of the inertia tensor.

Figure 4.24 shows the comparison of the identified system and the measured system's output measurements.

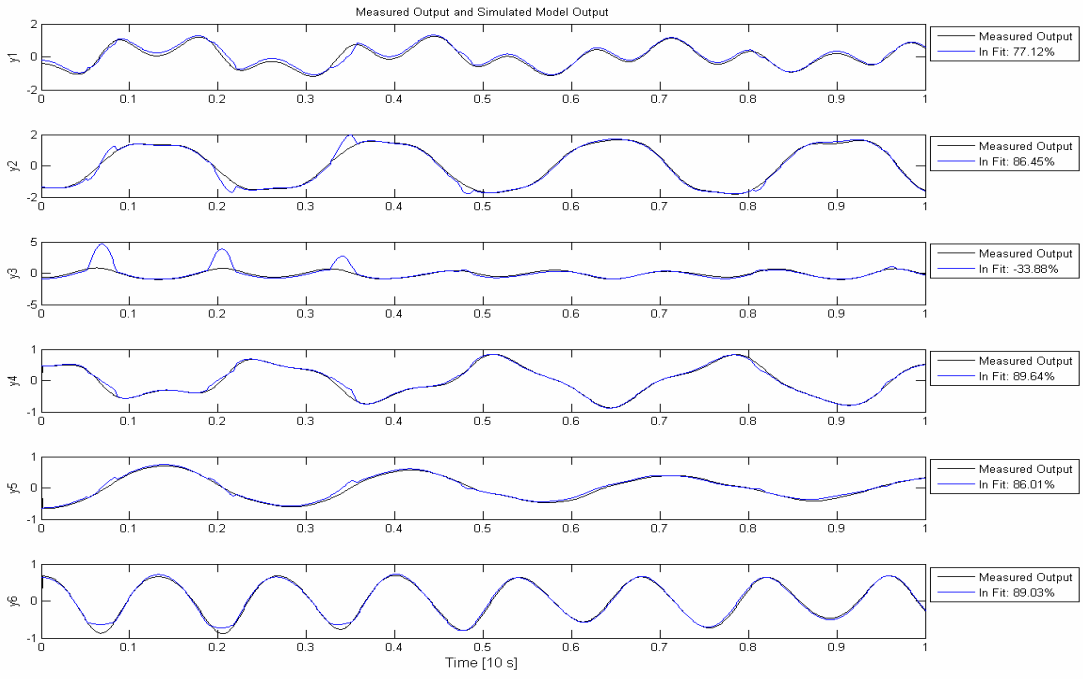

Figure 4.24 Comparison of the Identified System and the Measured System

4.9 Case Study 9

Table 4.9 Data for Case Study 9

CASE 9		
Cable Lengths [m]	2.5	
Coordinates of CG (initially) [m]	[2; 2.5; -2.5616]	
Mass [kg]	250	
Jxx [N.m^2]	1000	
Jyy [N.m^2]	1000	
Jzz [N.m^2]	1000	
Jxy [N.m^2]	50	
Jxz [N.m^2]	50	
Jyz [N.m^2]	50	
Coordinates of Hinge Points on the Ceiling [m]		
[0;0;0]		
[4;0;0]		
[0;5;0]		
[4;5;0]		
Body Dimensions [m]		
3x2x1 (Rectangular Prism)		
Coordinates of Hinge Points on the Body (wrt to their respective hinge points on the ceiling)		
[1;1;-2.0616]		
[1;-1;-2.0616]		
[-1;1;-2.0616]		
[-1;-1;-2.0616]		
Initial Conditions		
No Initial Displacement		
Applied Forces		
Force Magnitude [N]	**Point of Action [m]**	**Time interval [s]**
200	[0;-1.5;0]	[0.1,1.1]
Frequency of Forcing [Hz]		
0.7		
Initial Guess Vector for Inertia Tensor [N.m2]		
[750;200;200;750;200;750]		
Length of the Experiment [s]	**Sampling [s]**	
100	0.01	

4.9.1 The Results of the Experiment of Case Study 9

The resulting motion of the experiment can be observed in Figures 4.25, 4.26 and 4.27.

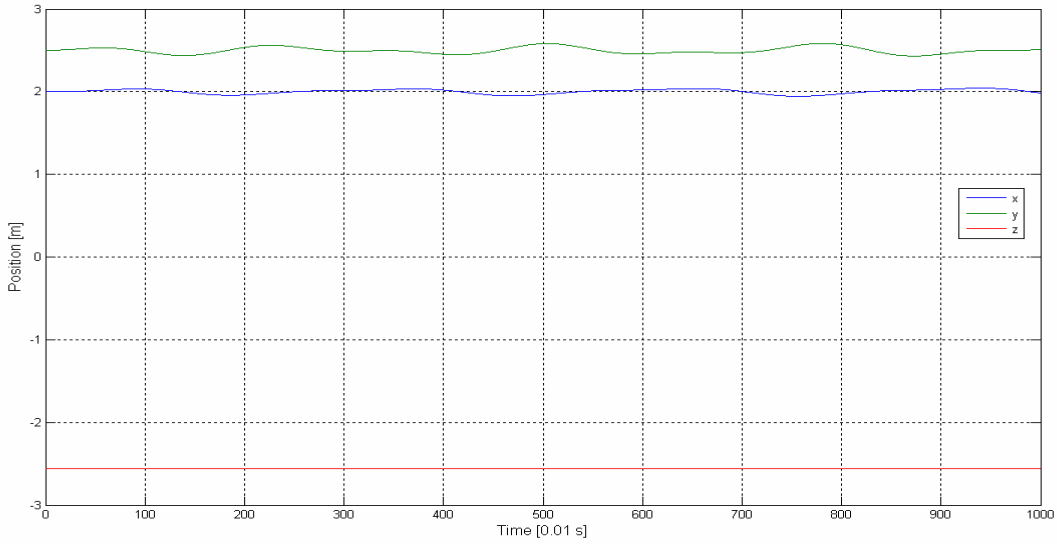

Figure 4.25 Position of CG

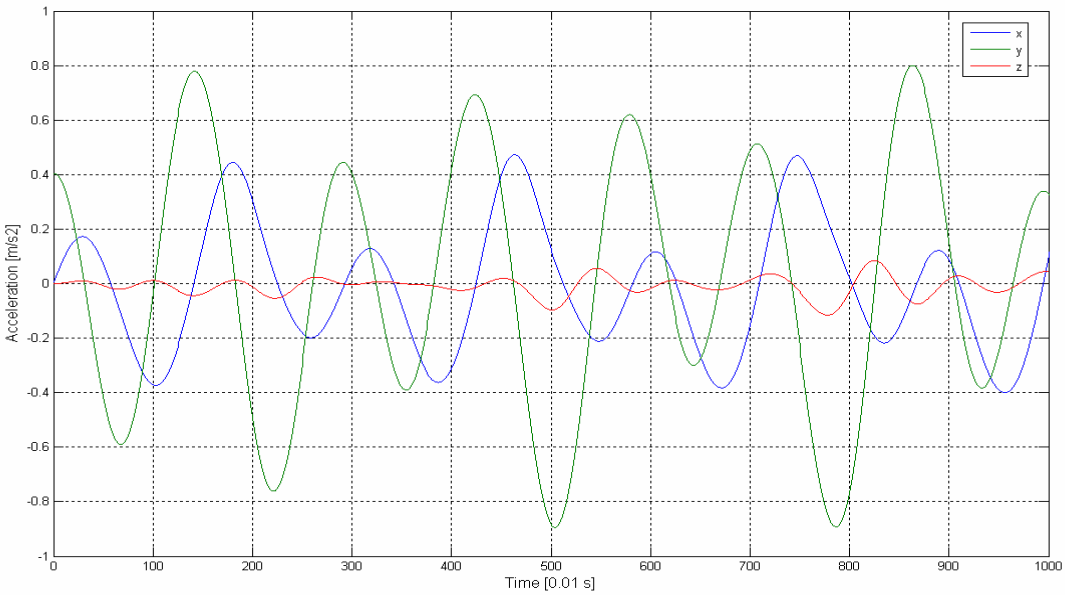

Figure 4.26 Acceleration of CG

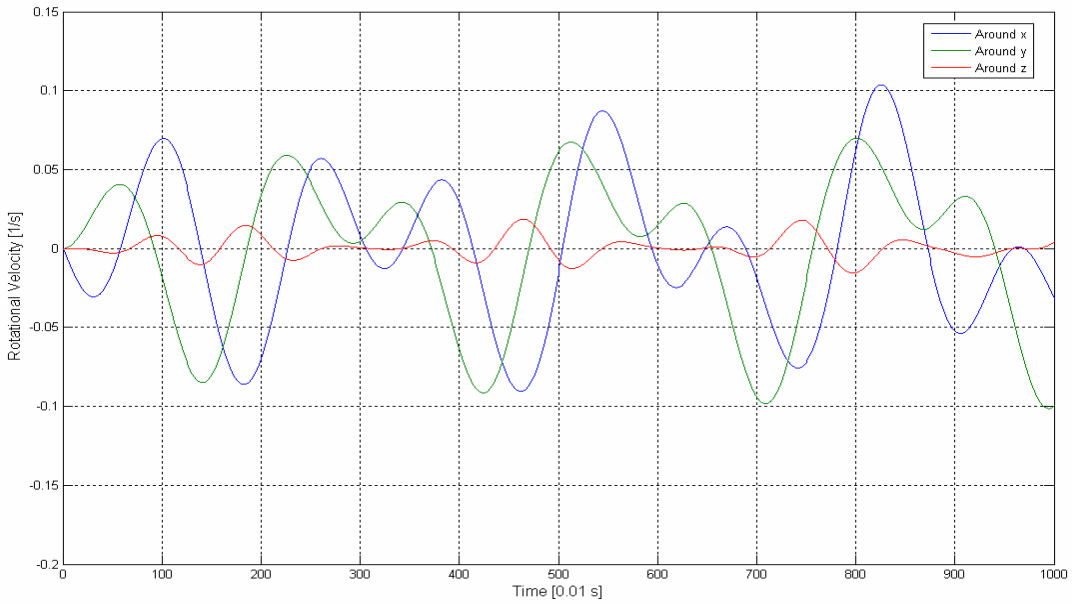

Figure 4.27 Rotational Velocity of the Body with respect to CG

4.9.2 The Results of the Identification Run for Case Study 9

Identification code calculated the following inertia tensor:

$$J = \begin{bmatrix} 999.2 & 45.4 & 50.7 \\ 45.4 & 1004 & 48.4 \\ 50.7 & 48.4 & 1002 \end{bmatrix}$$

Whereas the original tensor was:

$$J = \begin{bmatrix} 1000 & 50 & 50 \\ 50 & 1000 & 50 \\ 50 & 50 & 1000 \end{bmatrix}$$

Percentage error is:

$$\%Error = \begin{bmatrix} 0.08 & 9.2 & 1.4 \\ 9.2 & 0.4 & 3.2 \\ 1.4 & 3.2 & 0.2 \end{bmatrix}$$

Results of this case are found to be highly satisfactory. Error of the diagonal elements are less than 0.5 percent and the largest error of the off diagonal terms is less than 10 percent for a terms, which is usually negligibly small for real world cases.

Figure 4.28 shows the comparison of the identified system and the measured system's output measurements.

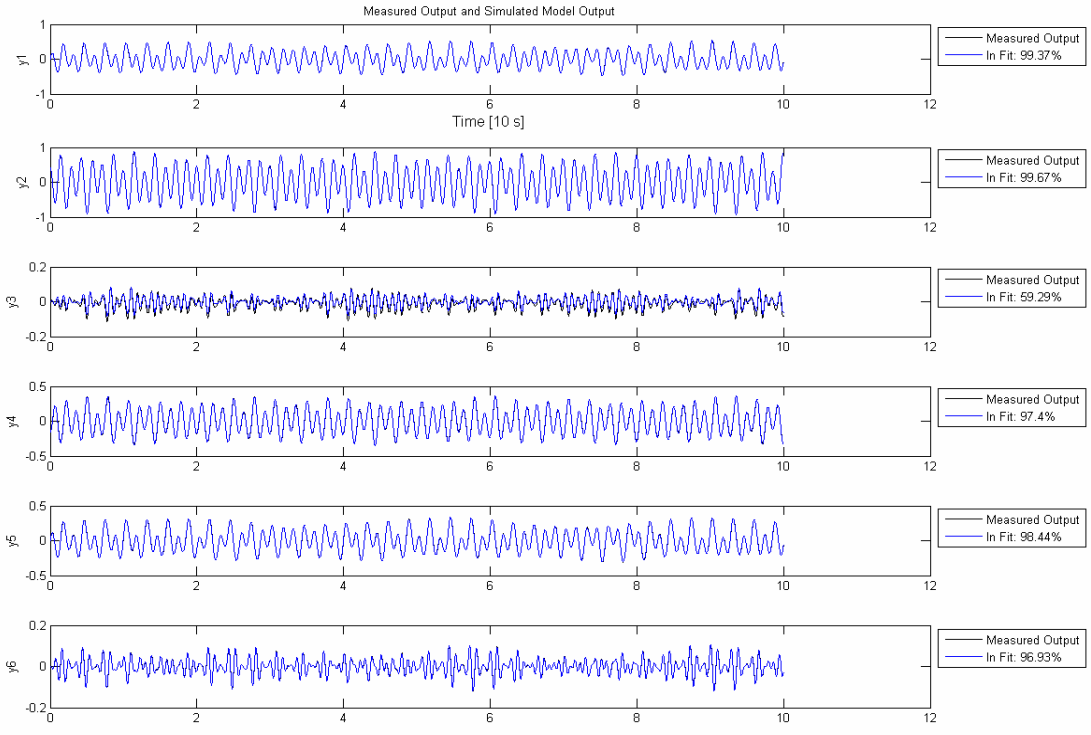

Figure 4.28 Comparison of the Identified System and the Measured System

4.10 Case Study 10

In this case the mass properties of 1998 Chevrolet Acura with one occupant and full fuel tank are used [32].

Table 4.10 Data for Case Study 10

CASE 10	
Coordinates of CG (initially) [m]	[1.97; 2.75; -2.874]
Mass [kg]	1975
Jxx [N.m^2]	3741
Jyy [N.m^2]	963
Jzz [N.m^2]	3973
Jxy [N.m^2]	0
Jxz [N.m^2]	0
Jyz [N.m^2]	168
Coordinates of Hinge Points on the Ceiling [m]	
[0;0;0]	
[4;0;0]	
[0;7.75;0]	
[4;7.75;0]	
Body Dimensions [m]	
2x5x2 (Rectangular Prism)	
Coordinates of Hinge Points on the Body (wrt to CG)	
[-0.985;-1.375;1.437]	
[1.015;-1.375;1.437]	
[-0.985;3.625;1.437]	
[1.015;3.625;1.437]	
Initial Conditions	
No Initial Displacement	
Applied Forces	
Force Magnitude [N]	**Point of Action (wrt CG) [m]**
200	[-0.985;-1.375;-0.563]
Frequency of Forcing [Hz]	
2.1	
Initial Guess Vector for Inertia Tensor [N.m2]	
[3000; 50; 50; 1250; 500; 3000]	
Length of the Experiment [s]	**Sampling [s]**
250	0.01

4.10.1 The Results of the Experiment of Case Study 10

The resulting motion of the experiment can be observed in Figures 4.29, 4.30, 4.31, 4.32, 4.33, 4.34, 4.35 and 4.36.

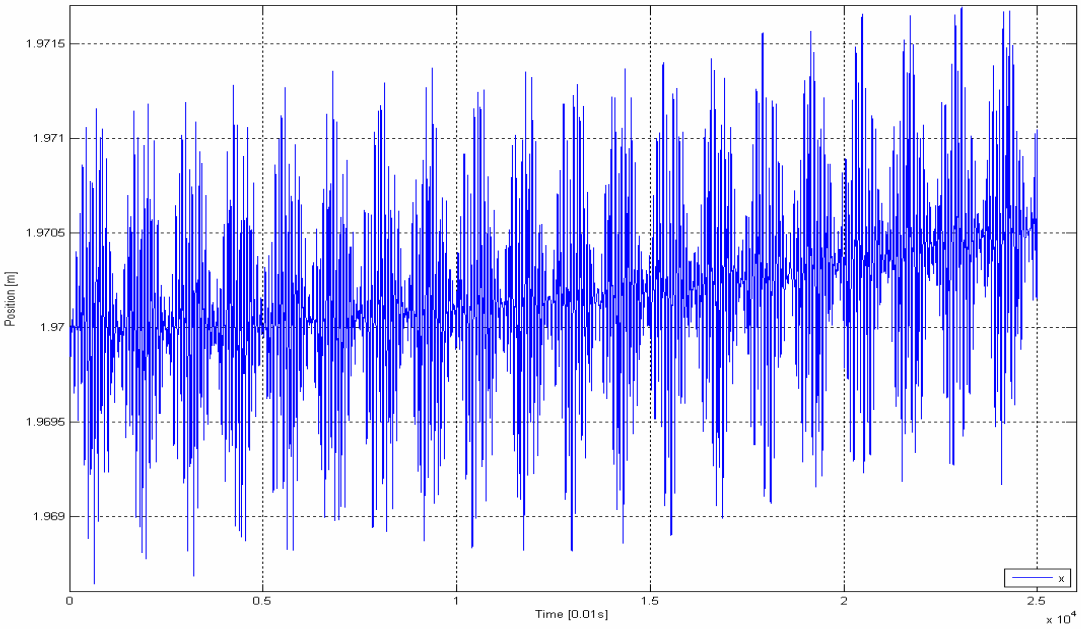

Figure 4.29 Position of x coordinate of CG

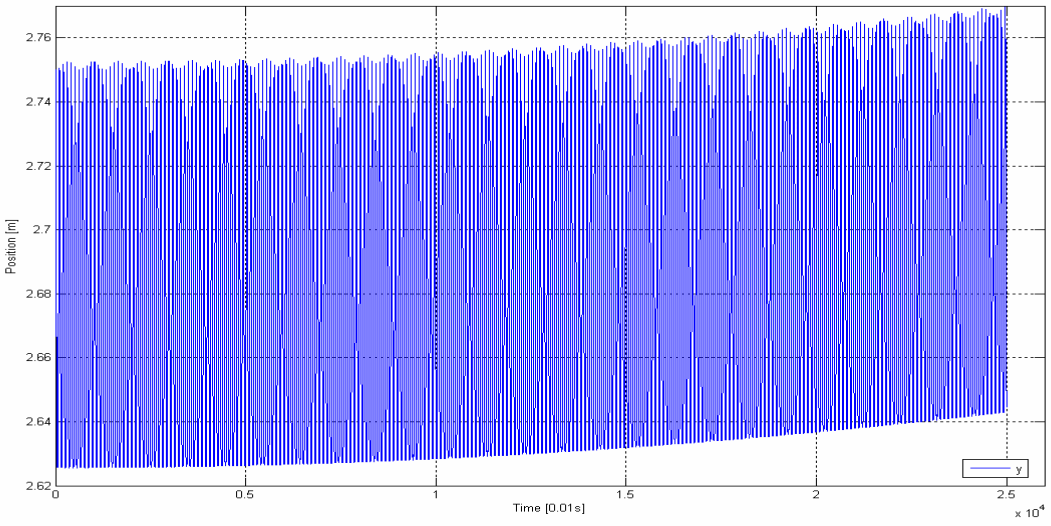

Figure 4.30 Position of y coordinate of CG

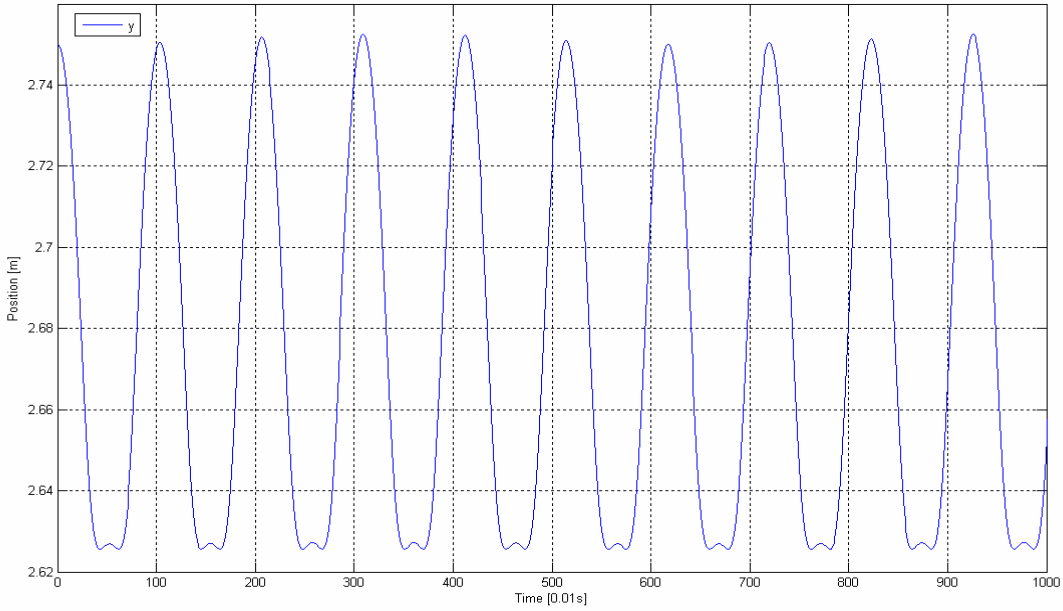

Figure 4.31 Figure 4.30 between [0,10]s

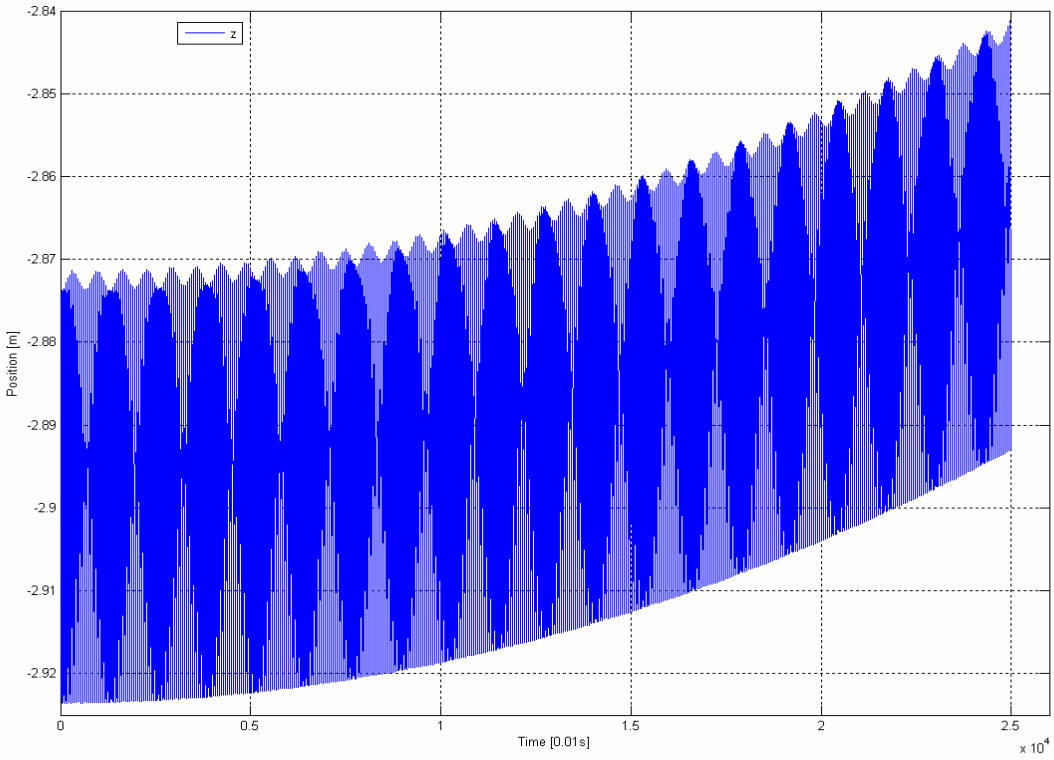

Figure 4.32 Position of z coordinate of CG

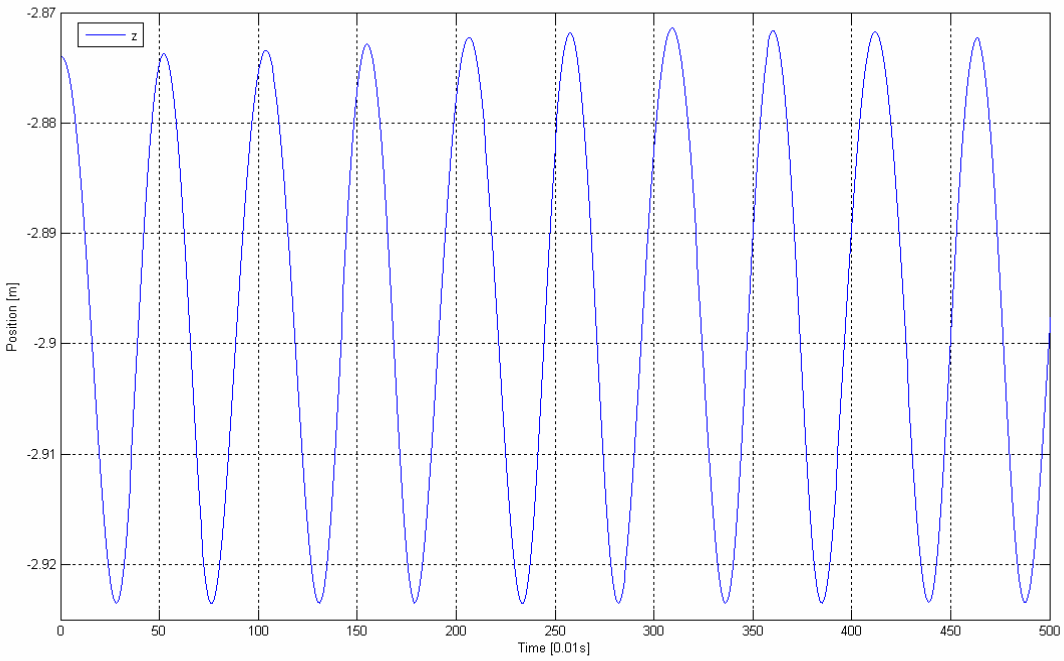

Figure 4.33 Figure 4.32 between [0,5]s

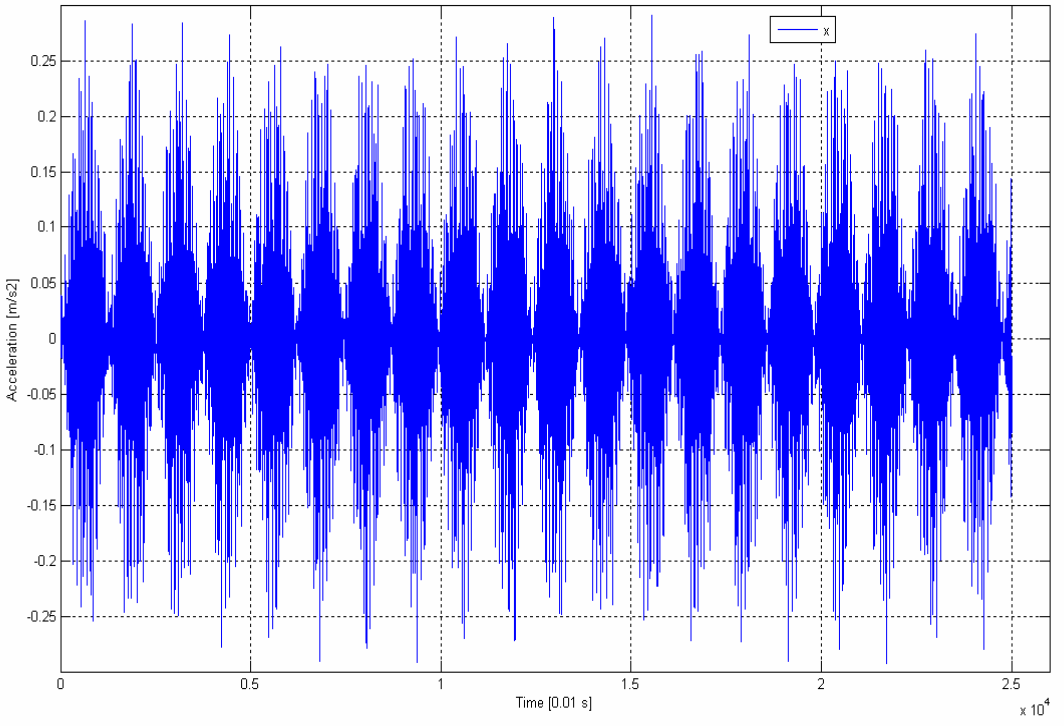

Figure 4.34 Acceleration of CG in x direction

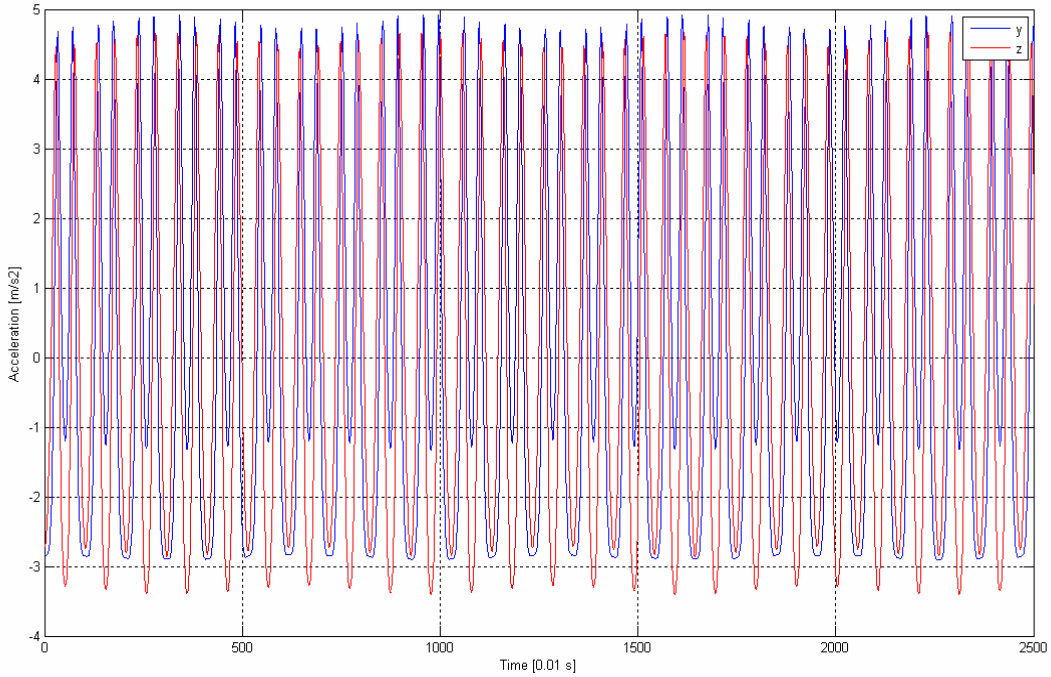

Figure 4.35 Acceleration of CG in y and z directions

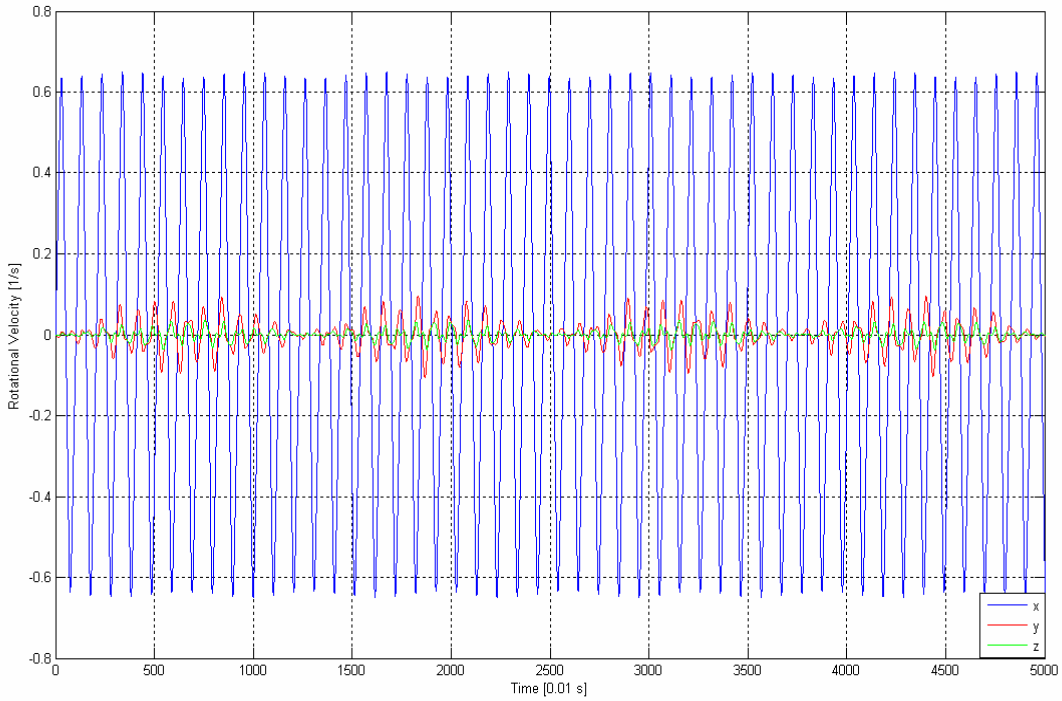

Figure 4.36 Rotational Velocity of the Body with respect to CG

4.10.2 The Results of the Identification Run for Case Study 10

Identification code calculated the following inertia tensor:

$$J = \begin{bmatrix} 3768.1 & -2 & 2 \\ -2 & 969.1 & 162.4 \\ 2 & 162.4 & 3837.2 \end{bmatrix}$$

Whereas the original tensor was:

$$J = \begin{bmatrix} 3741 & 0 & 0 \\ 0 & 963 & 168 \\ 0 & 168 & 3973 \end{bmatrix}$$

Percentage error is:

$$\%Error = \begin{bmatrix} 0.72 & \pm 2 & \pm 2 \\ \pm 2 & 0.63 & 3.32 \\ \pm 2 & 3.32 & 3.42 \end{bmatrix}$$

The vehicle used for this run is a sports utility vehicle (SUV). Results of this case are found to be highly satisfactory. The largest error of the diagonal elements is less than 3.5 percent and is acceptable for vehicle dynamics studies. Error of the off diagonal elements is well above required accuracy.

Figure 4.37 shows the comparison of the identified system and the measured system's output measurements.

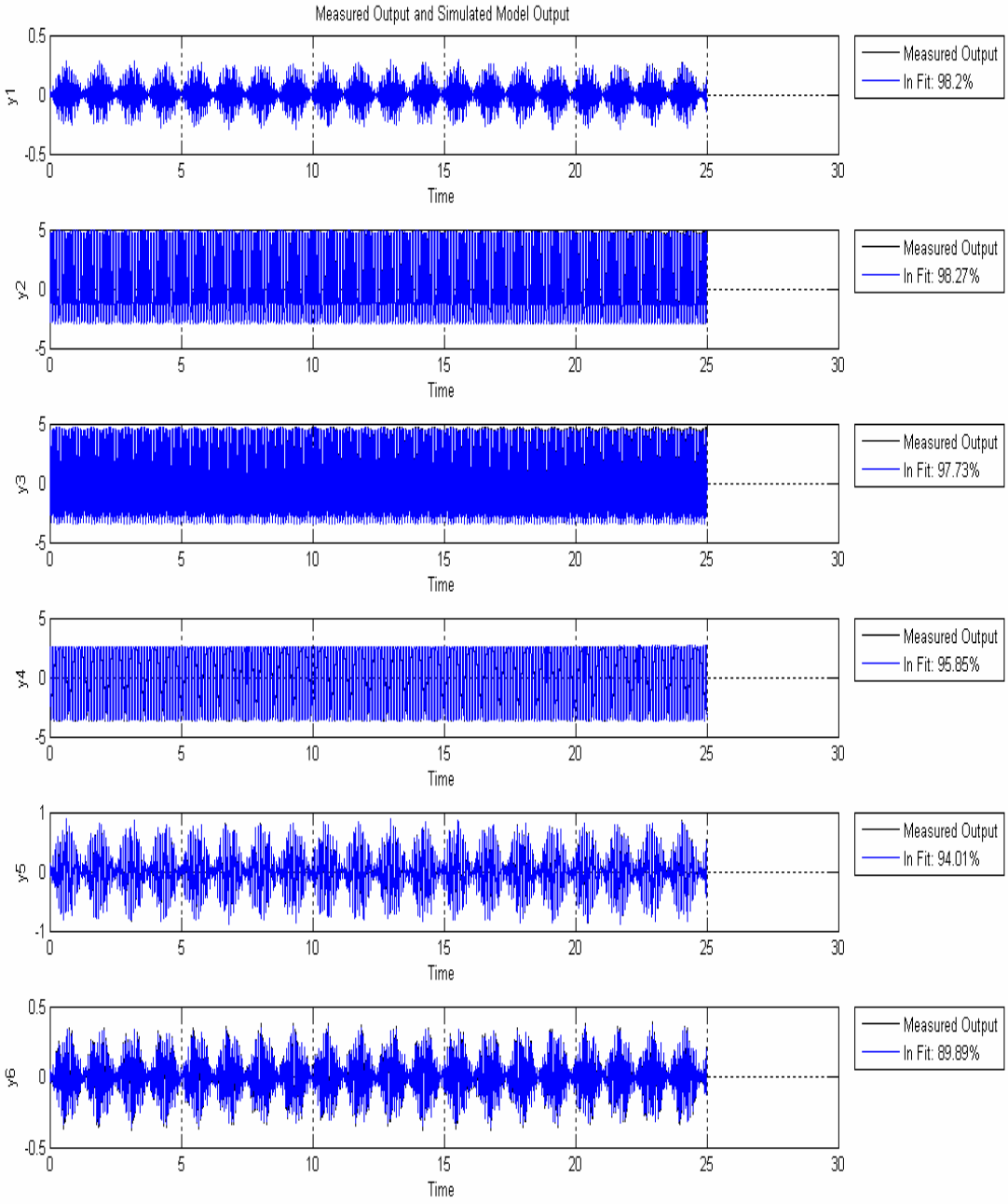

Figure 4.37 Comparison of the Identified System and the Measured System

4.11 Case Study 11

In this case the mass properties of 1998 Chevrolet Acura with one occupant and full fuel tank are used [32].

Table 4.11 Data for Case Study 11

CASE 11	
Coordinates of CG (initially) [m]	[1.97; 2.75; -2.874]
Mass [kg]	1975
Jxx [N.m^2]	3741
Jyy [N.m^2]	963
Jzz [N.m^2]	3973
Jxy [N.m^2]	0
Jxz [N.m^2]	0
Jyz [N.m^2]	168
Coordinates of Hinge Points on the Ceiling [m]	
[0;0;0]	
[4;0;0]	
[0;7.75;0]	
[4;7.75;0]	
Body Dimensions [m]	
2x5x2 (Rectangular Prism)	
Coordinates of Hinge Points on the Body (wrt to CG)	
[-0.985;-1.375;1.437]	
[1.015;-1.375;1.437]	
[-0.985;3.625;1.437]	
[1.015;3.625;1.437]	
Initial Conditions	
No Initial Displacement	
Applied Forces	
Force Magnitude [N]	**Point of Action (wrt CG) [m]**
400	[-0.985;-1.375;-0.563]
Frequency of Forcing [Hz]	
2.1	
Initial Guess Vector for Inertia Tensor [N.m2]	
[3000; 50; 50; 1250; 500; 3000]	
Length of the Experiment [s]	**Sampling [s]**
250	0.01

4.11.1 The Results of the Experiment of Case Study 11

The resulting motion of the experiment can be observed in Figures 4.38, 4.39, 4.40, 4.41, 4.42, 4.43, 4.44, 4.45 and 4.46.

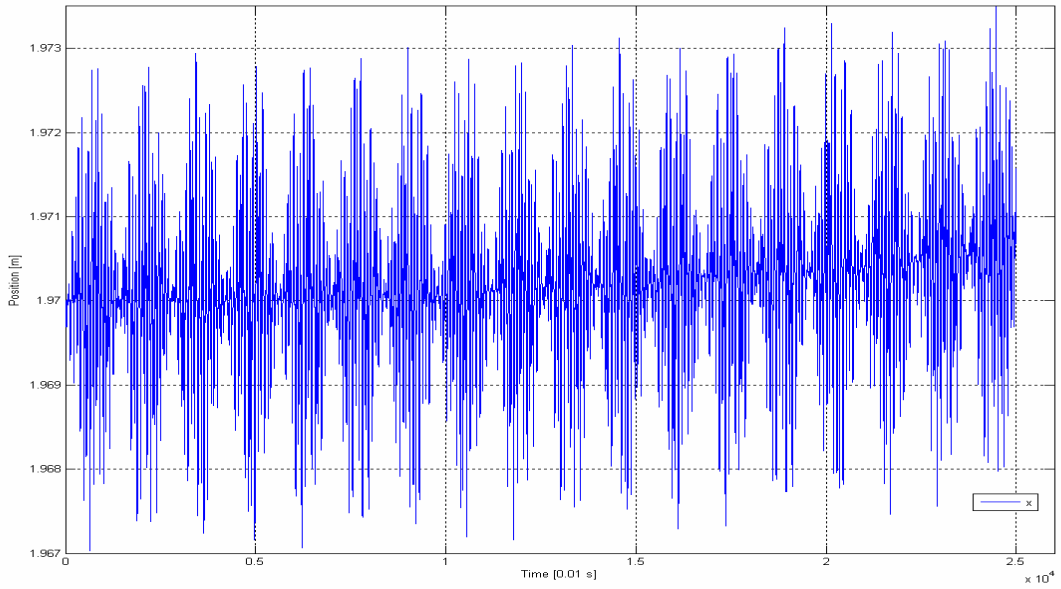

Figure 4.38 Position of x coordinate of CG

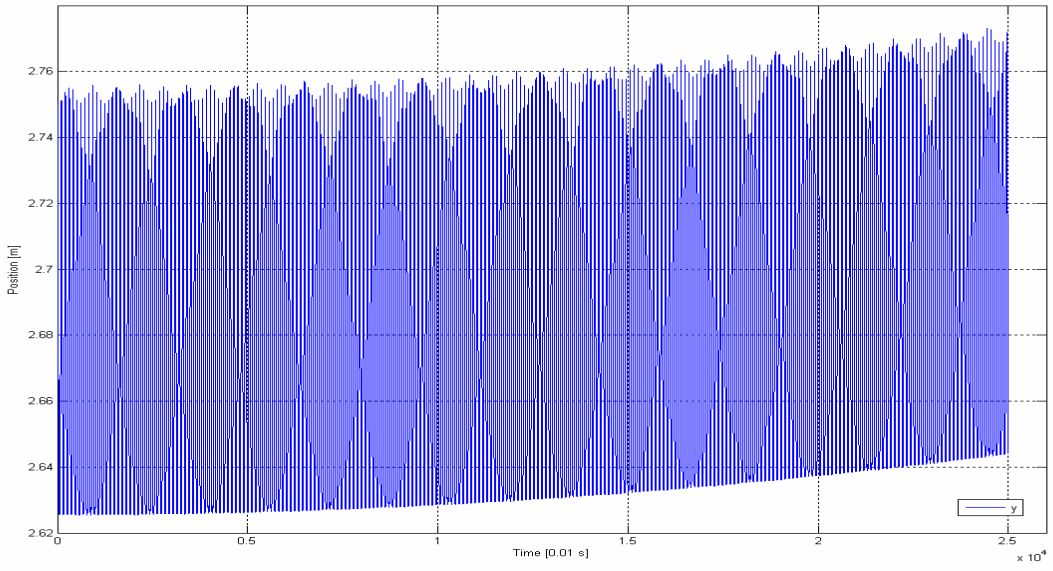

Figure 4.39 Position of y coordinate of CG

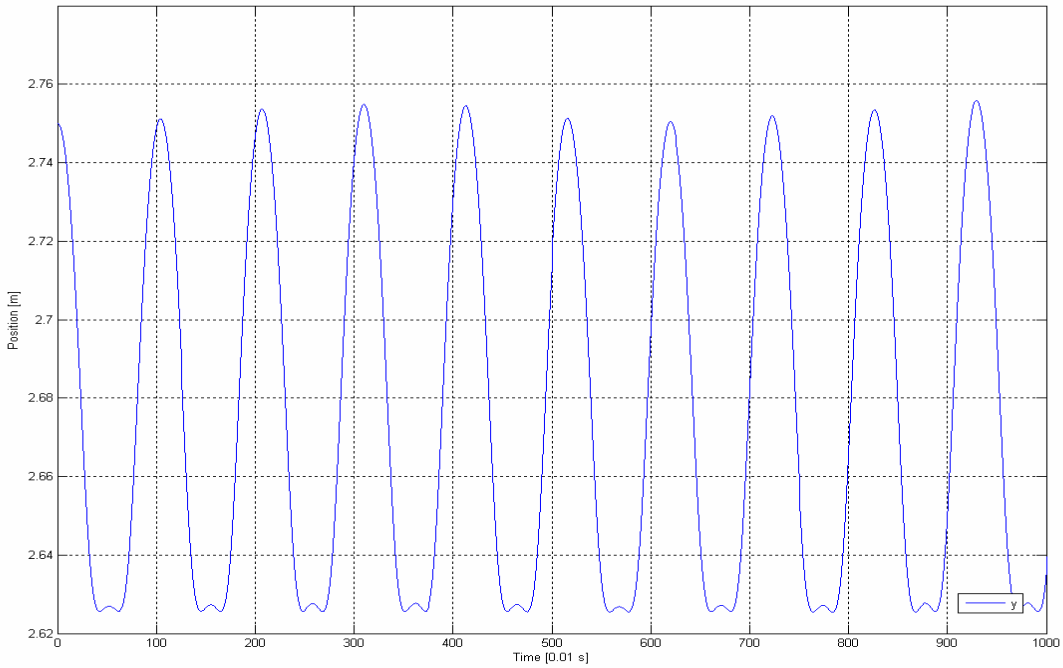

Figure 4.40 Figure 4.39 between [0,10]s

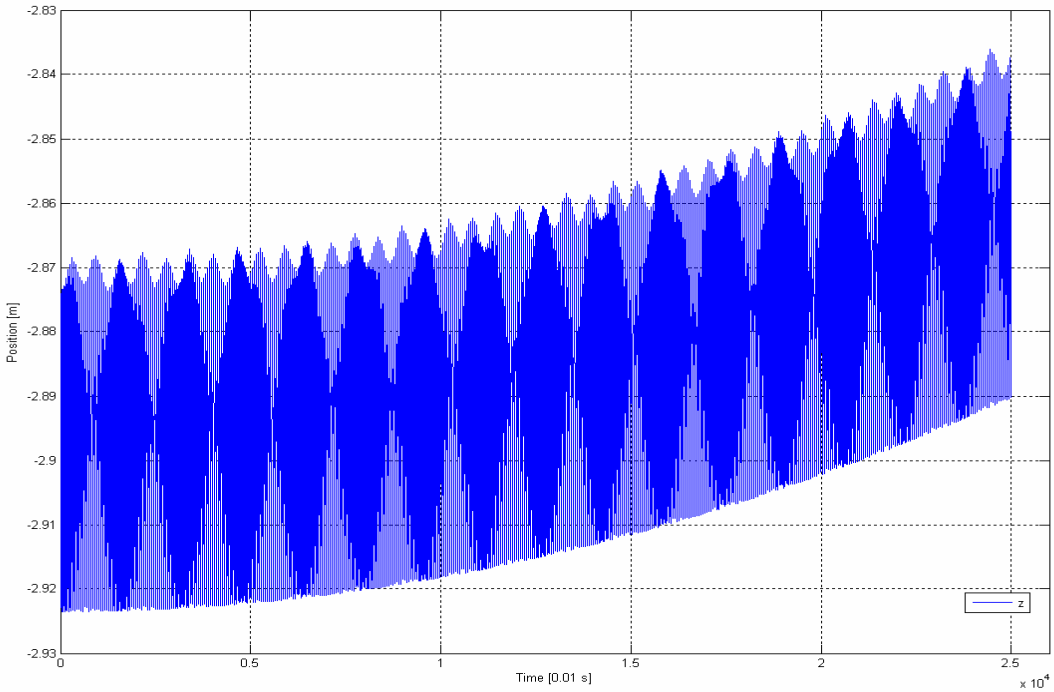

Figure 4.41 Position of z coordinate of CG

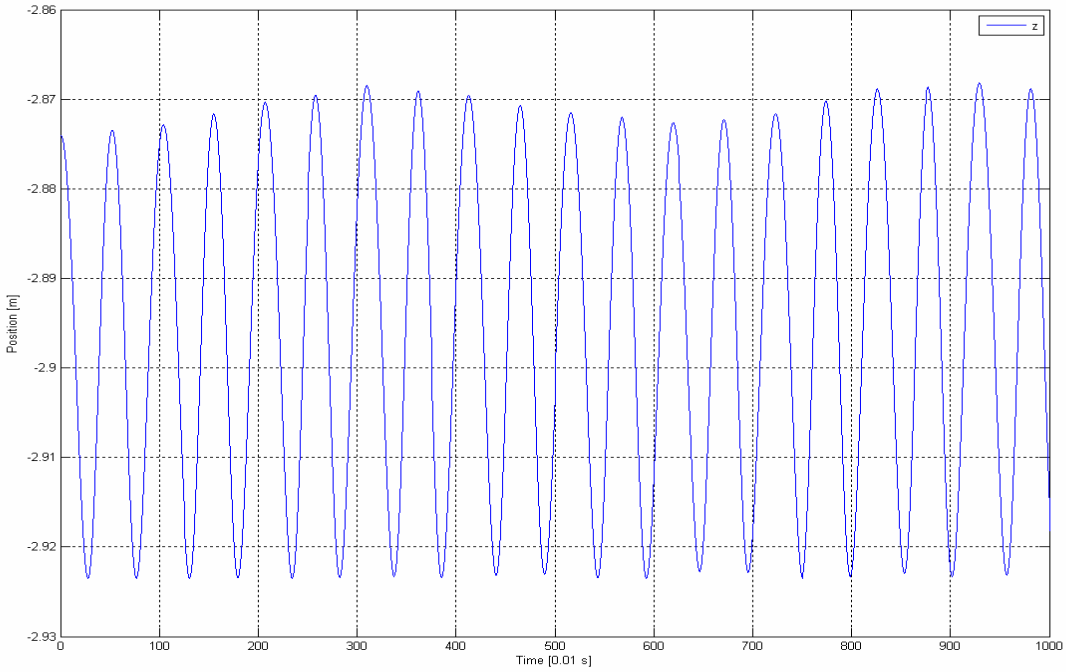

Figure 4.42 Figure 4.41 between [0,10]s

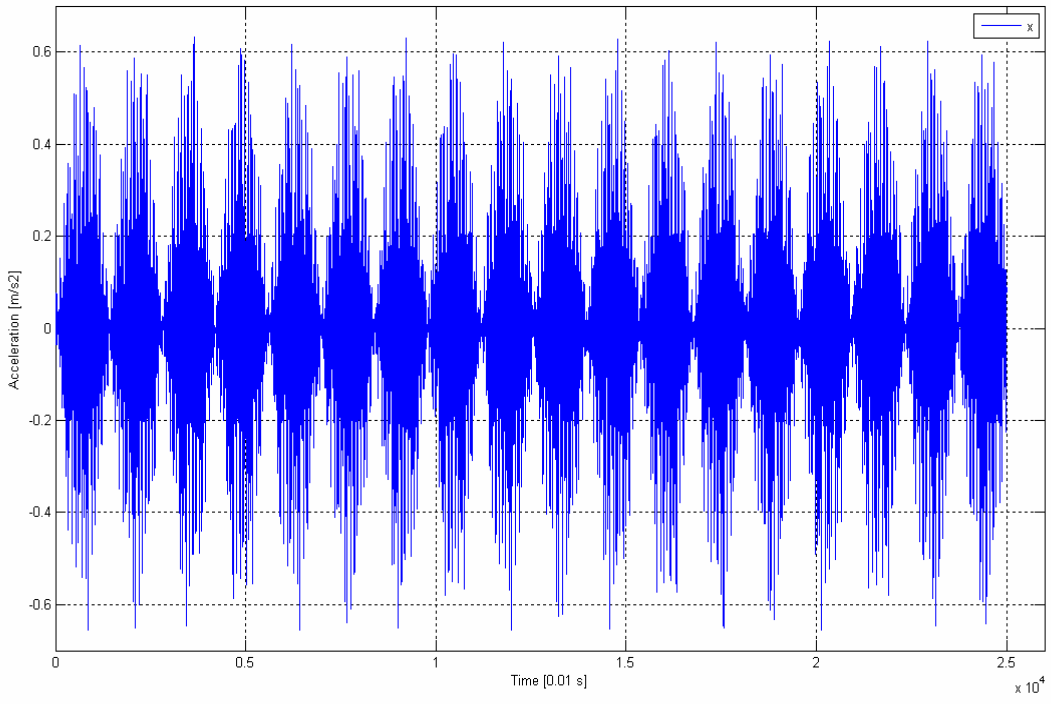

Figure 4.43 Acceleration of CG in x direction

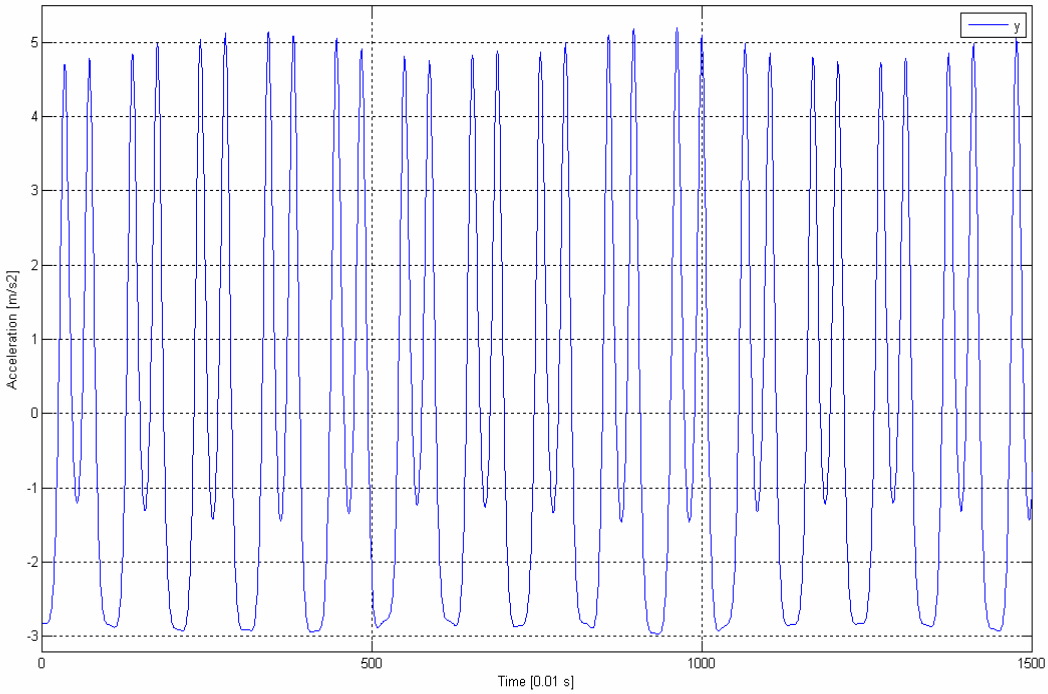

Figure 4.44 Acceleration of CG in y direction between [0,15]s

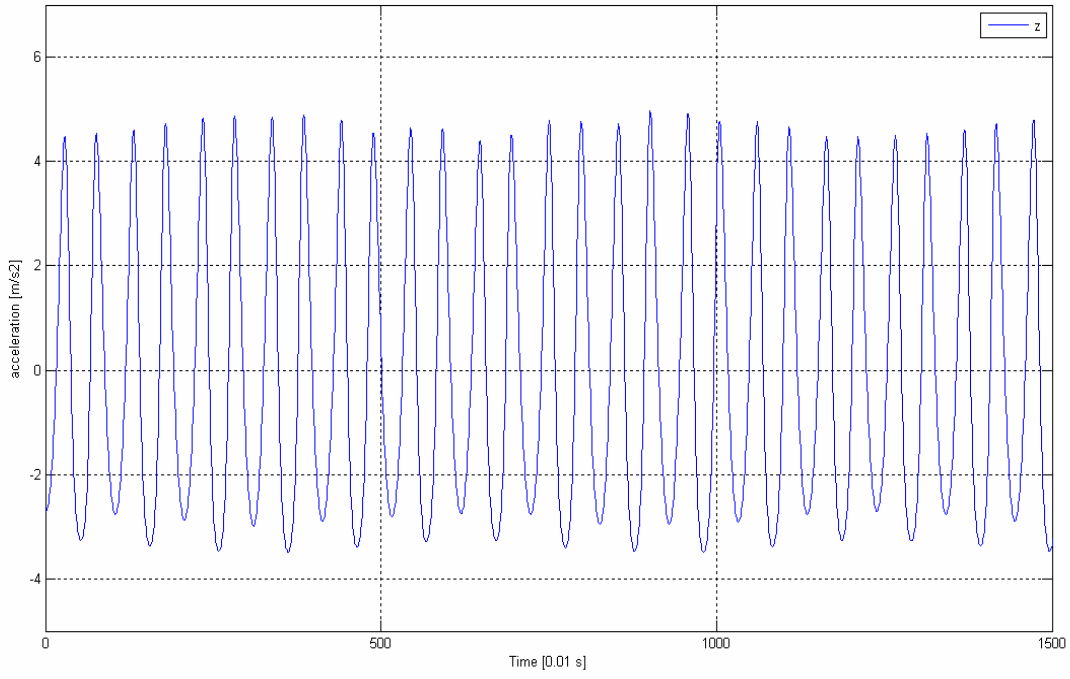

Figure 4.45 Acceleration of CG in z direction between [0,15]s

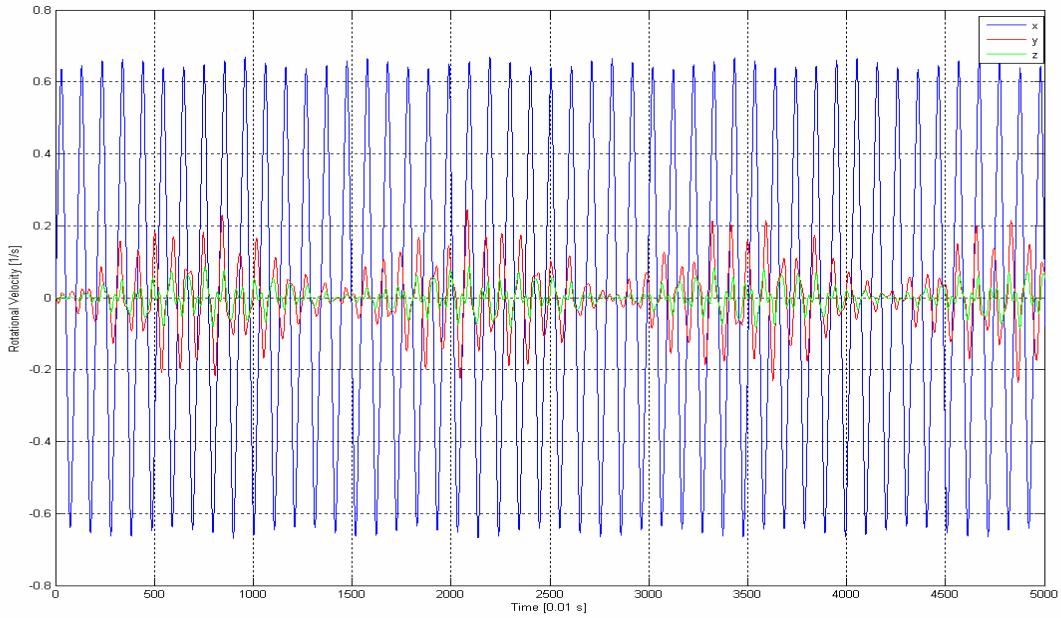

Figure 4.46 Rotational Velocity of the Body with respect to CG between [0,50]s

4.11.2 The Results of the Identification Run for Case Study 11

Identification code calculated the following inertia tensor:

$$J = \begin{bmatrix} 3772.7 & -3 & 13 \\ -3 & 969.3 & 165.8 \\ 13 & 165.8 & 3831.4 \end{bmatrix}$$

Whereas the original tensor was:

$$J = \begin{bmatrix} 3741 & 0 & 0 \\ 0 & 963 & 168 \\ 0 & 168 & 3973 \end{bmatrix}$$

Percentage error is:

$$\%Error = \begin{bmatrix} 0.85 & \pm 3 & \pm 13 \\ \pm 3 & 0.65 & 1.3 \\ \pm 13 & 1.3 & 3.56 \end{bmatrix}$$

Accuray of this case is in acceptable range. The largest error of the diagonal elements is less than 4 percent and is acceptable for vehicle dynamics studies. Error of the off diagonal elements is less tha 1.5 percent.

Figure 4.47 shows the comparison of the identified system and the measured system's output measurements.

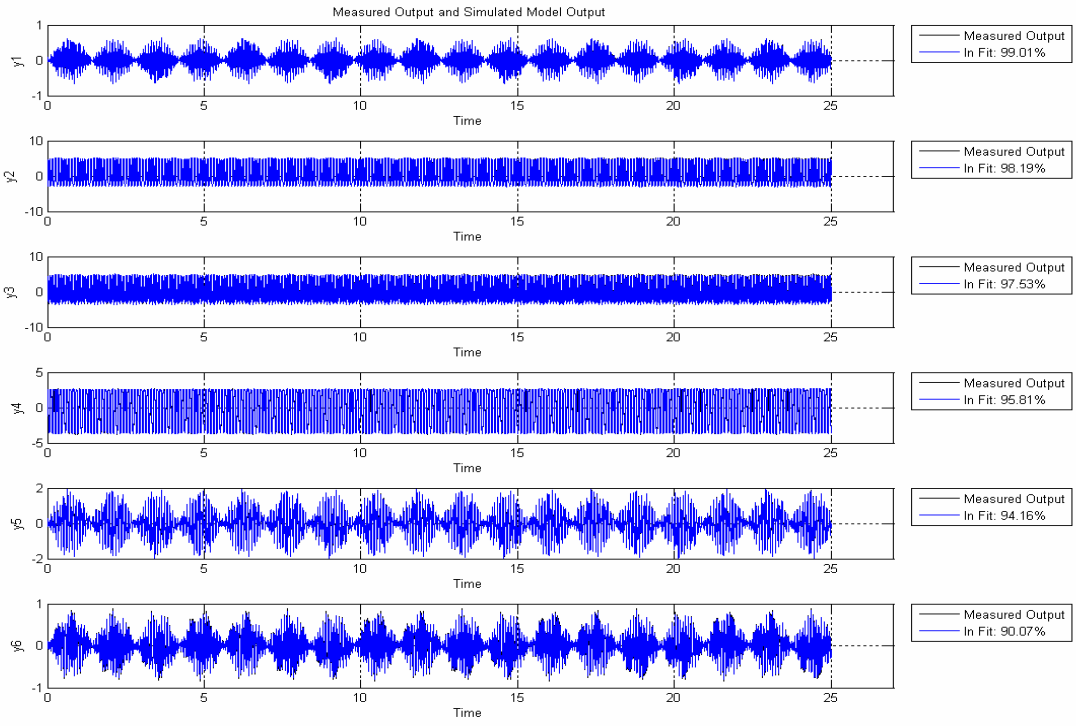

Figure 4.47 Comparison of the Identified System and the Measured System

4.12 Case Study 12

In this case the mass properties of 1998 Chevrolet Metro (Suzuki Swift) with one occupant and full fuel tank are used [32].

Table 4.12 Data for Case Study 12

CASE 12	
Coordinates of CG (initially) [m]	[1.4; 2.065; -2.252]
Mass [kg]	880
Jxx [N.m^2]	987
Jyy [N.m^2]	274
Jzz [N.m^2]	1102
Jxy [N.m^2]	0
Jxz [N.m^2]	0
Jyz [N.m^2]	32
Coordinates of Hinge Points on the Ceiling [m]	
[0;0;0]	
[3.5;0;0]	
[0;5;0]	
[3.5;5;0]	
Body Dimensions [m]	
1.5x2.5x1.5 (Rectangular Prism)	
Coordinates of Hinge Points on the Body (wrt to CG)	
[-0.7;-1.0325;1.126]	
[0.8;-1.0325;1.126]	
[-0.7;1..4675;1.126]	
[0.8;1.4675;1.126]	
Initial Conditions	
No Initial Displacement	
Applied Forces	
Force Magnitude [N]	**Point of Action (wrt CG) [m]**
200	[-0.7;-1.0325;-0.374]
Frequency of Forcing [Hz]	
2.1	
Initial Guess Vector for Inertia Tensor [N.m2]	
[700; 10; 10; 350; 50; 1000]	
Length of the Experiment [s]	**Sampling [s]**
250	0.01

4.12.1 The Results of the Experiment of Case Study 12

The resulting motion of the experiment can be observed in Figures 4.48, 4.49, 4.50, 4.51, 4.52, 4.53, 4.54.

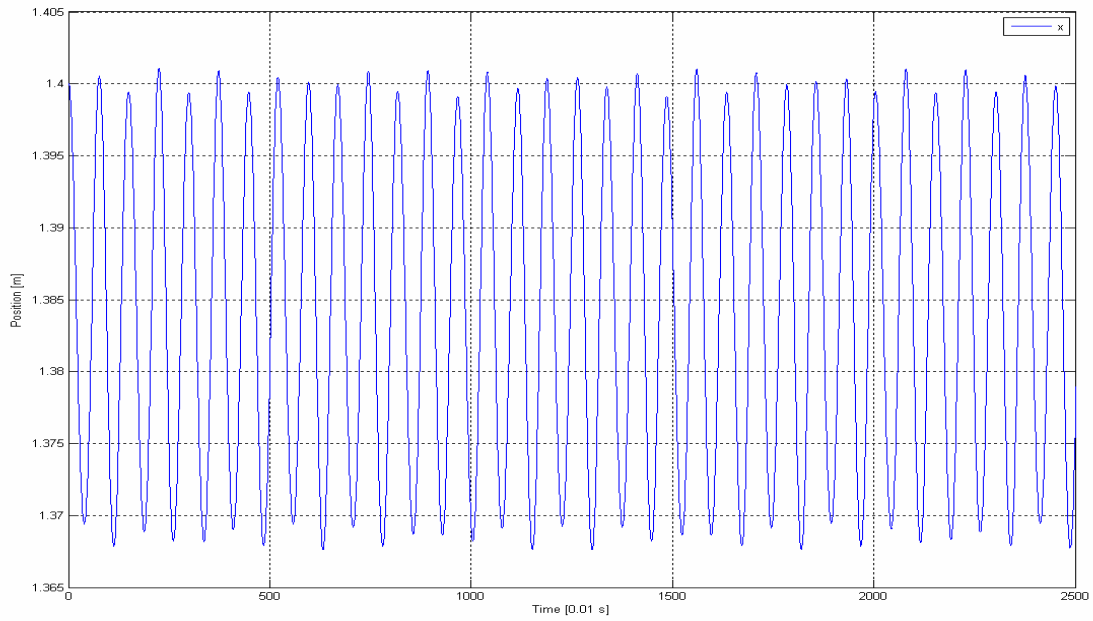

Figure 4.48 Position of x coordinate of CG between [0,25] s

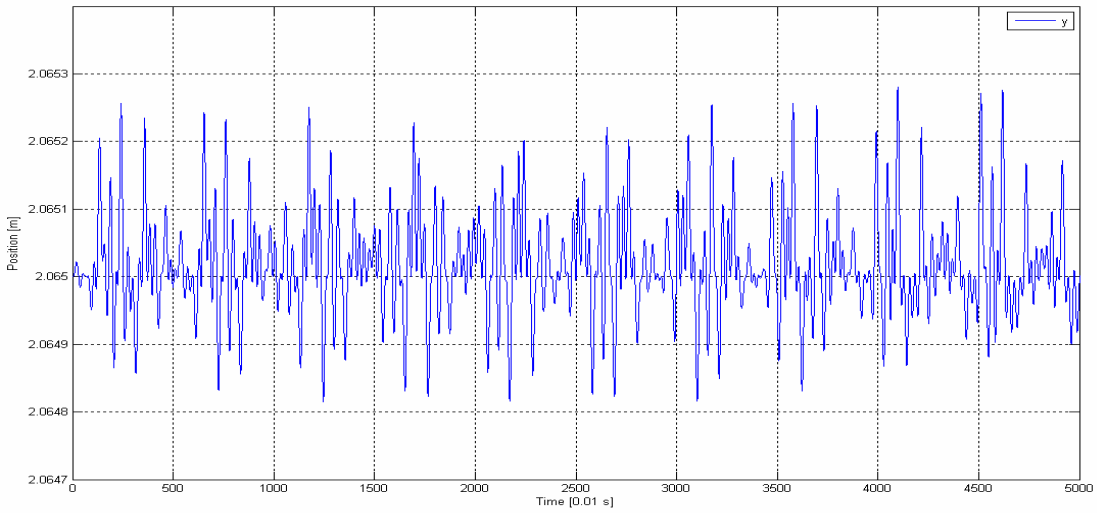

Figure 4.49 Position of y coordinate of CG between [0,50] s

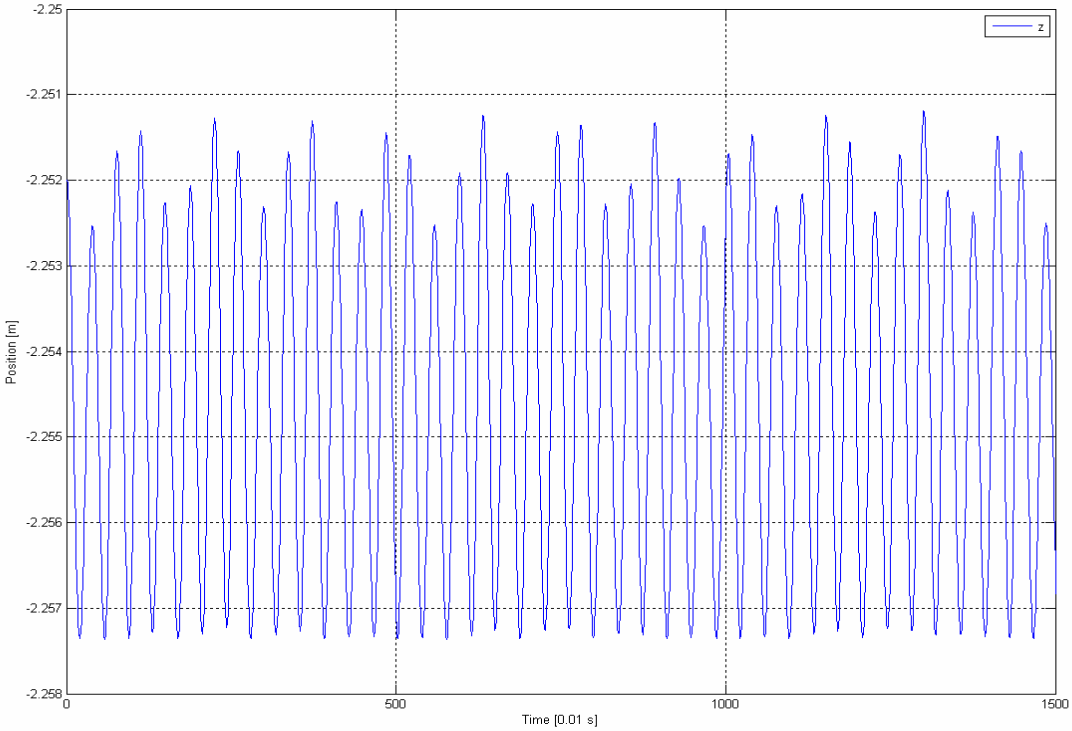

Figure 4.50 Position of z coordinate of CG between [0,15]s

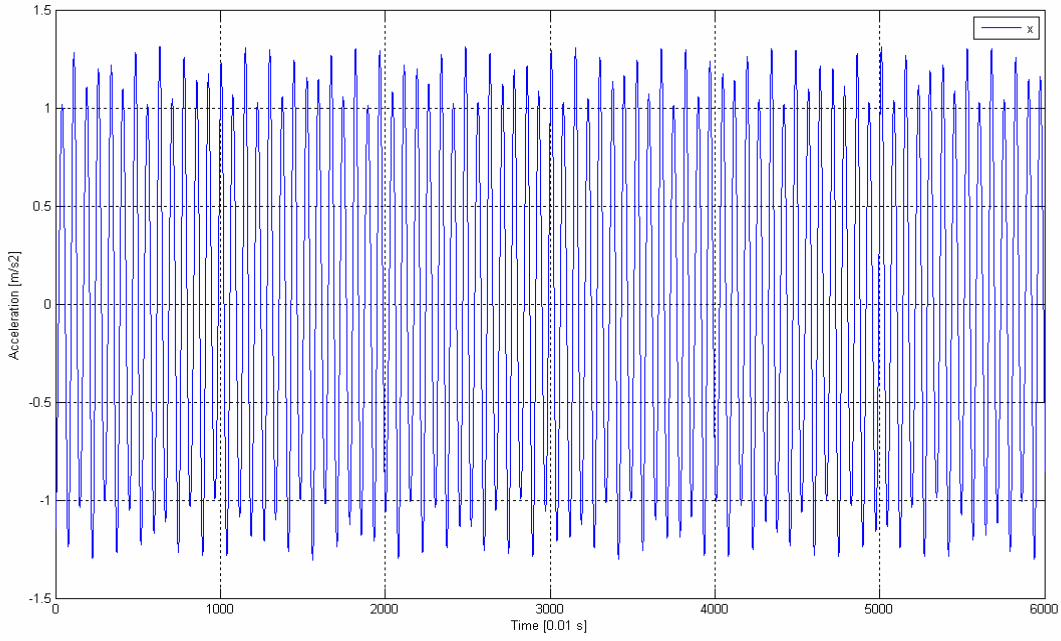

Figure 4.51 Acceleration of CG in x direction between [0,60]s

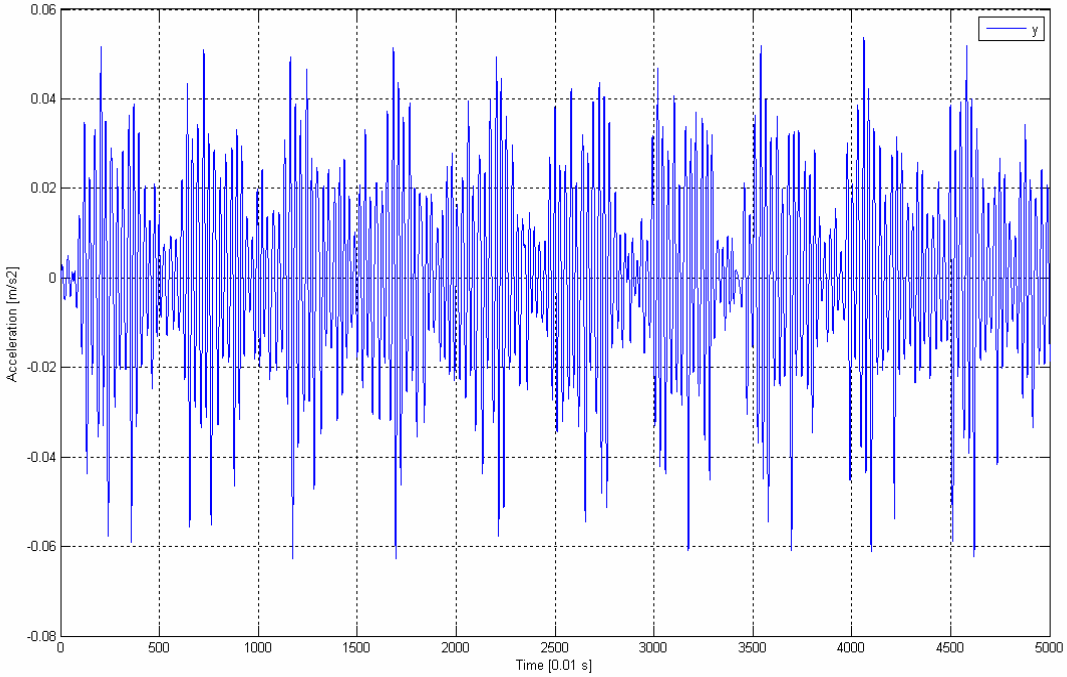

Figure 4.52 Acceleration of CG in y direction between [0,50]s

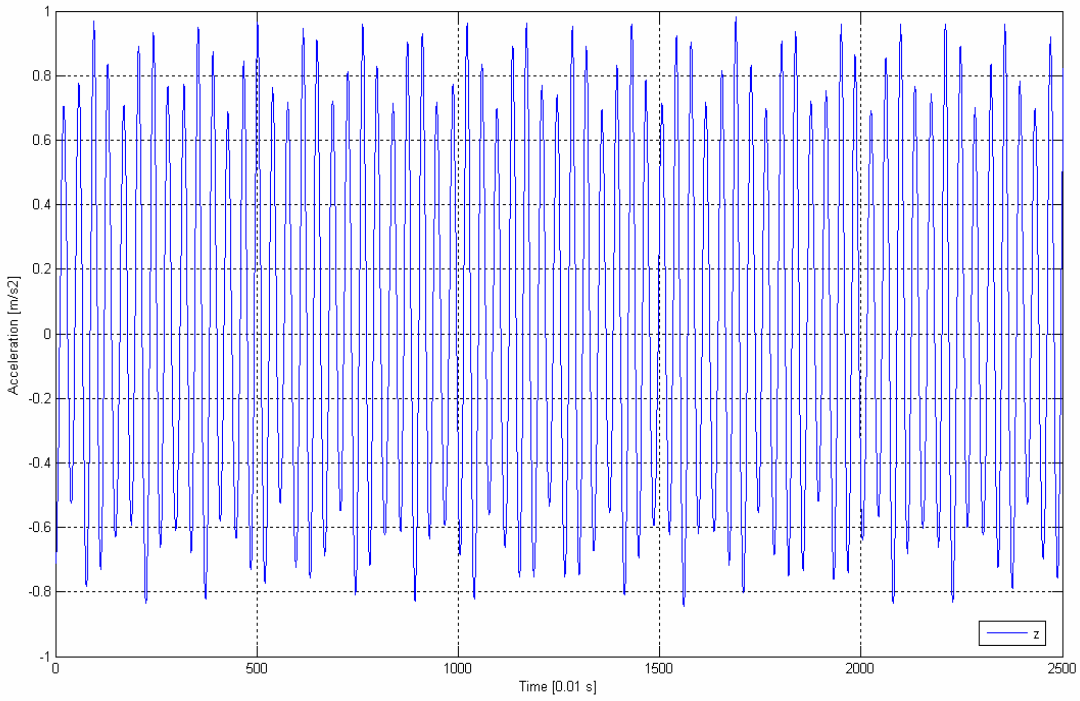

Figure 4.53 Acceleration of CG in z direction between [0,25]s

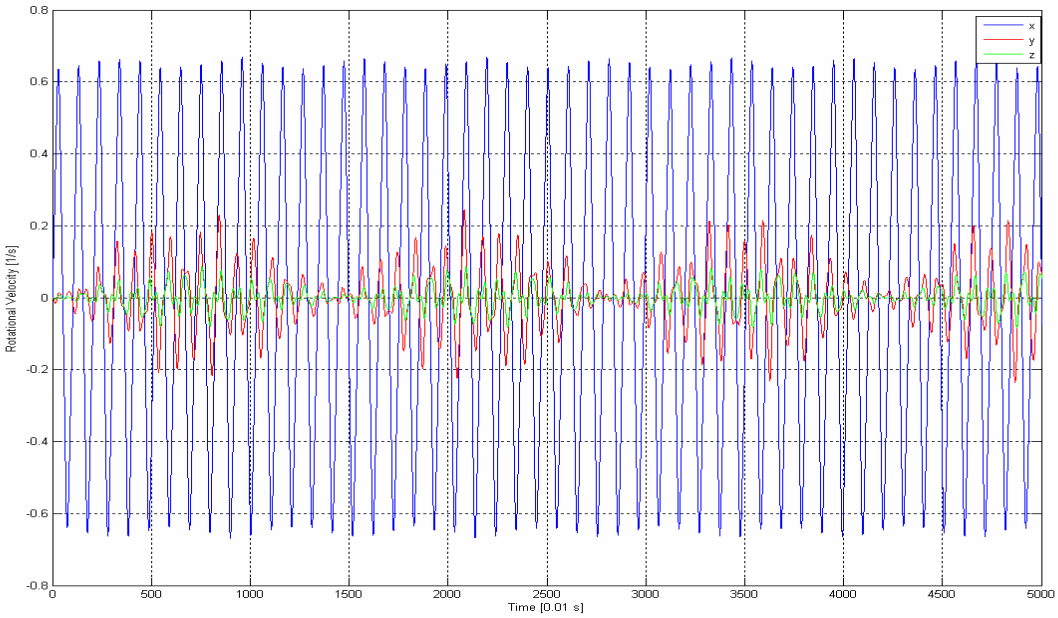

Figure 4.54 Rotational Velocity of the Body with respect to CG between [0,50]s

4.12.2 The Results of the Identification Run for Case Study 12

Identification code calculated the following inertia tensor:

$$J = \begin{bmatrix} 987 & 0 & 0 \\ 0 & 274 & 32 \\ 0 & 32 & 1102 \end{bmatrix}$$

Whereas the original tensor was:

$$J = \begin{bmatrix} 971.5 & 6 & 5.1 \\ 6 & 287.2 & 36.9 \\ 5.1 & 36.9 & 1082.1 \end{bmatrix}$$

Percentage error is:

$$\%Error = \begin{bmatrix} 1.57 & \pm 6 & \pm 5.1 \\ \pm 6 & 4.82 & 15.3 \\ \pm 5.1 & 15.3 & 1.81 \end{bmatrix}$$

Although 15 percent error in off diagonal elements look high, absolute value of that components is very low when compared to diagonal elements, thus the error is not significant and the alues are still good enough for vehicle dynamics studies.

Figure 4.55 shows the comparison of the identified system and the measured system's output measurements.

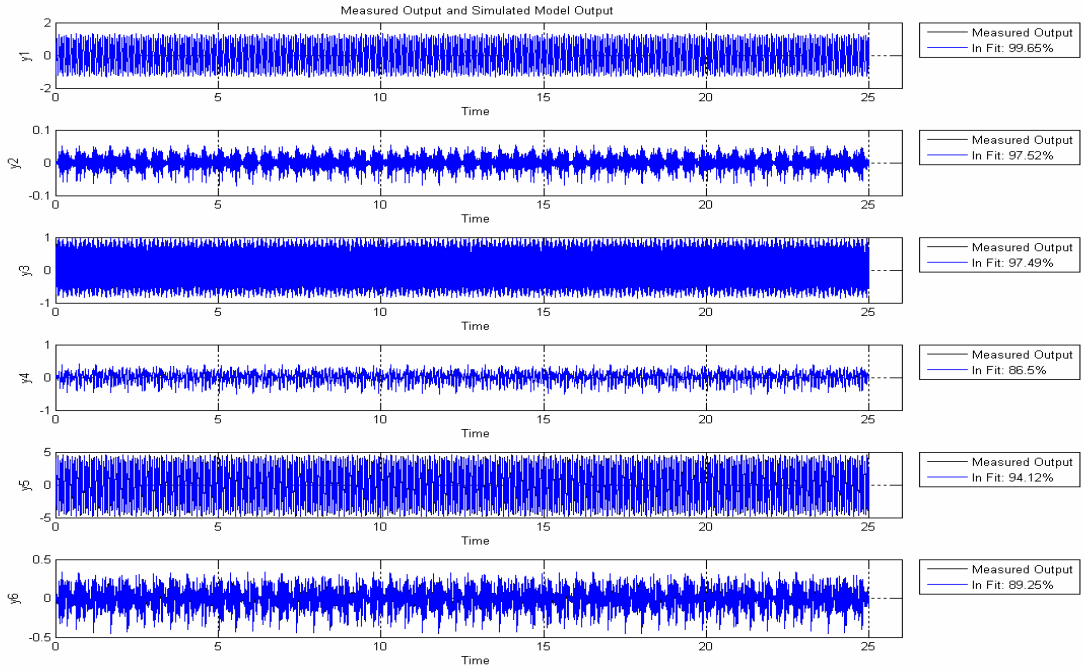

Figure 4.55 Comparison of the Identified System and the Measured System

4.13 Case Study 13

In this case the mass properties of 1998 Chevrolet Metro (Suzuki Swift) with one occupant and full fuel tank are used [32].

Table 4.13 Data for Case Study 13

CASE 13	
Coordinates of CG (initially) [m]	[1.4; 2.065; -2.252]
Mass [kg]	880
Jxx [N.m^2]	987
Jyy [N.m^2]	274
Jzz [N.m^2]	1102
Jxy [N.m^2]	0
Jxz [N.m^2]	0
Jyz [N.m^2]	32
Coordinates of Hinge Points on the Ceiling [m]	
[0;0;0]	
[3.5;0;0]	
[0;5;0]	
[3.5;5;0]	
Body Dimensions [m]	
1.5x2.5x1.5 (Rectangular Prism)	
Coordinates of Hinge Points on the Body (wrt to CG)	
[-0.7;-1.0325;1.126]	
[0.8;-1.0325;1.126]	
[-0.7;1..4675;1.126]	
[0.8;1.4675;1.126]	
Initial Conditions	
No Initial Displacement	
Applied Forces	
Force Magnitude [N]	**Point of Action (wrt CG) [m]**
200	[-0.7;-1.0325;-0.374]
Frequency of Forcing [Hz]	
1.05	
Initial Guess Vector for Inertia Tensor [N.m2]	
[700; 10; 10; 350; 50; 1000]	
Length of the Experiment [s]	**Sampling [s]**
250	0.01

4.13.1 The Results of the Experiment of Case Study 13

The resulting motion of the experiment can be observed in Figures 4.56, 4.57, 4.58, 4.59, 4.60, 4.61, 4.62, 4.63 and 4.64.

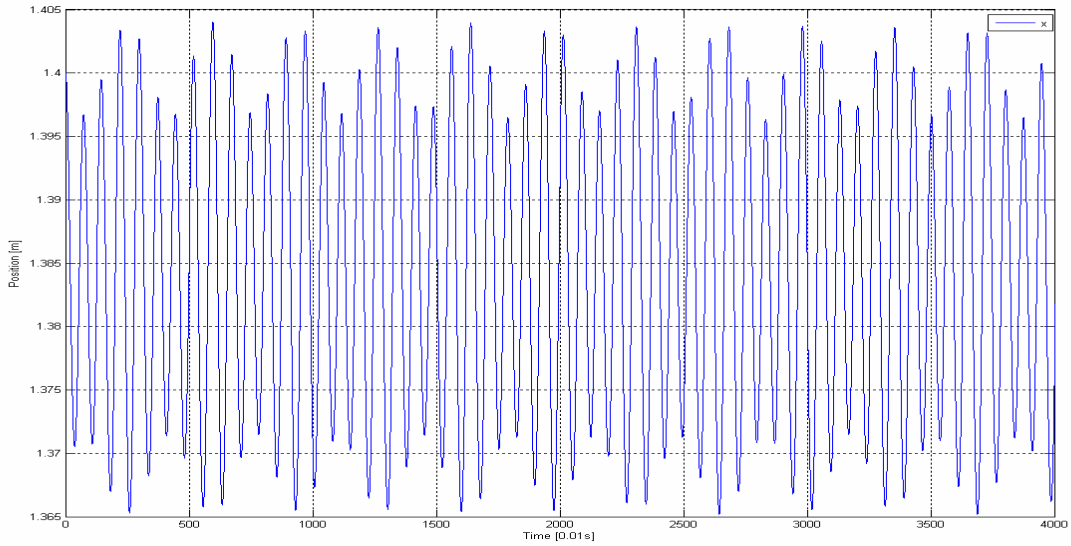

Figure 4.56 Position of x coordinate of CG between [0,40] s

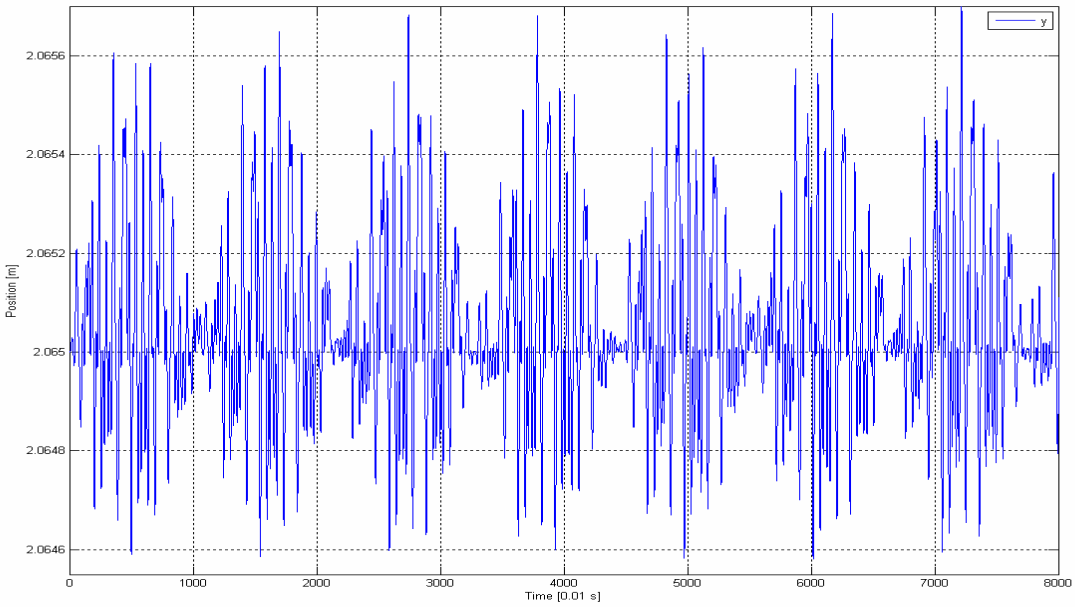

Figure 4.57 Position of y coordinate of CG between [0,80] s

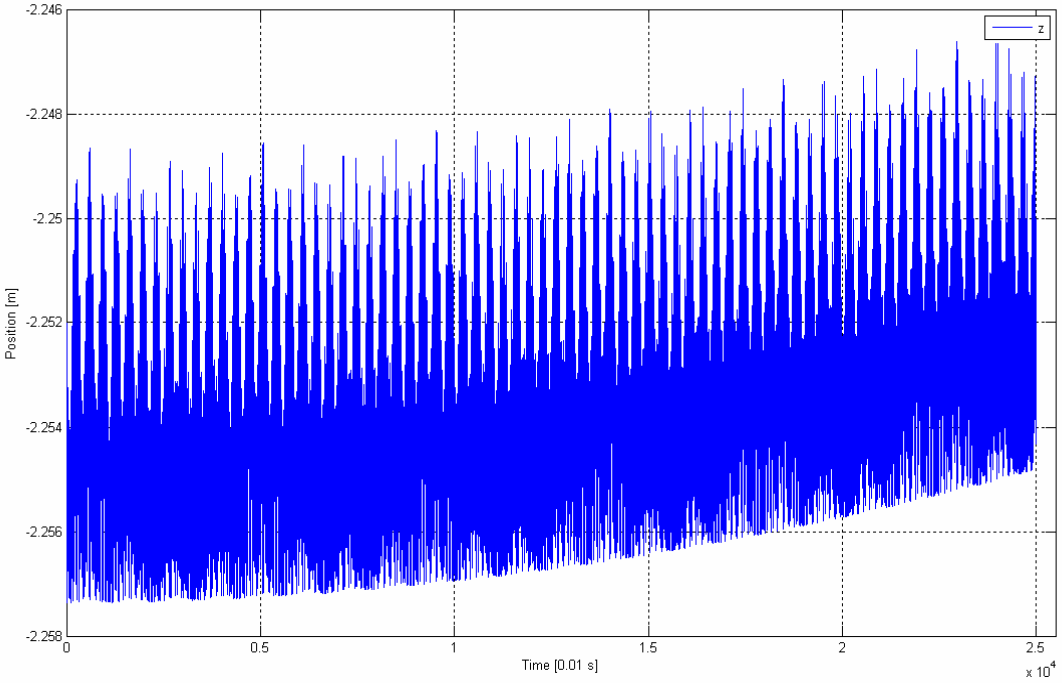

Figure 4.58 Position of z coordinate of CG

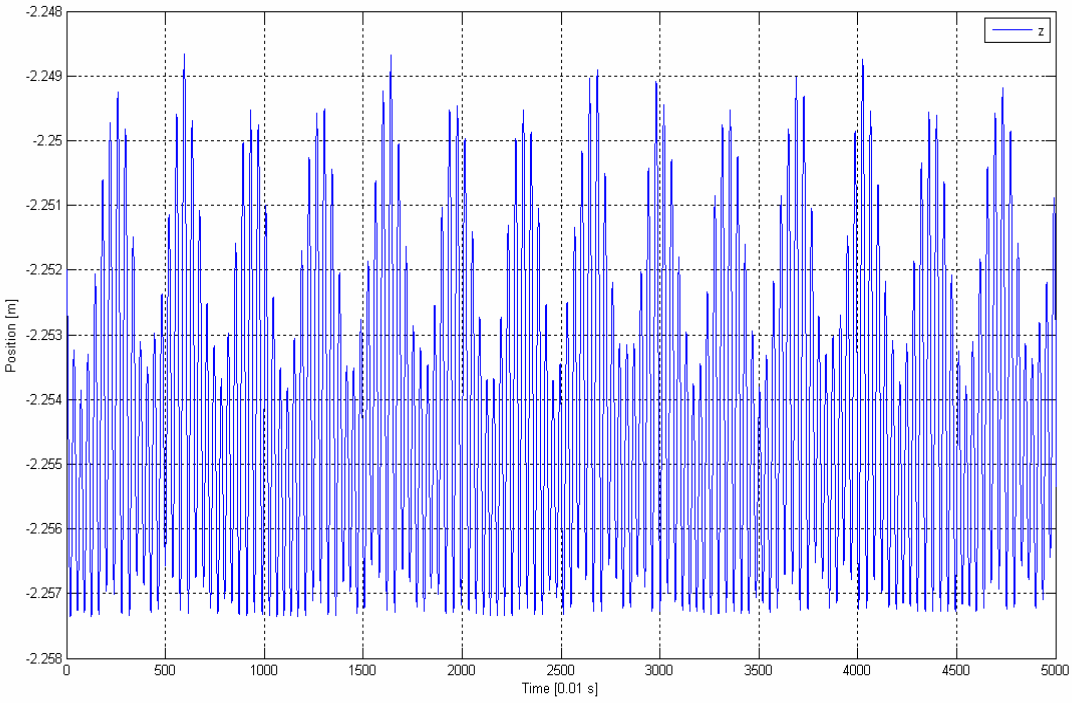

Figure 4.59 Position of z coordinate of CG between [0,50] s

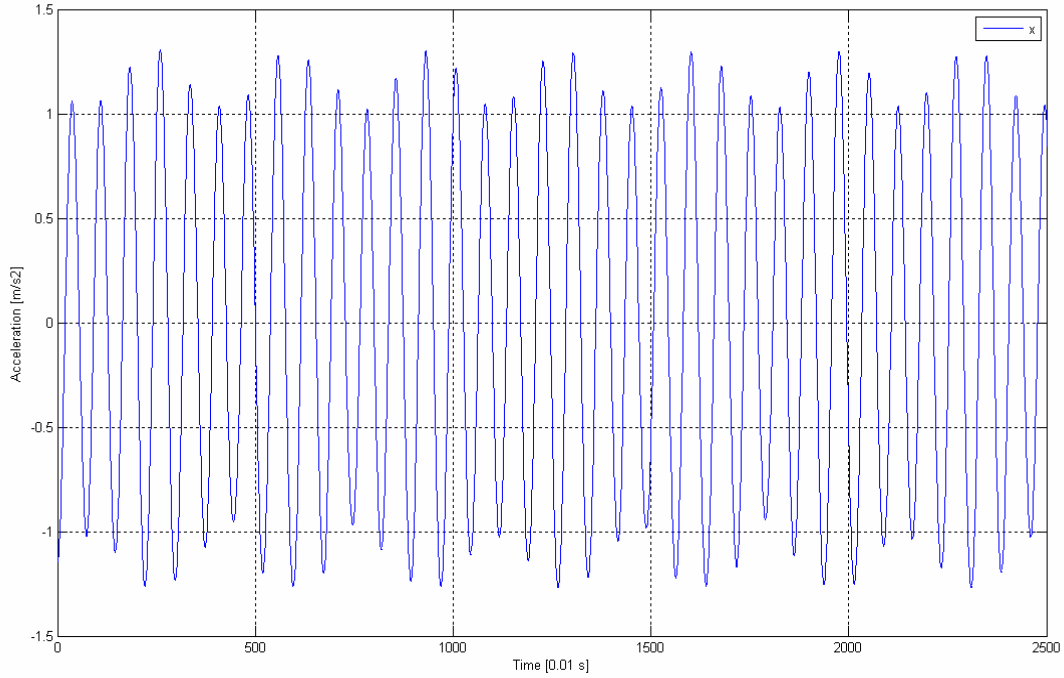

Figure 4.60 Acceleration of CG in x direction between [0,25]s

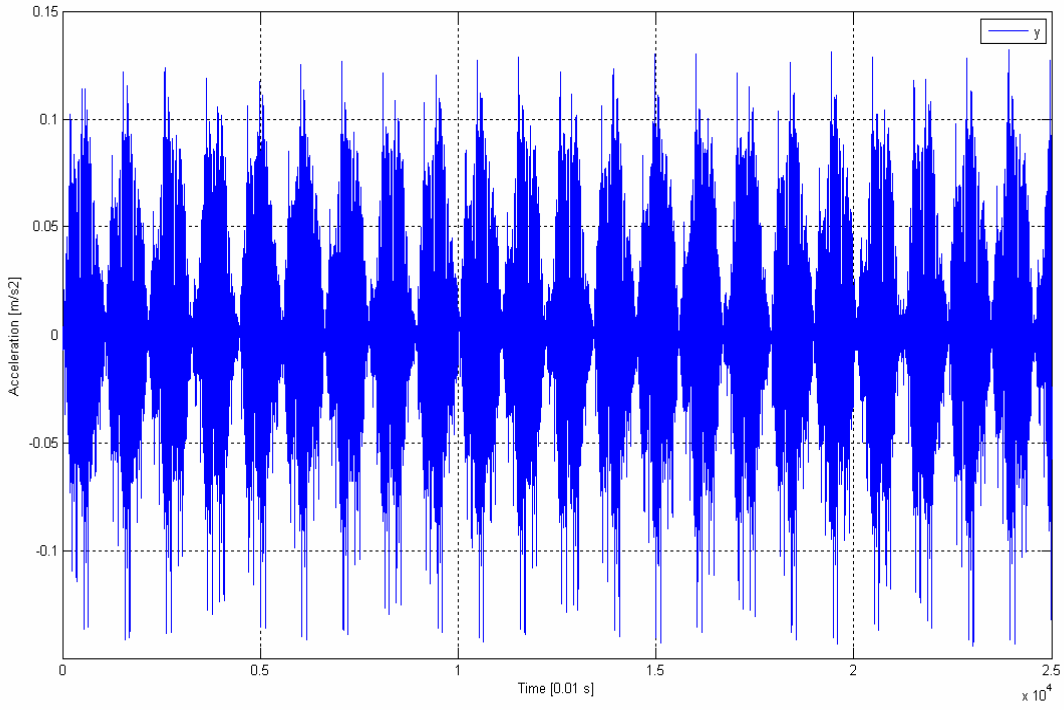

Figure 4.61 Acceleration of CG in y direction

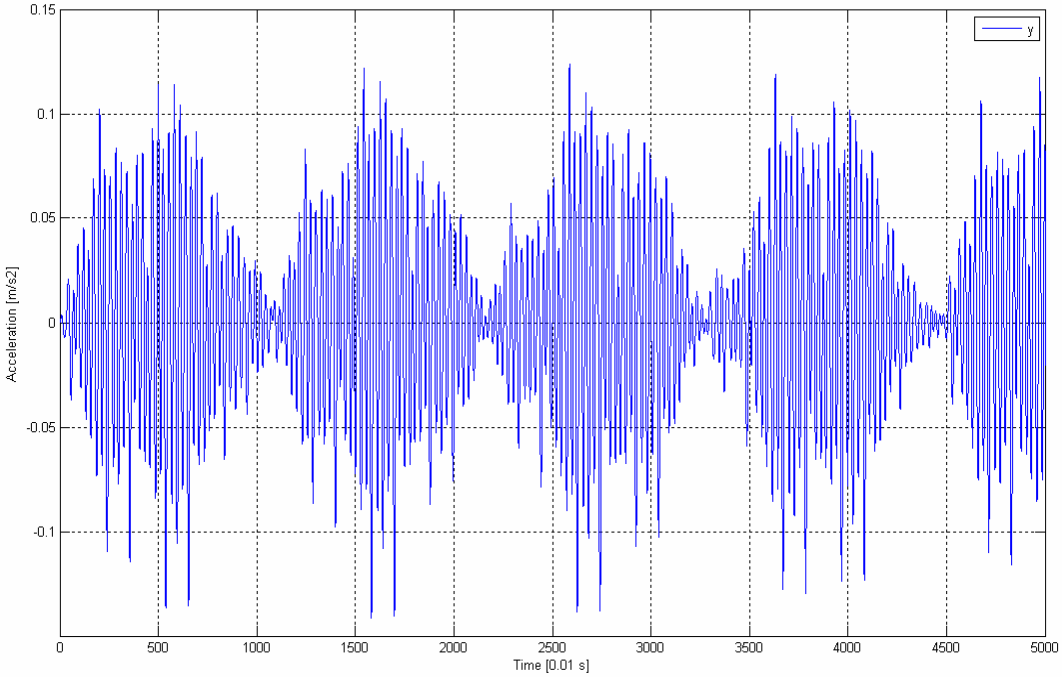

Figure 4.62 Acceleration of CG in y direction between [0,50]s

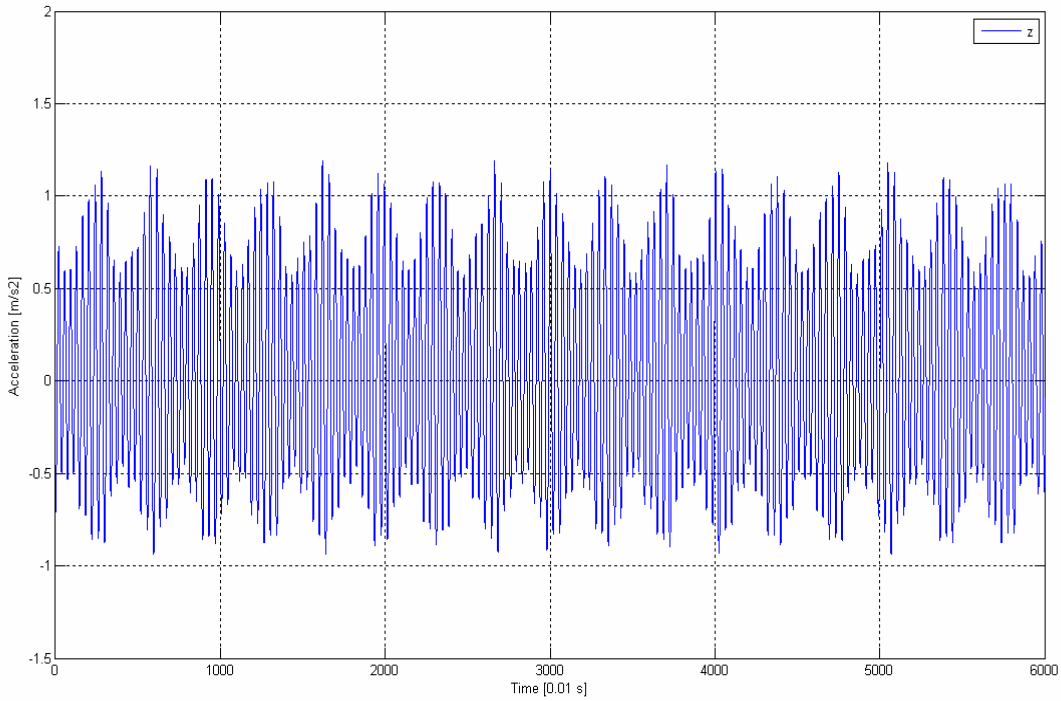

Figure 4.63 Acceleration of CG in z direction between [0,60]s

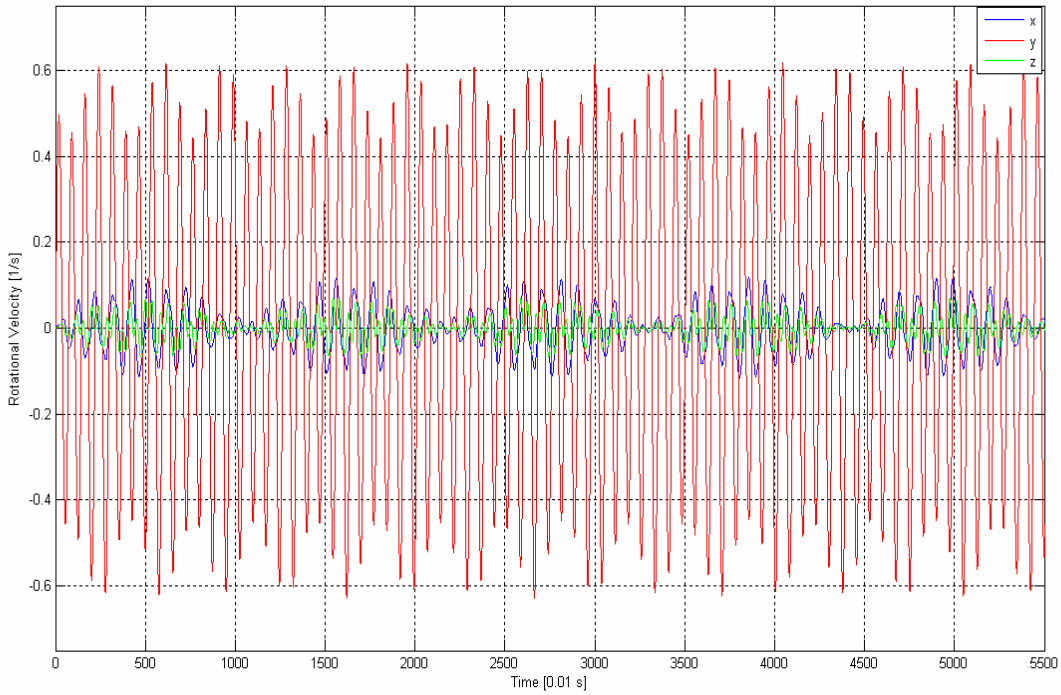

Figure 4.64 Rotational Velocity of the Body with respect to CG between [0,50]s

4.13.2 The Results of the Identification Run for Case Study 13

Identification code calculated the following inertia tensor:

$$J = \begin{bmatrix} 968.2 & -0.4 & 10.2 \\ -0.4 & 279.3 & 34.4 \\ 10.2 & 34.4 & 1082.6 \end{bmatrix}$$

Whereas the original tensor was:

$$J = \begin{bmatrix} 987 & 0 & 0 \\ 0 & 274 & 32 \\ 0 & 32 & 1102 \end{bmatrix}$$

Percentage error is:

$$\%Error = \begin{bmatrix} 1.90 & \pm 0.4 & \pm 10.2 \\ \pm 0.4 & 1.93 & 7.5 \\ \pm 10.2 & 7.5 & 1.76 \end{bmatrix}$$

The same data set from the previous case is used with halved frequency. The error of off diagonal elements is not high in this case, with a maximum of 7.5 percent. Diagonal elements are very accurately identified. igure 4.65 shows the comparison of the identified system and the measured system's output measurements.

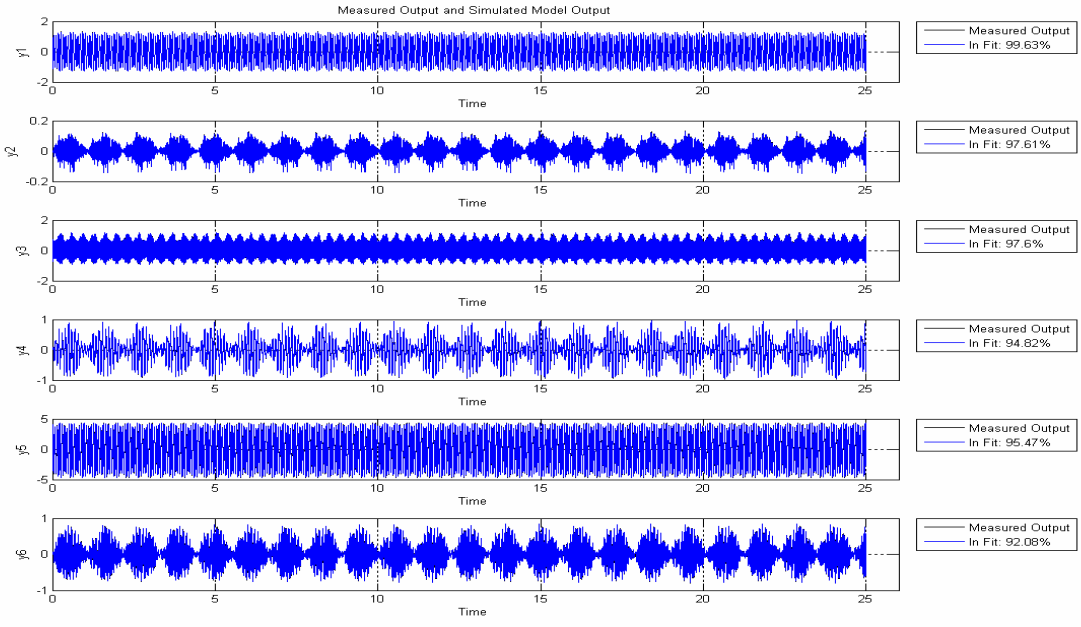

Figure 4.65 Comparison of the Identified System and the Measured System

4.14 Case Study 14

In this case the mass properties of 1998 Honda Civic with one occupant and full fuel tank are used [32].

Table 4.14 Data for Case Study 14

CASE 14	
Coordinates of CG (initially) [m]	[1.6; 2.256; -2.274]
Mass [kg]	1145
Jxx [N.m^2]	1617
Jyy [N.m^2]	365
Jzz [N.m^2]	1785
Jxy [N.m^2]	0
Jxz [N.m^2]	0
Jyz [N.m^2]	70
Coordinates of Hinge Points on the Ceiling [m]	
[0;0;0]	
[4;0;0]	
[0;6;0]	
[4;6;0]	
Body Dimensions [m]	
1.6x3x1.5 (Rectangular Prism)	
Coordinates of Hinge Points on the Body (wrt to CG)	
[-0.8;-1.128;1.137]	
[0.8;-1.128;1.137]	
[-0.8;1.672;1.137]	
[0.8;1.672;1.137]	
Initial Conditions	
No Initial Displacement	
Applied Forces	
Force Magnitude [N]	**Point of Action (wrt CG) [m]**
200	[-0.8;-1.128;-0.363]
Frequency of Forcing [Hz]	
1.05	
Initial Guess Vector for Inertia Tensor [N.m2]	
[1000; 10; 10; 300; 40; 1000]	
Length of the Experiment [s]	**Sampling [s]**
250	0.01

4.14.1 The Results of the Experiment of Case Study 14

The resulting motion of the experiment can be observed in Figures 4.66, 4.67, 4.68, 4.69, 4.70, 4.71, 4.72, 4.73, 4.74, 4.75, 4.76, 4.77.

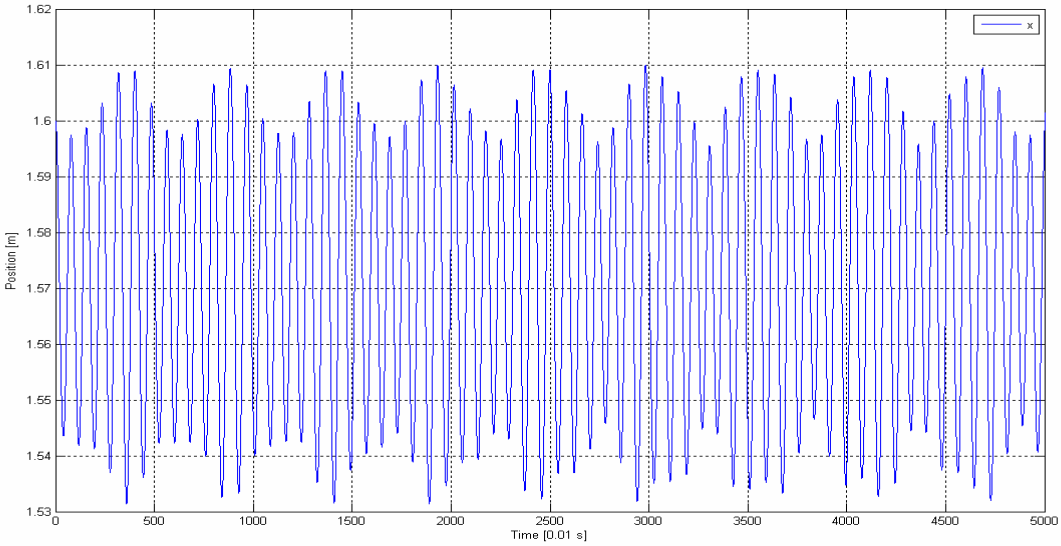

Figure 4.66 Position of x coordinate of CG between [0,50] s

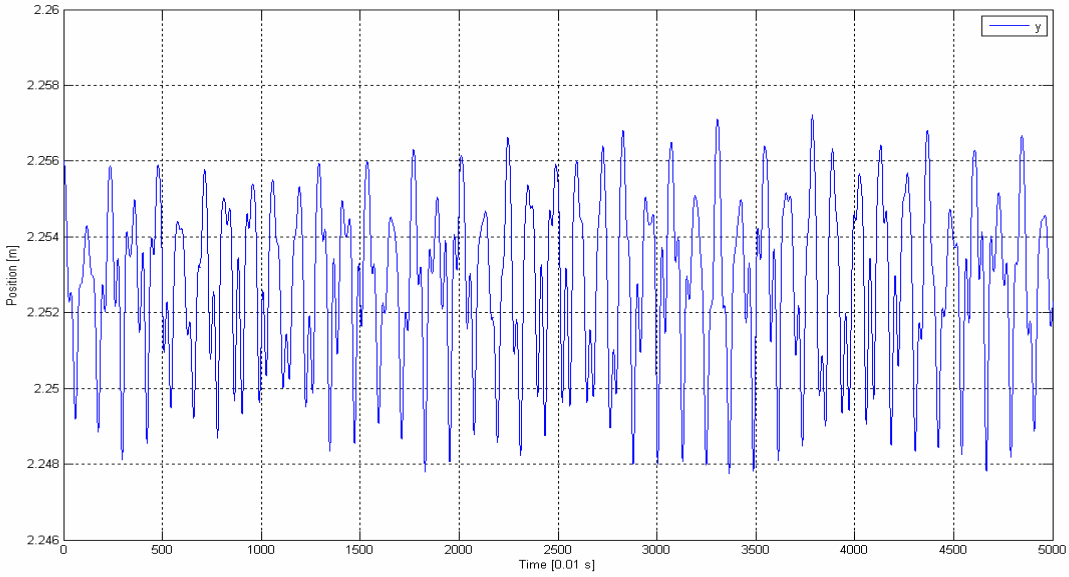

Figure 4.67 Position of y coordinate of CG between [0,50] s

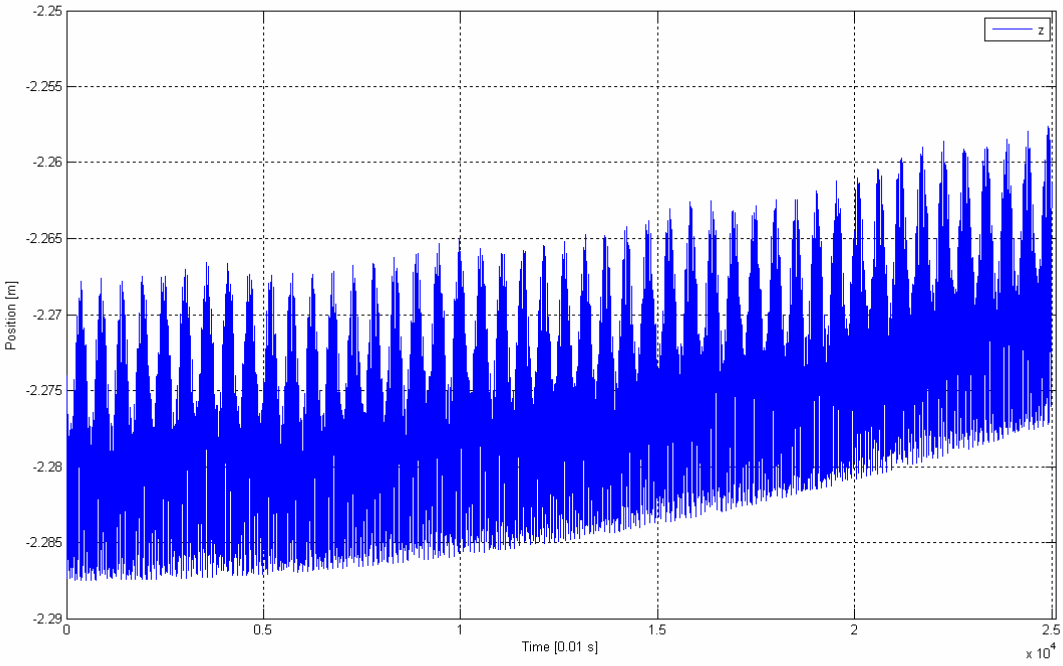

Figure 4.68 Position of z coordinate of CG

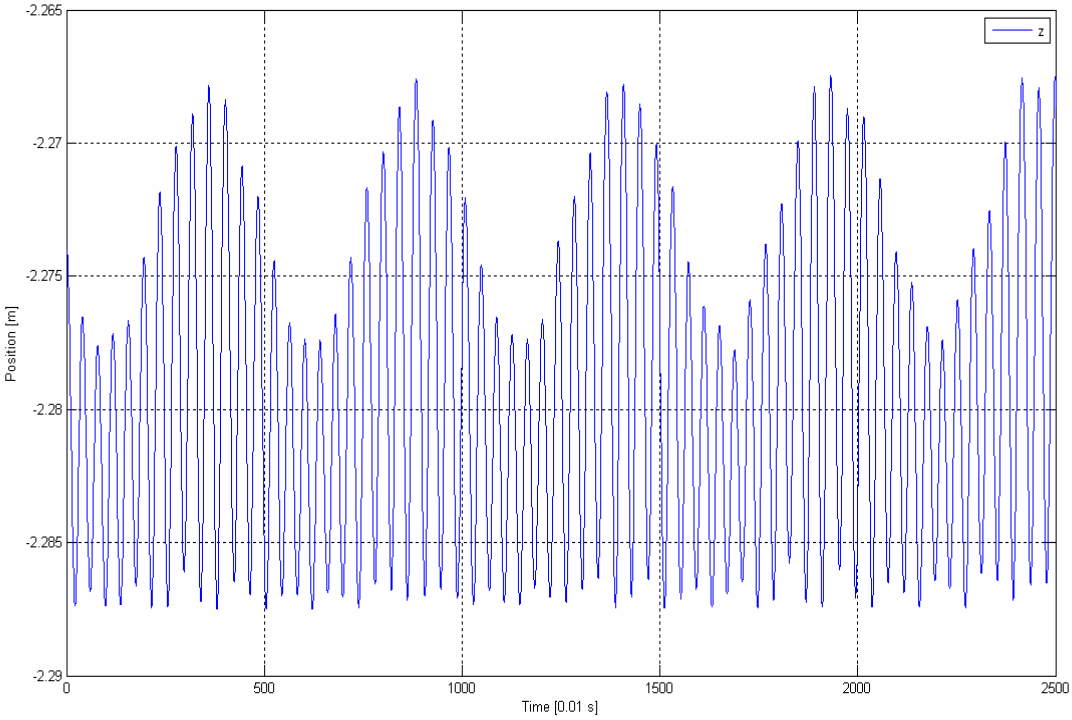

Figure 4.69 Position of z coordinate of CG between [0,25] s

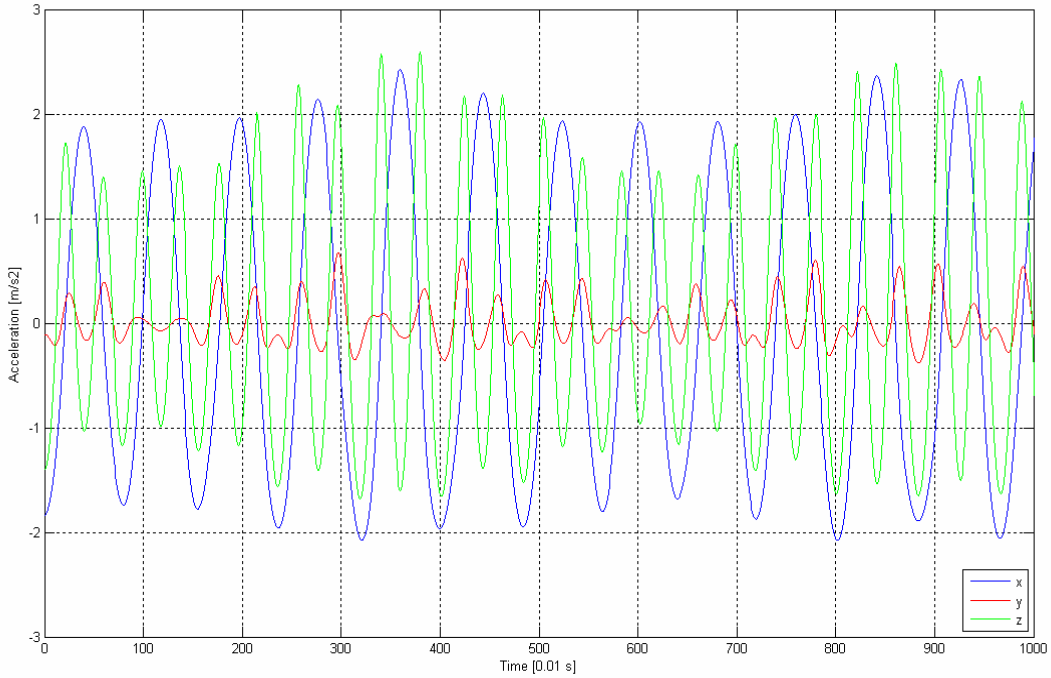

Figure 4.70 Acceleration of CG in between [0,10]s

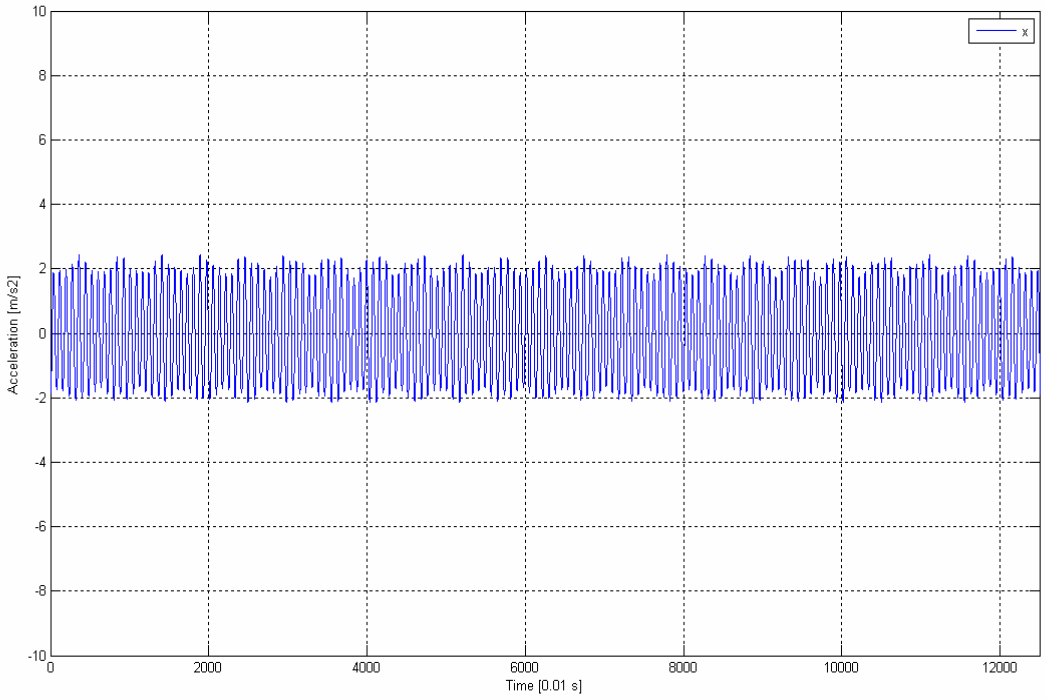

Figure 4.71 Acceleration of CG in x direction between [0,125] s

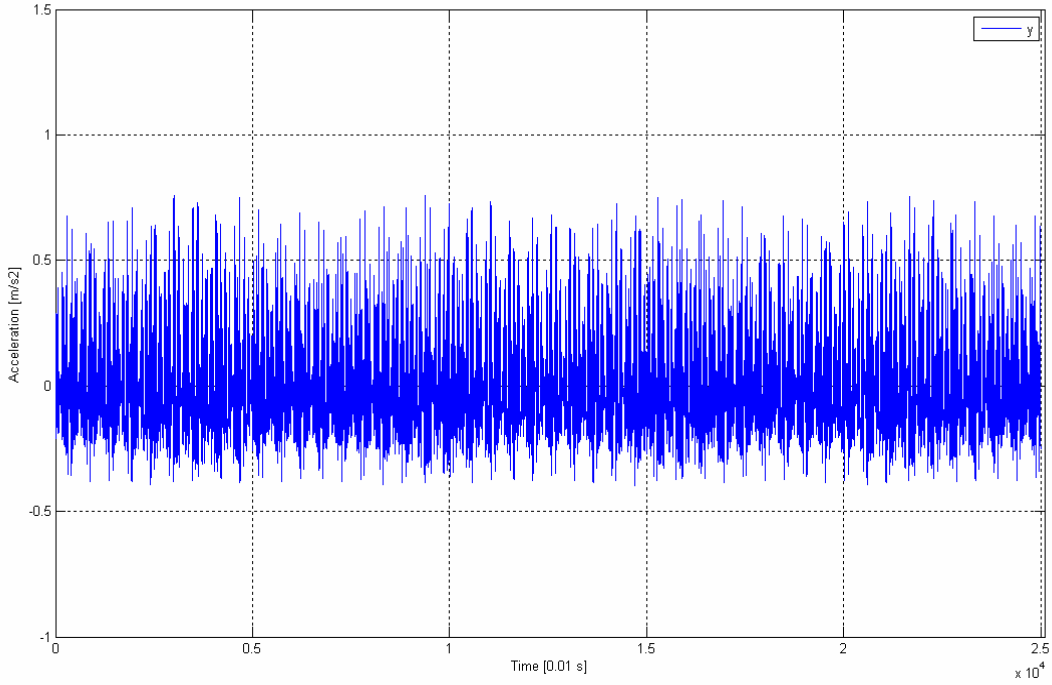

Figure 4.72 Acceleration of CG in y direction

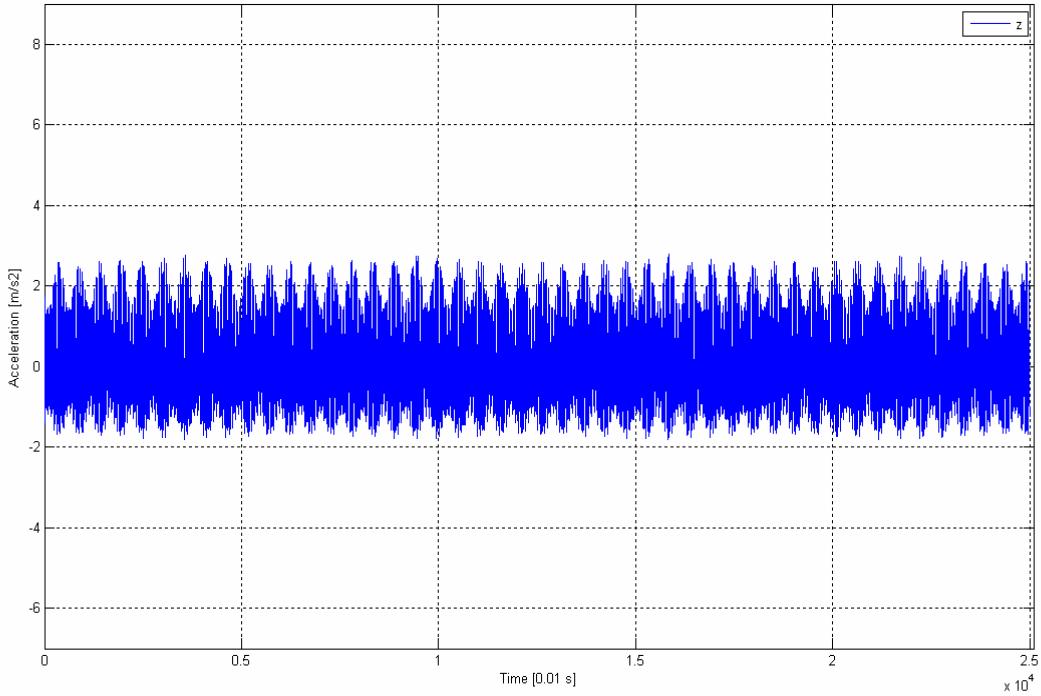

Figure 4.73 Acceleration of CG in z direction

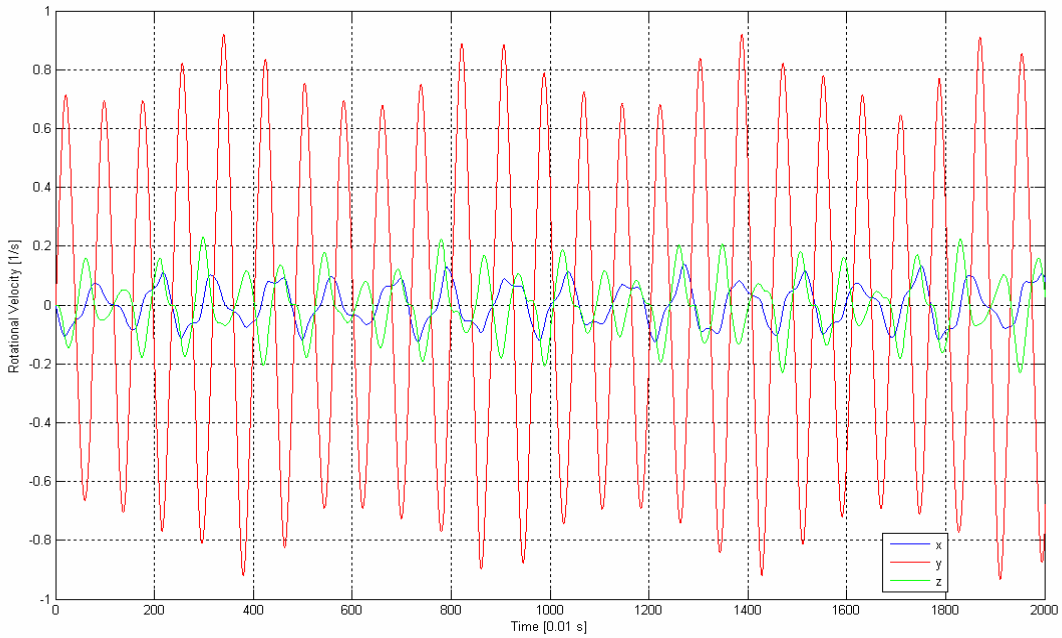

Figure 4.74 Rotational Velocity of the Body with respect to CG between [0,20]s

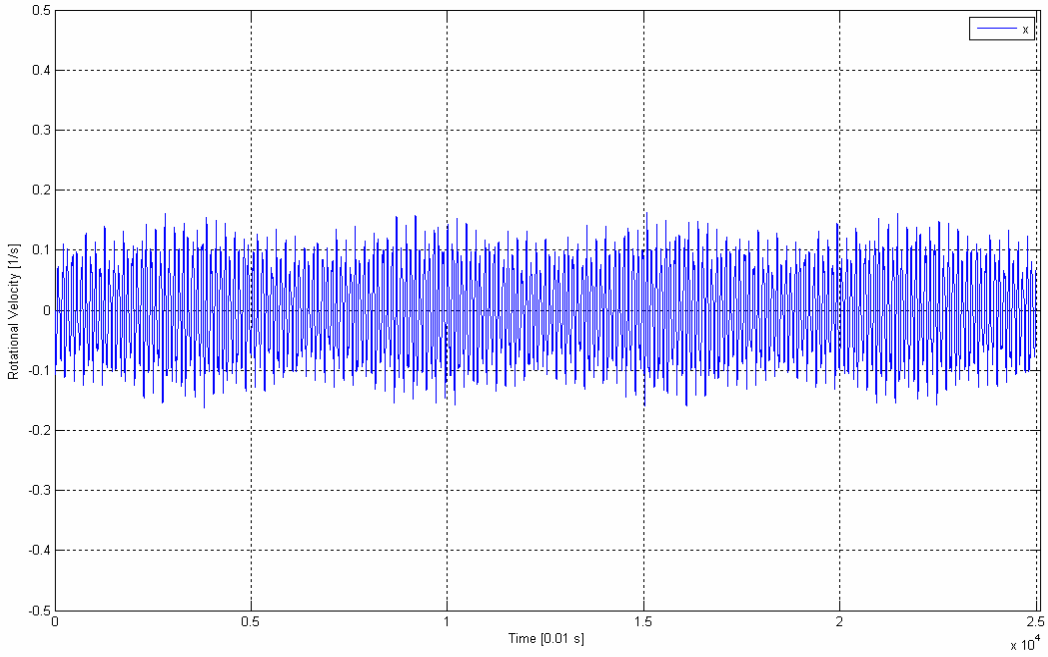

Figure 4.75 Rotational Velocity of the Body with respect to CG around x axis

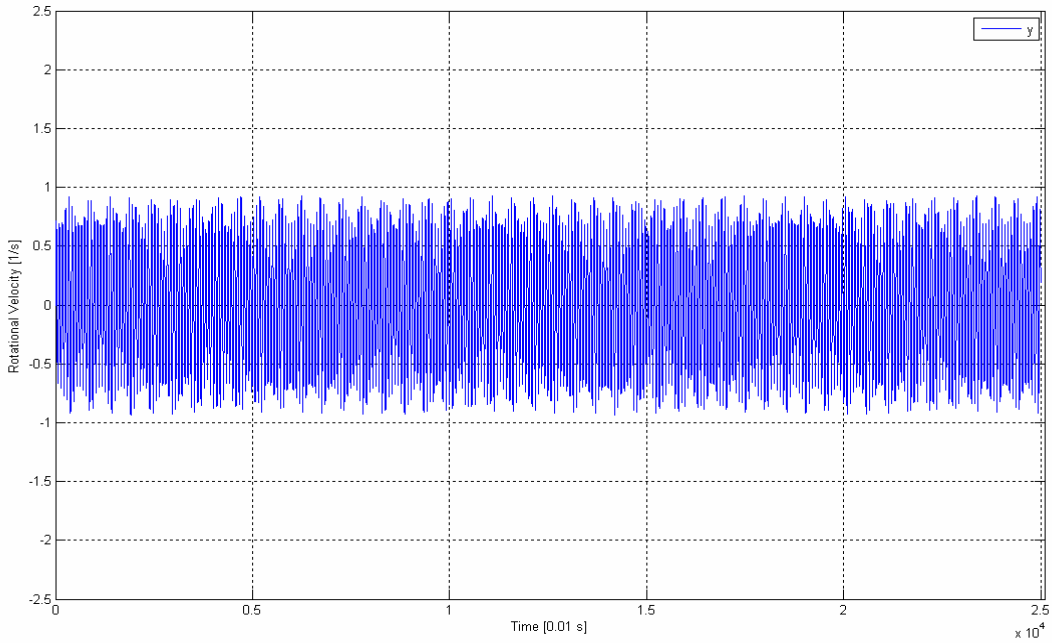

Figure 4.76 Rotational Velocity of the Body with respect to CG around y axis

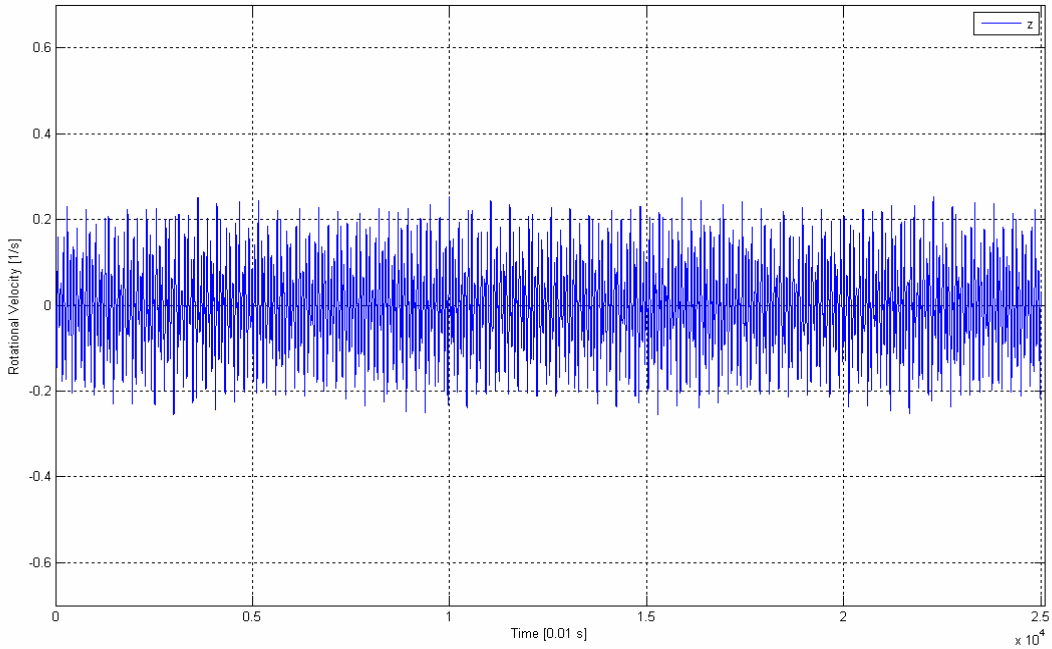

Figure 4.77 Rotational Velocity of the Body with respect to CG around z axis

4.14.2 The Results of the Identification Run for Case Study 14

Identification code calculated the following inertia tensor:

$$J = \begin{bmatrix} 1542.4 & -1.4 & -0.8 \\ -1.4 & 364.9 & 63 \\ -0.8 & 63 & 1731 \end{bmatrix}$$

Whereas the original tensor was:

$$J = \begin{bmatrix} 1617 & 0 & 0 \\ 0 & 365 & 70 \\ 0 & 70 & 1785 \end{bmatrix}$$

Percentage error is:

$$\%Error = \begin{bmatrix} 4.61 & \pm 1.4 & \pm 0.8 \\ \pm 1.4 & 0.03 & 10 \\ \pm 0.8 & 10 & 3.03 \end{bmatrix}$$

In this case, the mass properties of Honda Civic [32] is used, which is a car that is also available on Turkish market. Maximum error of diagonal elements is again lower than 5 percent and maximum error of off diagonal elements is 10 percent. The results are satisfying in terms of vehicle dynamics studies.

Figure 4.78 shows the comparison of the identified system and the measured system's output measurements.

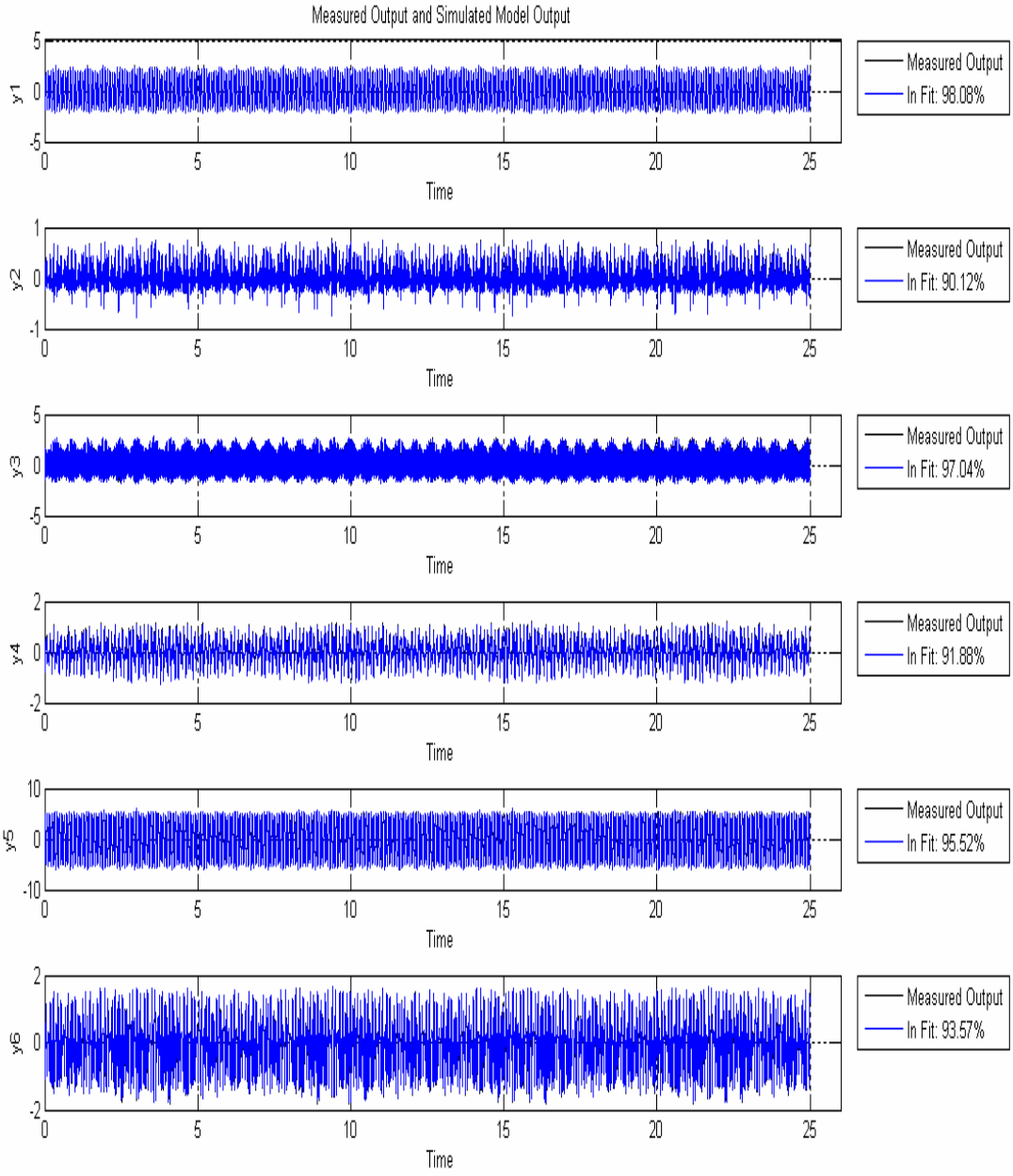

Figure 4.78 Comparison of the Identified System and the Measured System

4.15 Case Study 15

In this case the mass properties of 1998 Honda Civic with one occupant and full fuel tank are used [32].

Table 4.15 Data for Case Study 15

CASE 15	
Coordinates of CG (initially) [m]	[1.6; 2.256; -2.274]
Mass [kg]	1145
Jxx [N.m^2]	1617
Jyy [N.m^2]	365
Jzz [N.m^2]	1785
Jxy [N.m^2]	0
Jxz [N.m^2]	0
Jyz [N.m^2]	70
Coordinates of Hinge Points Points on the Ceiling [m]	
[0;0;0]	
[4;0;0]	
[0;6;0]	
[4;6;0]	
Body Dimensions [m]	
1.6x3x1.5 (Rectangular Prism)	
Coordinates of Hinge Points on the Body (wrt to CG)	
[-0.8;-1.128;1.137]	
[0.8;-1.128;1.137]	
[-0.8;1.672;1.137]	
[0.8;1.672;1.137]	
Initial Conditions	
No Initial Displacement	
Applied Forces	
Force Magnitude [N]	**Point of Action (wrt CG) [m]**
200	[-0.8;-1.128;-0.363]
Frequency of Forcing [Hz]	
2.1	
Initial Guess Vector for Inertia Tensor [N.m2]	
[1000; 10; 10; 300; 40; 1000]	
Length of the Experiment [s]	**Sampling [s]**
250	0.01

4.15.1 The Results of the Experiment of Case Study 15

The resulting motion of the experiment can be observed in Figures 4.79, 4.80, 4.81, 4.82, 4.83, 4.84, 4.85, 4.86, 4.87, 4.88, 4.89.

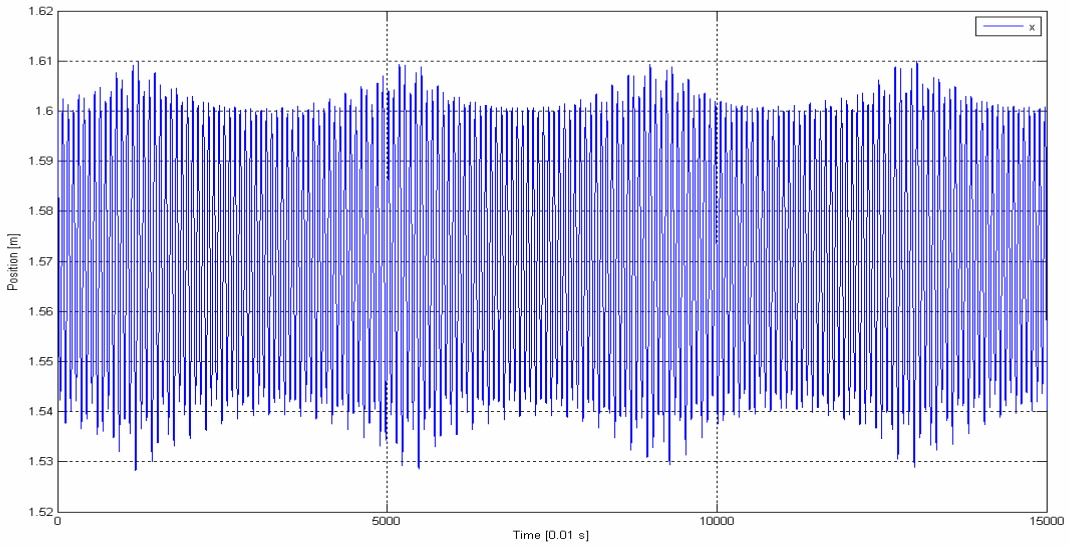

Figure 4.79 Position of x coordinate of CG between [0,150] s

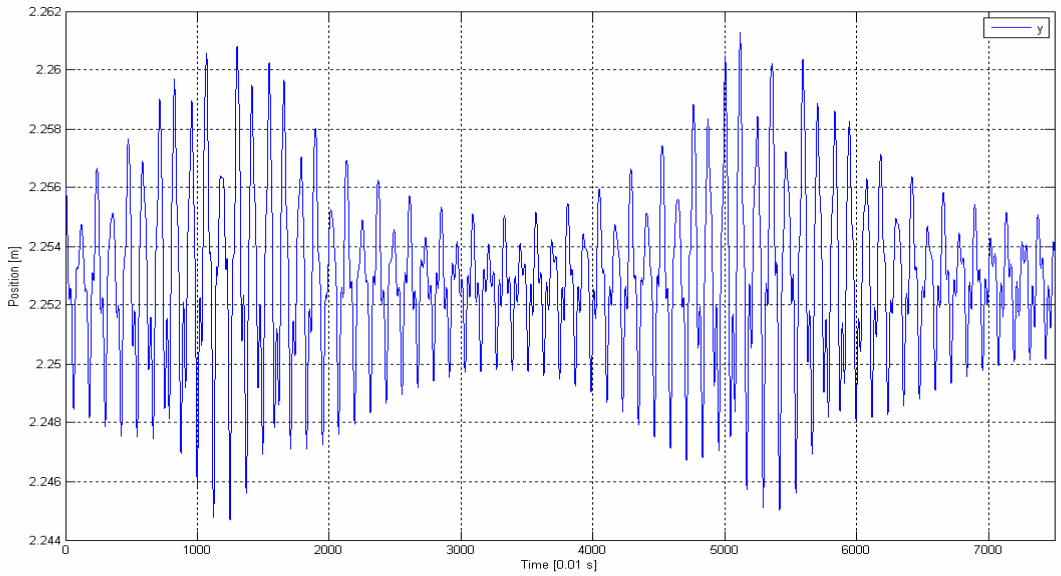

Figure 4.80 Position of y coordinate of CG between [0,75] s

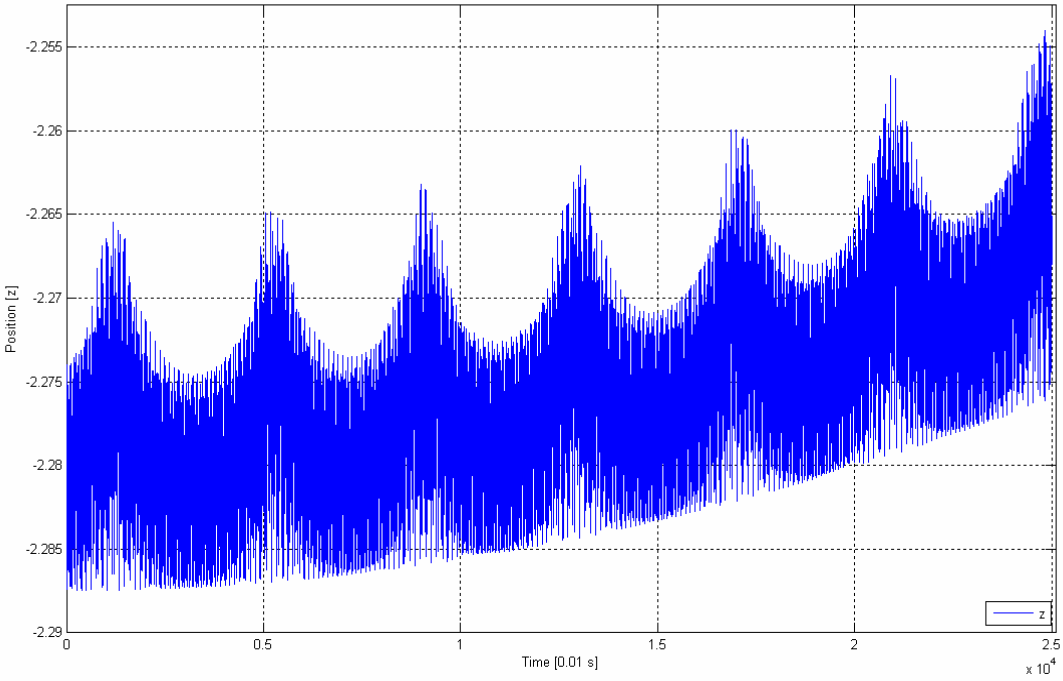

Figure 4.81 Position of z coordinate of CG

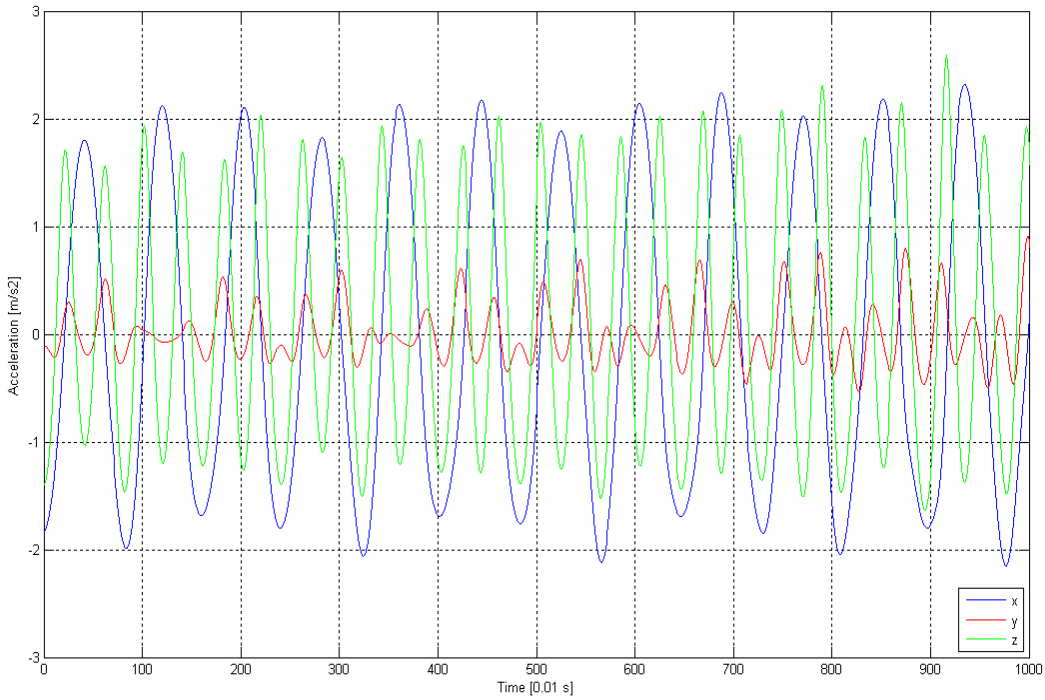

Figure 4.82 Acceleration of CG in between [0,10]s

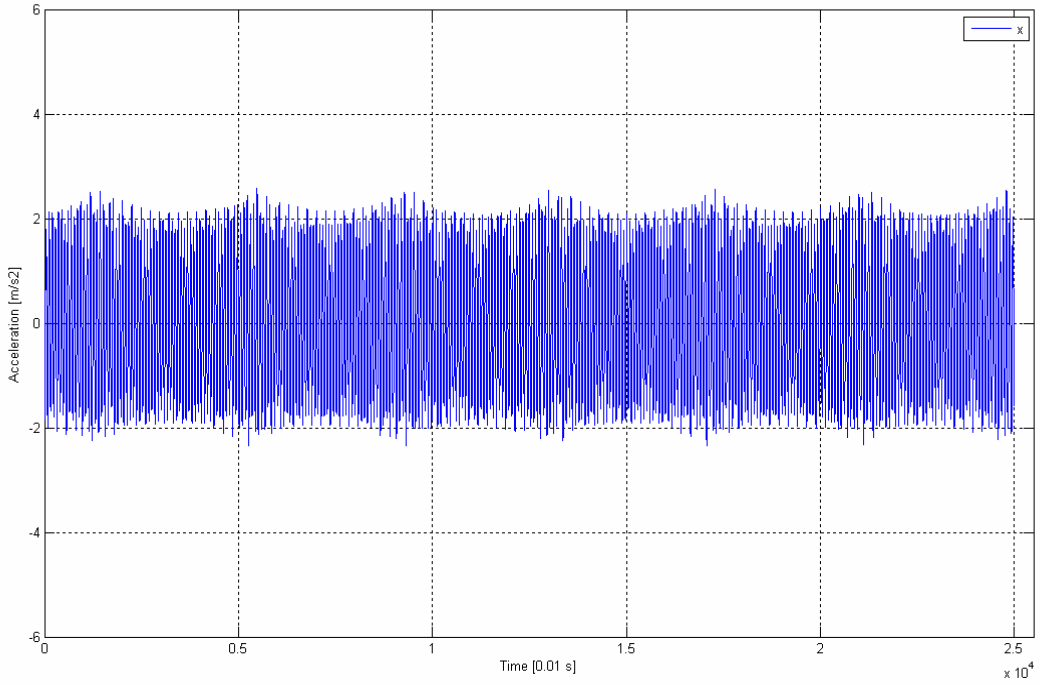

Figure 4.83 Acceleration of CG in x direction

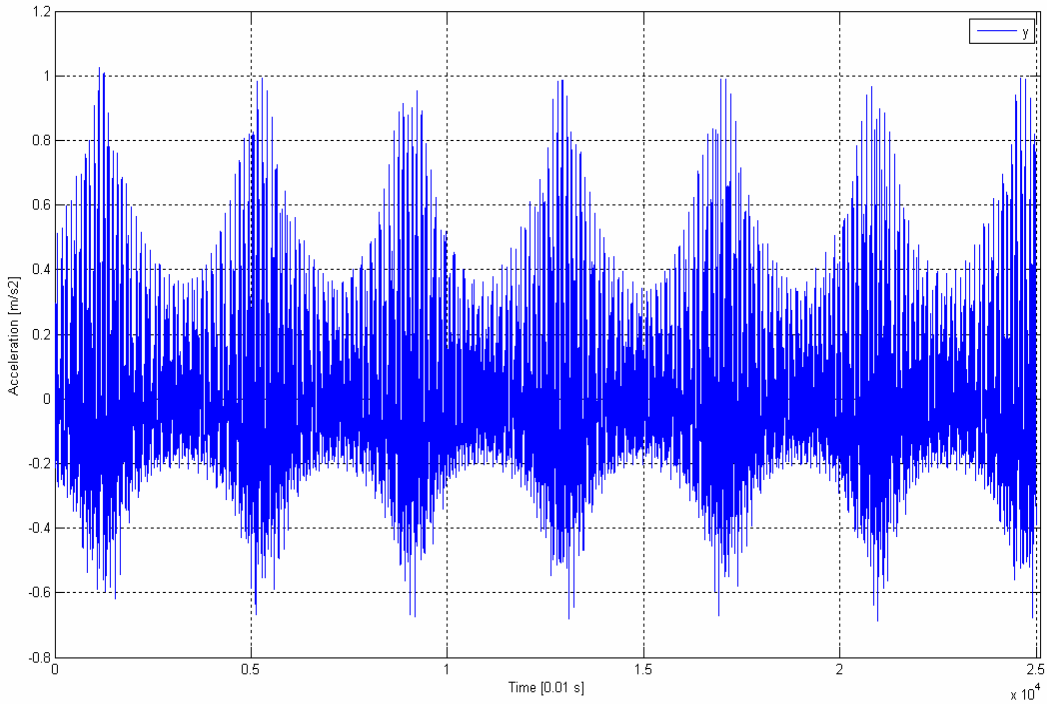

Figure 4.84 Acceleration of CG in y direction

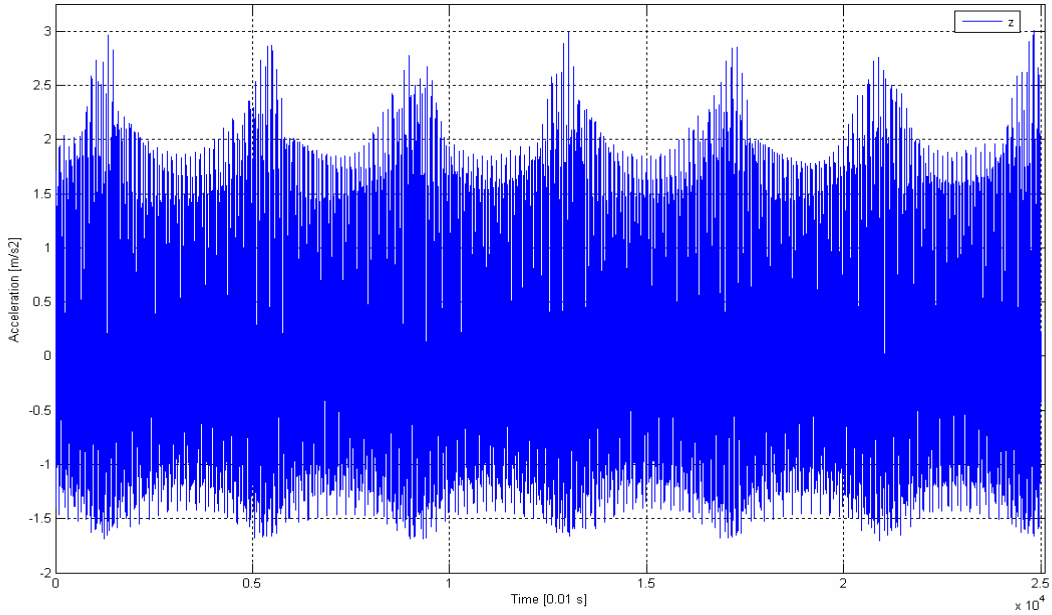

Figure 4.85 Acceleration of CG in z direction

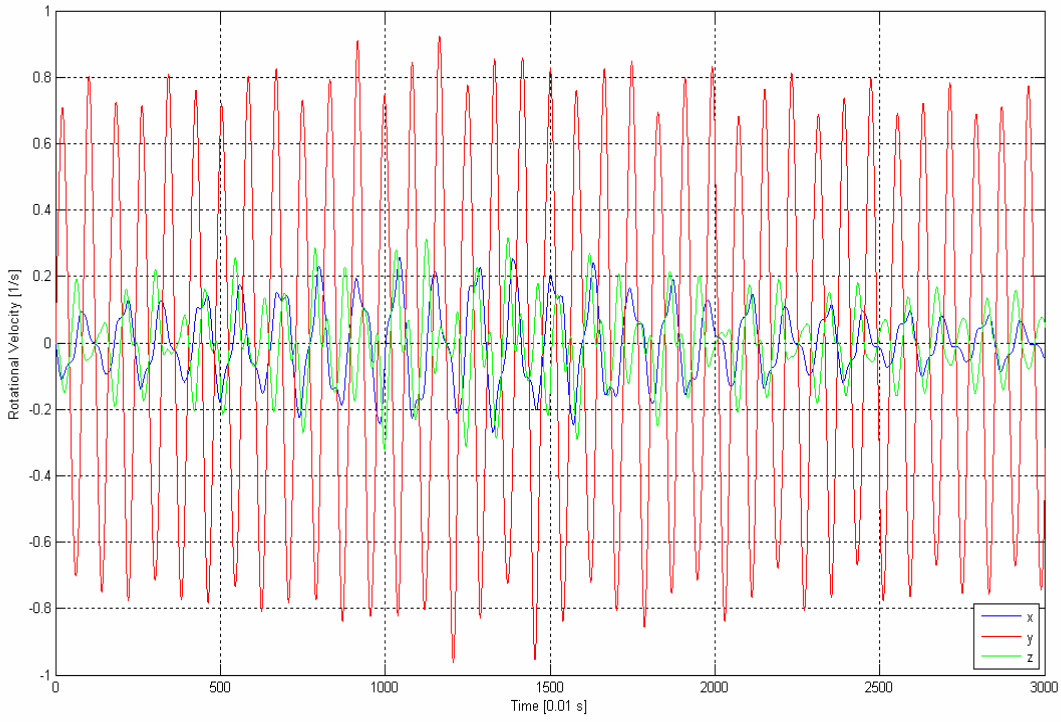

Figure 4.86 Rotational Velocity of the Body with respect to CG between [0,20]s

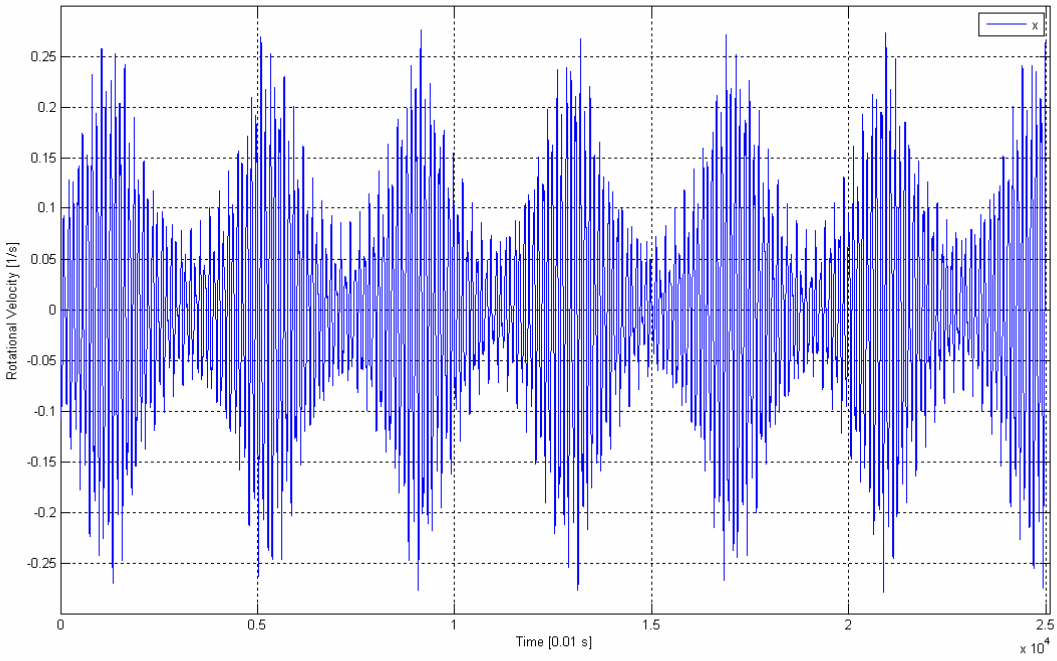

Figure 4.87 Rotational Velocity of the Body with respect to CG around x axis

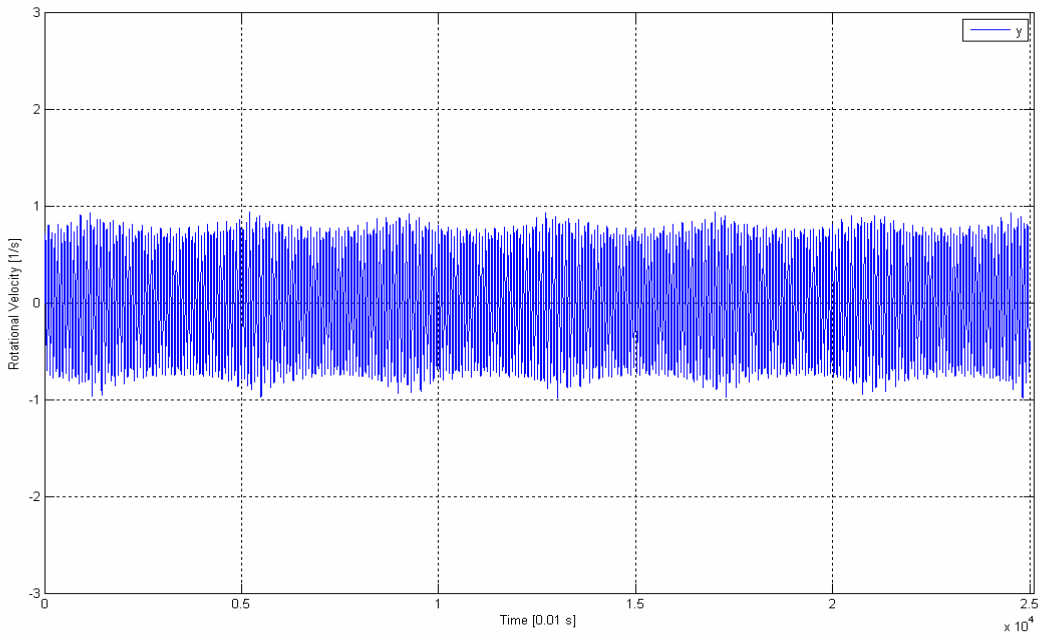

Figure 4.88 Rotational Velocity of the Body with respect to CG around y axis

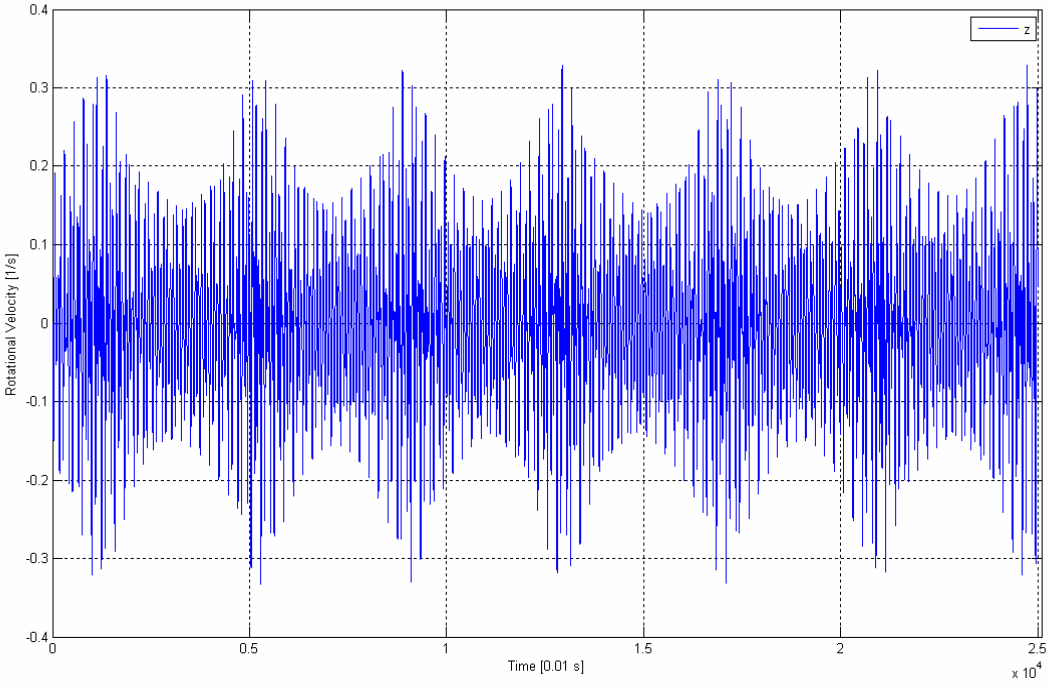

Figure 4.89 Rotational Velocity of the Body with respect to CG around z axis

4.15.2 The Results of the Identification Run for Case Study 15

Identification code calculated the following inertia tensor:

$$J = \begin{bmatrix} 1594.5 & -2.7 & 4.3 \\ -2.7 & 369.9 & 54.4 \\ 4.3 & 54.4 & 1675.4 \end{bmatrix}$$

Whereas the original tensor was:

$$J = \begin{bmatrix} 1617 & 0 & 0 \\ 0 & 365 & 70 \\ 0 & 70 & 1785 \end{bmatrix}$$

Percentage error is:

$$\%Error = \begin{bmatrix} 1.39 & \pm 2.7 & \pm 4.3 \\ \pm 2.7 & 1.34 & 22.3 \\ \pm 4.3 & 22.3 & 6.14 \end{bmatrix}$$

This case uses the same data set from the previous case except for the fact that the forcing frequency is doubled. The error on the first two diagonal elements decreased whereas the error on the yaw moment of inertia and roll/yaw product of inertia increased. Still the accuracy is acceptable for most vehicle studies.

Figure 4.90 shows the comparison of the identified system and the measured system's output measurements.

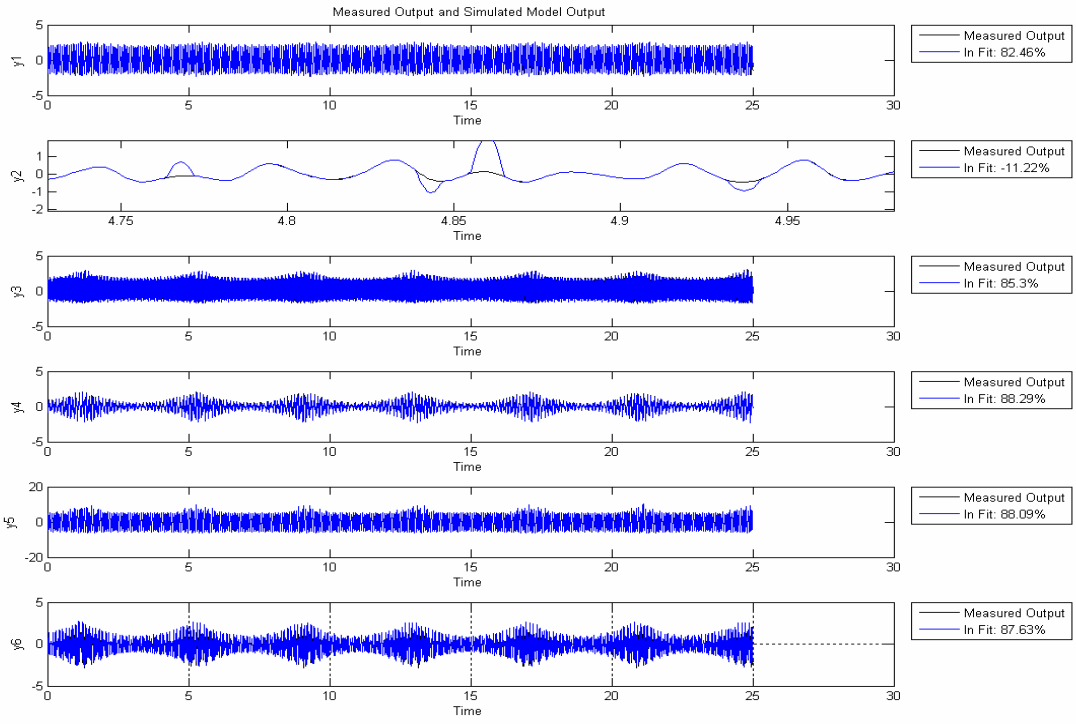

Figure 4.90 Comparison of the Identified System and the Measured System

4.16 Case Study 16

In this case the mass properties of 1998 Jeep Cherokee with one occupant and full fuel tank are used [32].

Table 4.16 Data for Case Study 16

CASE 16	
Coordinates of CG (initially) [m]	[1.6; 2.5; -2.58]
Mass [kg]	1810
Jxx [N.m^2]	2894
Jyy [N.m^2]	695
Jzz [N.m^2]	3101
Jxy [N.m^2]	0
Jxz [N.m^2]	0
Jyz [N.m^2]	102
Coordinates of Hinge Points on the Ceiling [m]	
[0;0;0]	
[4;0;0]	
[0;5.2;0]	
[4;5.2;0]	
Body Dimensions [m]	
1.6x2.5x1.75 (Rectangular Prism)	
Coordinates of Hinge Points on the Body (wrt to CG)	
[-0.8;-1.25;1.29]	
[0.8;-1.25;1.29]	
[-0.8;1.25;1.29]	
[0.8;1.25;1.29]	
Initial Conditions	
No Initial Displacement	
Applied Forces	
Force Magnitude [N]	**Point of Action (wrt CG) [m]**
200	[-0.8;-1.25;-0.46]
Frequency of Forcing [Hz]	
1.05	
Initial Guess Vector for Inertia Tensor [N.m2]	
[1000; 10; 10; 300; 40; 1000]	
Length of the Experiment [s]	**Sampling [s]**
150	0.01

4.16.1 The Results of the Experiment of Case Study 16

The resulting motion of the experiment can be observed in Figures 4.91, 4.92, 4.93, 4.94, 4.95, 4.96, 4.97, 4.98, 4.99, 4.100, 4.101, 4.102, 4.103.

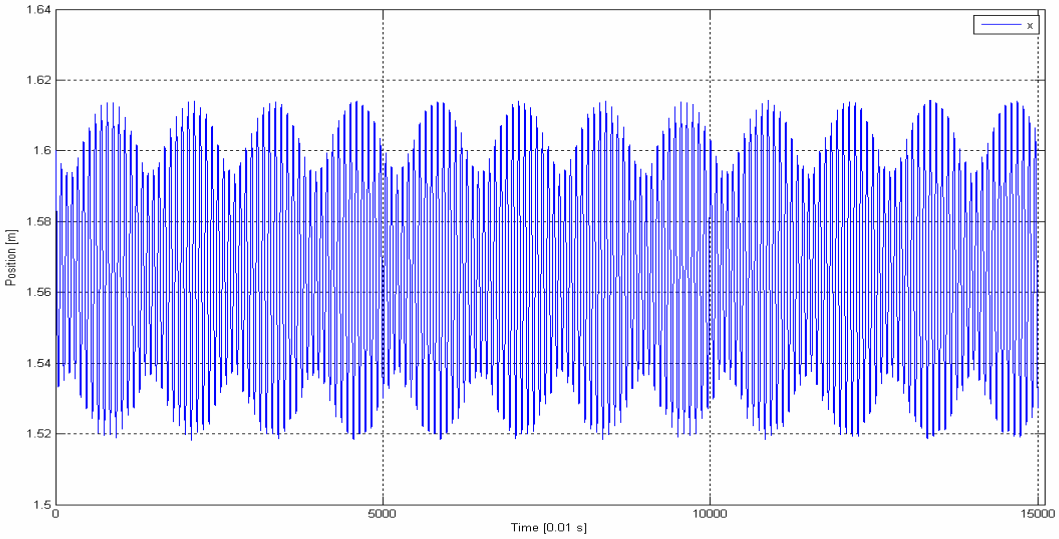

Figure 4.91 Position of x coordinate of CG

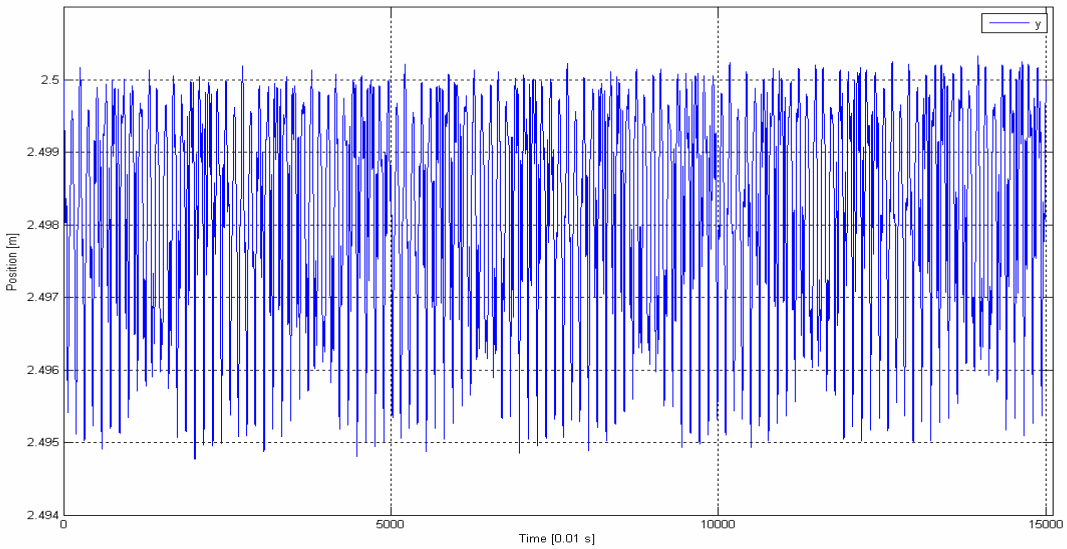

Figure 4.92 Position of y coordinate of CG

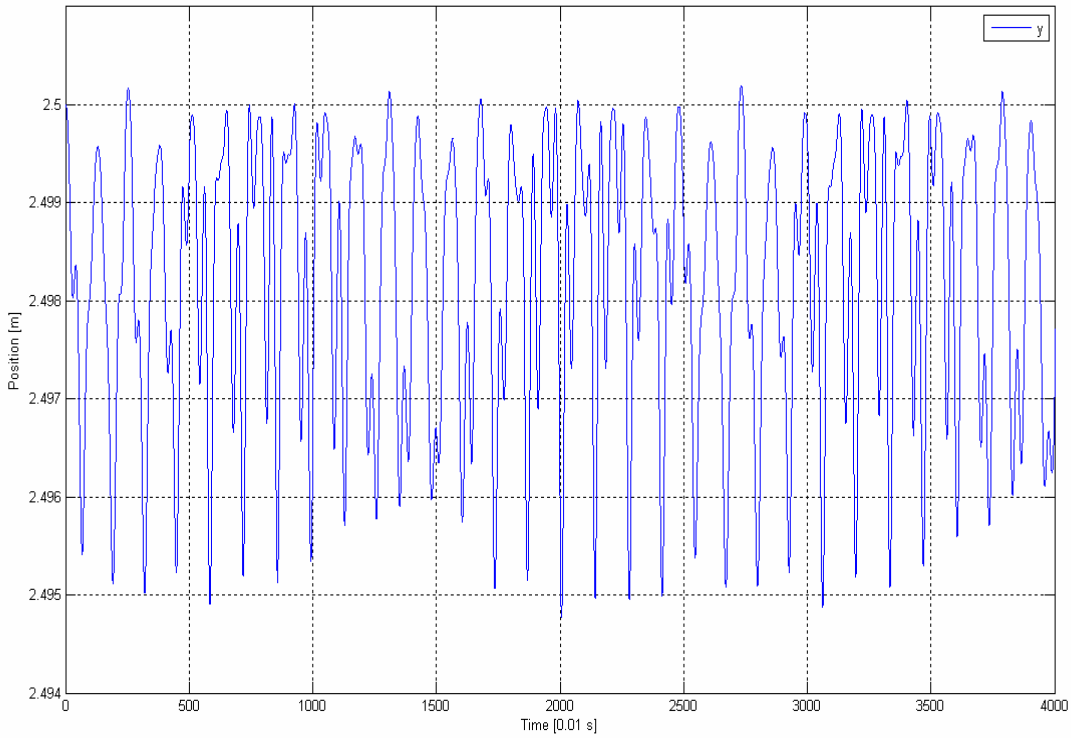

Figure 4.93 Position of y coordinate of CG between [0,40] s

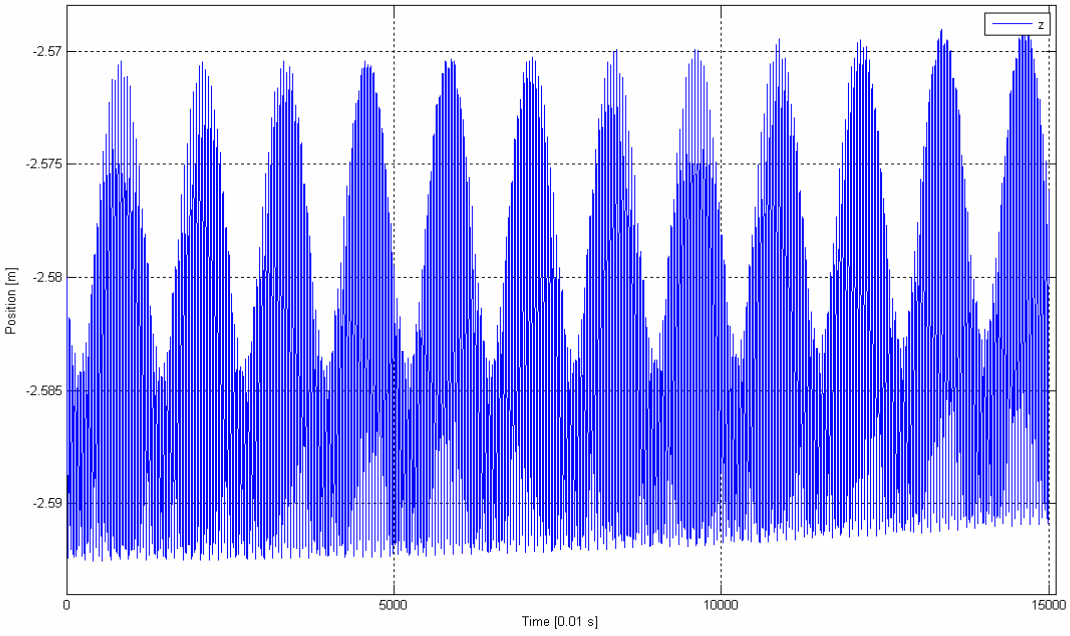

Figure 4.94 Position of z coordinate of CG

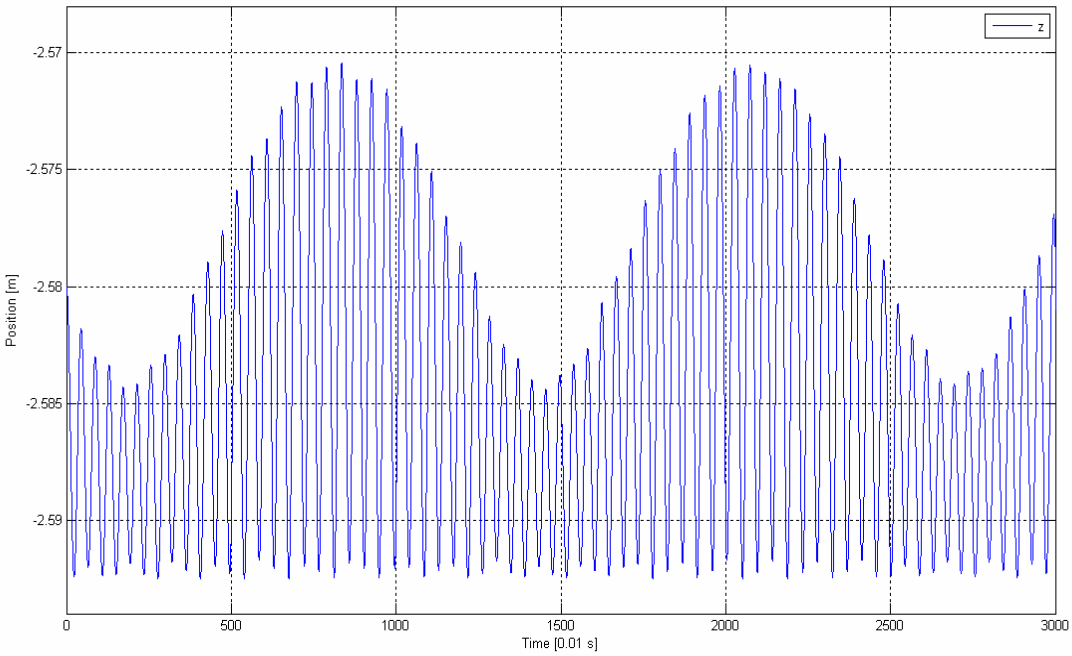

Figure 4.95 Position of z coordinate of CG between [0,30] s

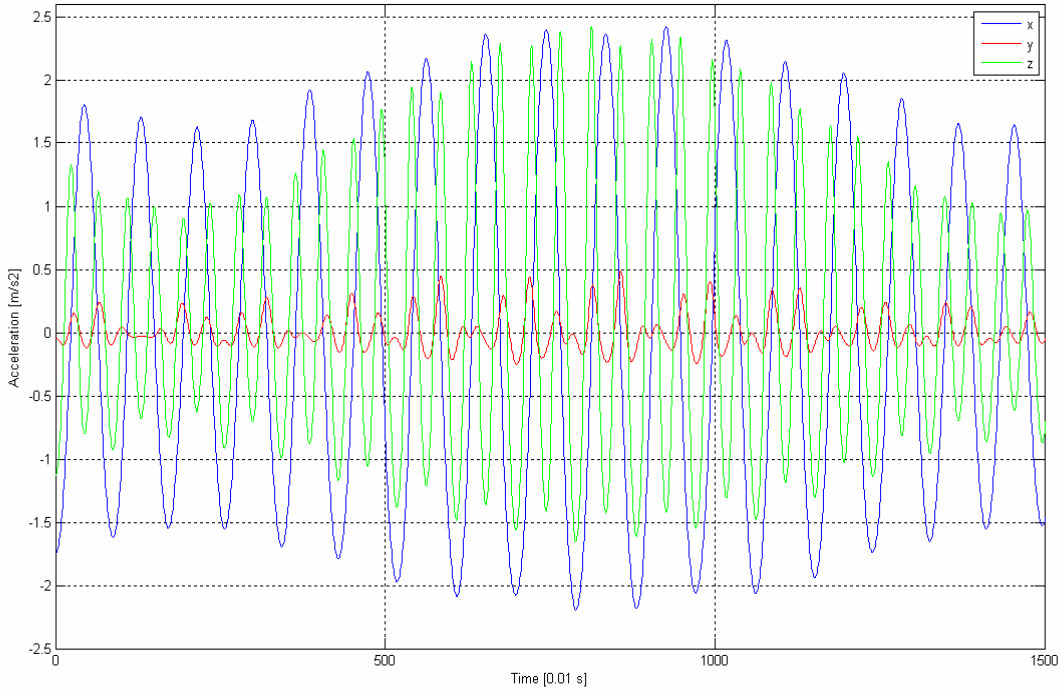

Figure 4.96 Acceleration of CG in between [0,15]s

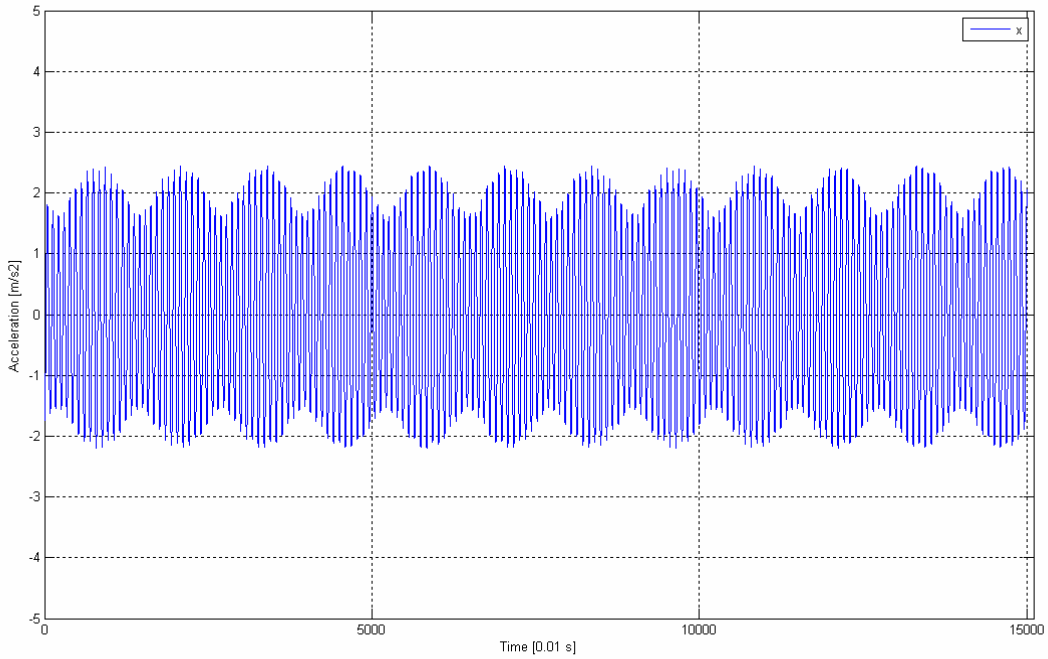

Figure 4.97 Acceleration of CG in x direction

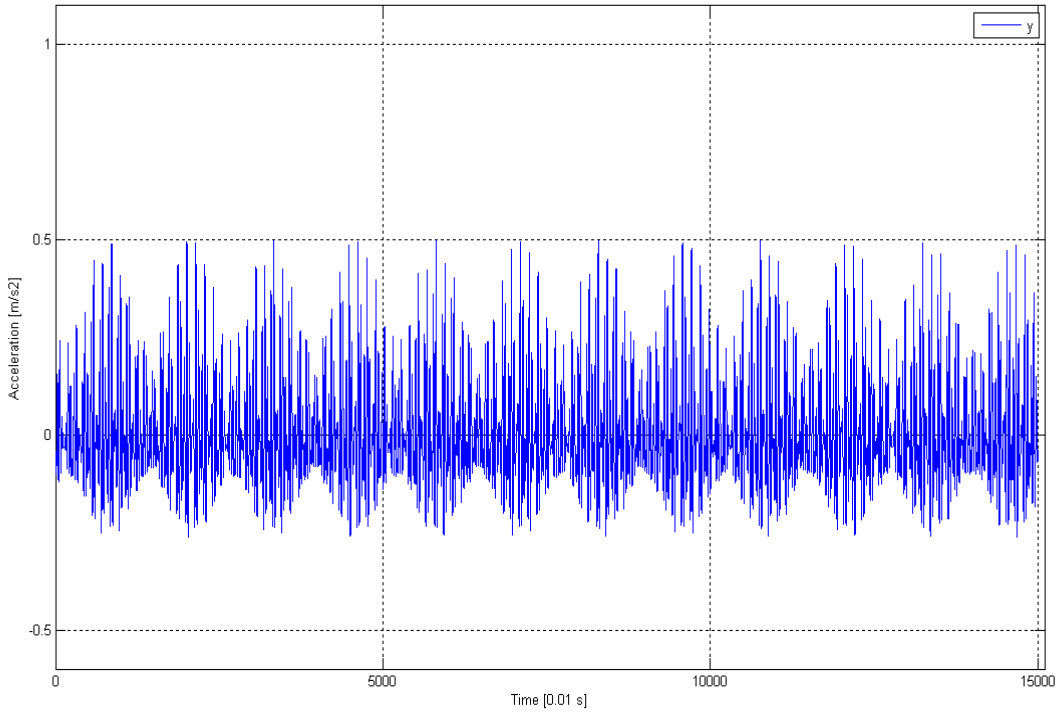

Figure 4.98 Acceleration of CG in y direction

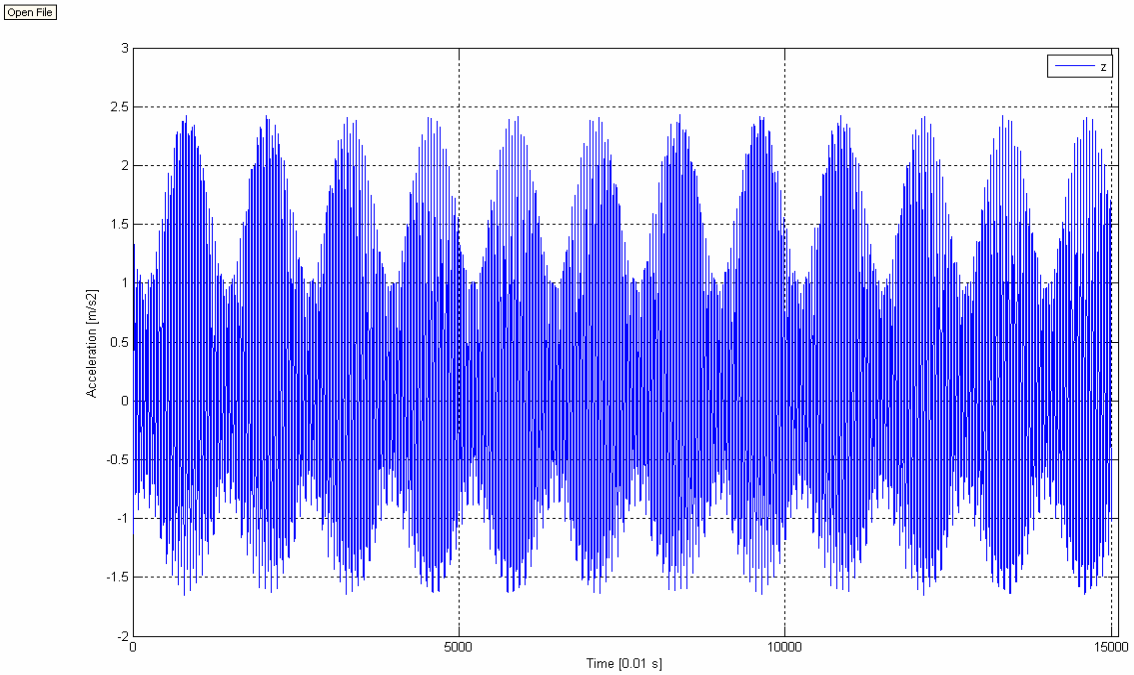

Figure 4.99 Acceleration of CG in z direction

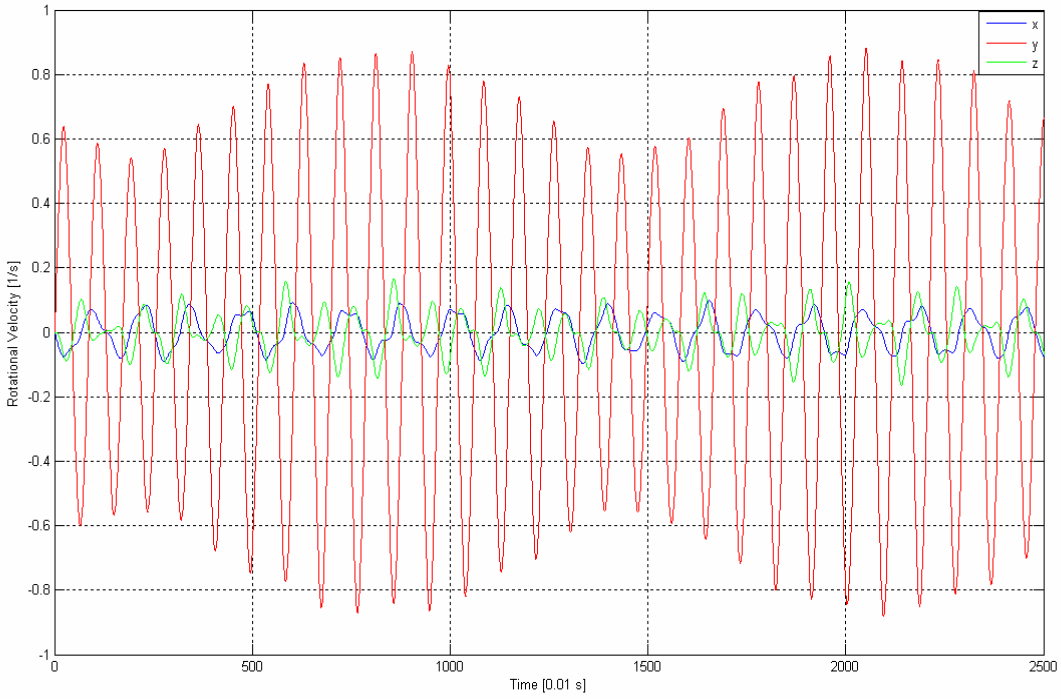

Figure 4.100 Rotational Velocity of the Body with respect to CG between [0,25]s

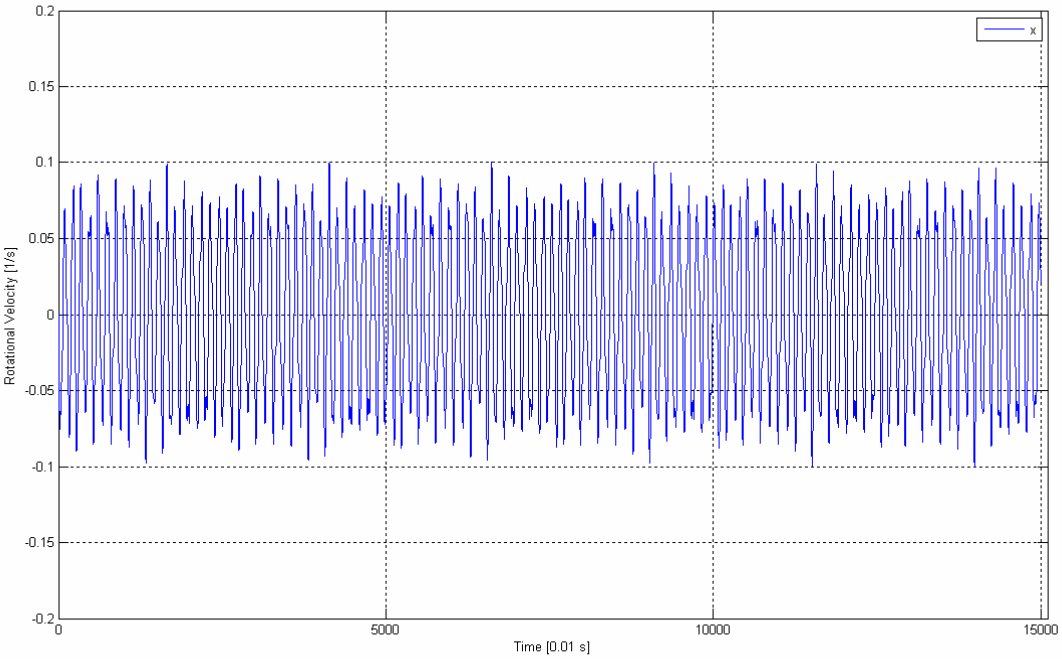

Figure 4.101 Rotational Velocity of the Body with respect to CG around x axis

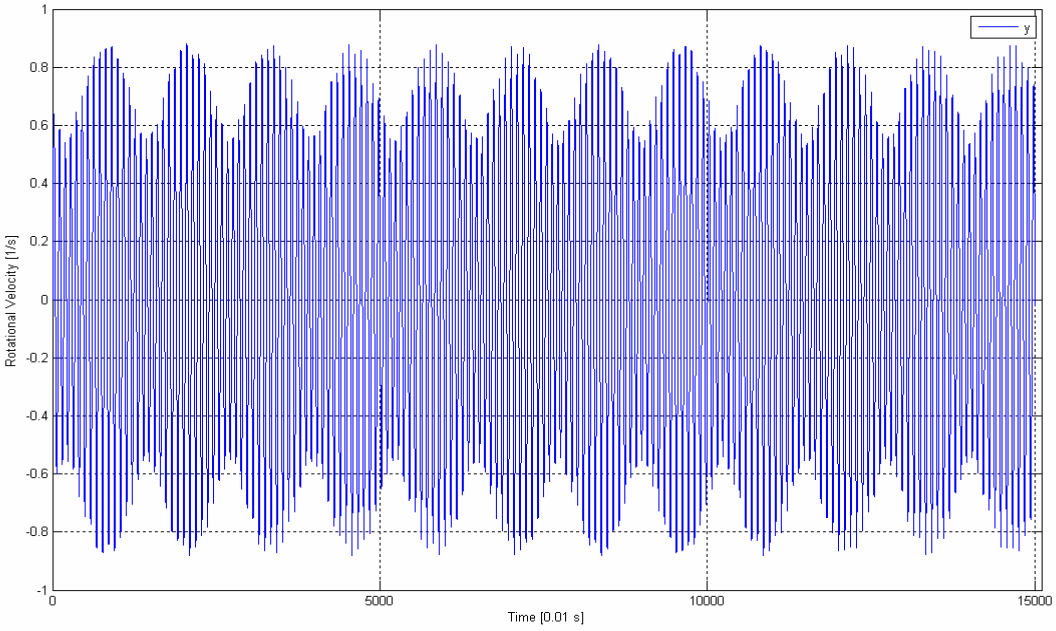

Figure 4.102 Rotational Velocity of the Body with respect to CG around y axis

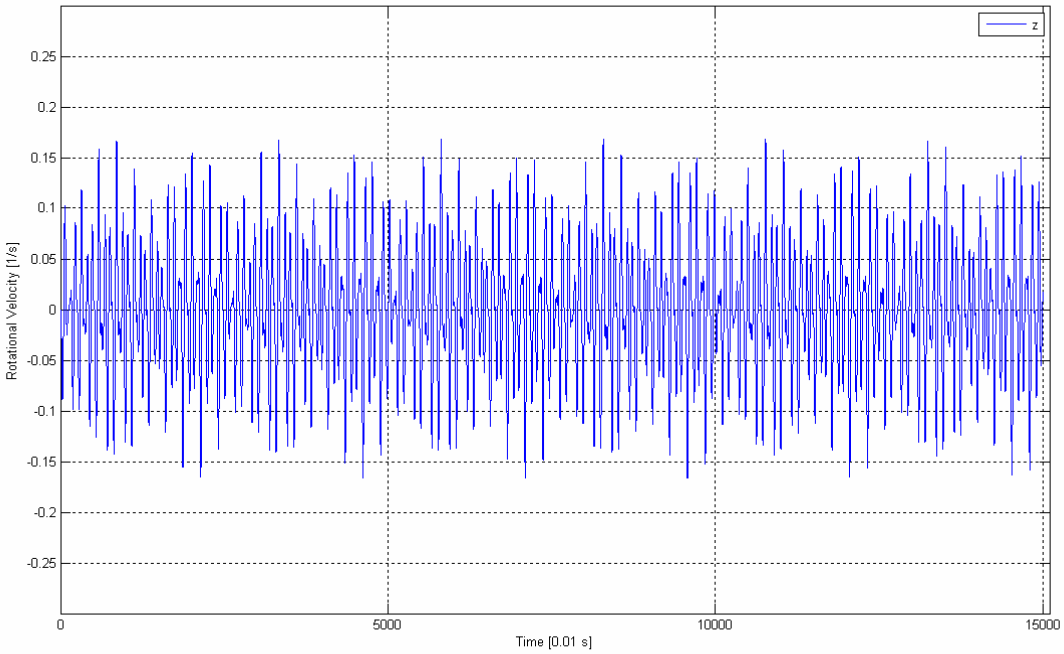

Figure 4.103 Rotational Velocity of the Body with respect to CG around z axis

4.16.2 The Results of the Identification Run for Case Study 16

Identification code calculated the following inertia tensor:

$$J = \begin{bmatrix} 2778.2 & -2.5 & 1.0 \\ -2.5 & 691.9 & 93.9 \\ 1.0 & 93.9 & 2984.8 \end{bmatrix}$$

Whereas the original tensor was:

$$J = \begin{bmatrix} 2894 & 0 & 0 \\ 0 & 695 & 102 \\ 0 & 102 & 3101 \end{bmatrix}$$

Percentage error is:

$$\%Error = \begin{bmatrix} 4.00 & \pm 2.5 & \pm 1.0 \\ \pm 2.5 & 0.45 & 7.94 \\ \pm 1.0 & 7.94 & 3.75 \end{bmatrix}$$

The vehicle used in this case is Jeep Cherokee, and is available on Turkish market. The cas is a SUV class vehicle. Accuray of all components of the inertia tensor are acceptable to used on other vehicle dynamics studies.

Figure 4.104 shows the comparison of the identified system and the measured system's output measurements.

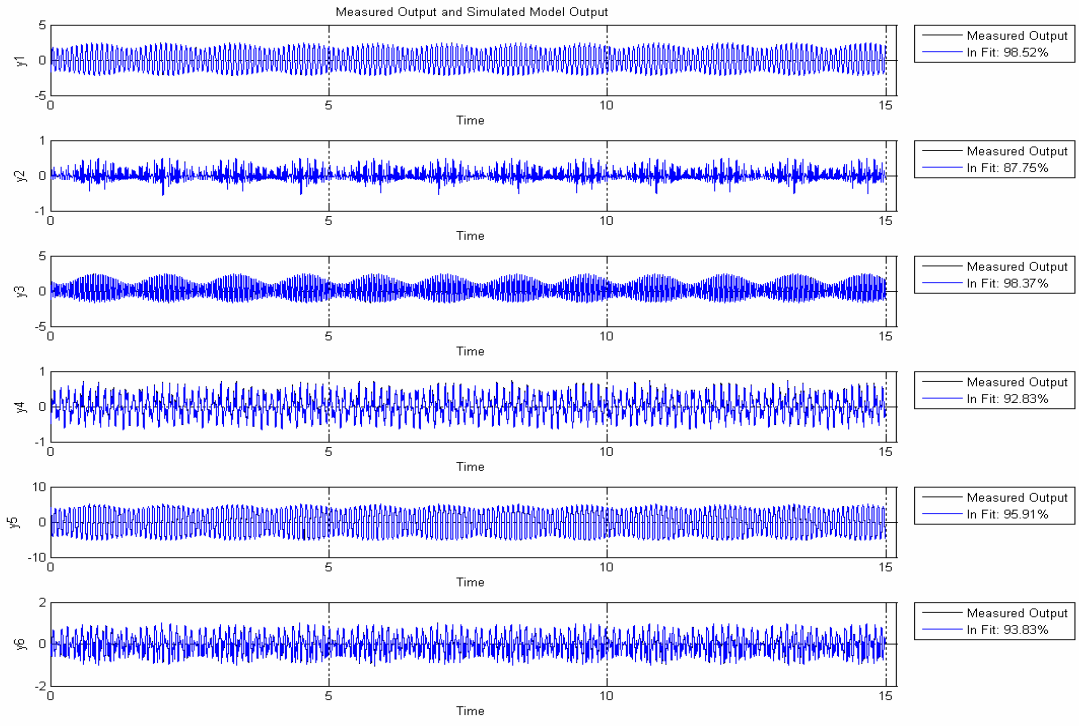

Figure 4.104 Comparison of the Identified System and the Measured System

4.17 Case Study 17

In this case the mass properties of 1998 Jeep Cherokee with one occupant and full fuel tank are used [32].

Table 4.17 Data for Case Study 17

CASE 17	
Coordinates of CG (initially) [m]	[1.6; 2.5; -2.58]
Mass [kg]	1810
Jxx [N.m^2]	2894
Jyy [N.m^2]	695
Jzz [N.m^2]	3101
Jxy [N.m^2]	0
Jxz [N.m^2]	0
Jyz [N.m^2]	102
Coordinates of Hinge Points on the Ceiling [m]	
[0;0;0]	
[4;0;0]	
[0;5.2;0]	
[4;5.2;0]	
Body Dimensions [m]	
1.6x2.5x1.75 (Rectangular Prism)	
Coordinates of Hinge Points on the Body (wrt to CG)	
[-0.8;-1.25;1.29]	
[0.8;-1.25;1.29]	
[-0.8;1.25;1.29]	
[0.8;1.25;1.29]	
Initial Conditions	
No Initial Displacement	
Applied Forces	
Force Magnitude [N]	**Point of Action (wrt CG) [m]**
200	[-0.8;-1.25;-0.46]
Frequency of Forcing [Hz]	
1.05	
Initial Guess Vector for Inertia Tensor [N.m2]	
[1000; 10; 10; 300; 40; 1000]	
Length of the Experiment [s]	**Sampling [s]**
100	0.01

4.17.1 The Results of the Experiment of Case Study 17

The resulting motion is the same as that of Case Study 16 in first 100 seconds.

4.17.1 The Results of the Identification Run for Case Study 17

Identification code calculated the following inertia tensor:

$$J = \begin{bmatrix} 2778.3 & -1.9 & 2.2 \\ -1.9 & 690 & 94.4 \\ 2.2 & 94.4 & 2985.0 \end{bmatrix}$$

Whereas the original tensor was:

$$J = \begin{bmatrix} 2894 & 0 & 0 \\ 0 & 695 & 102 \\ 0 & 102 & 3101 \end{bmatrix}$$

Percentage error is:

$$\%Error = \begin{bmatrix} 4.0 & \pm 1.9 & \pm 2.2 \\ \pm 1.9 & 0.72 & 7.45 \\ \pm 2.2 & 7.45 & 3.74 \end{bmatrix}$$

Same data set and the same forcing in the pervious case is used, but the time interval used in identification is shortened. The amount of error for all elements are nearly the same as the last case.

Figure 4.105 shows the comparison of the identified system and the measured system's output measurements.

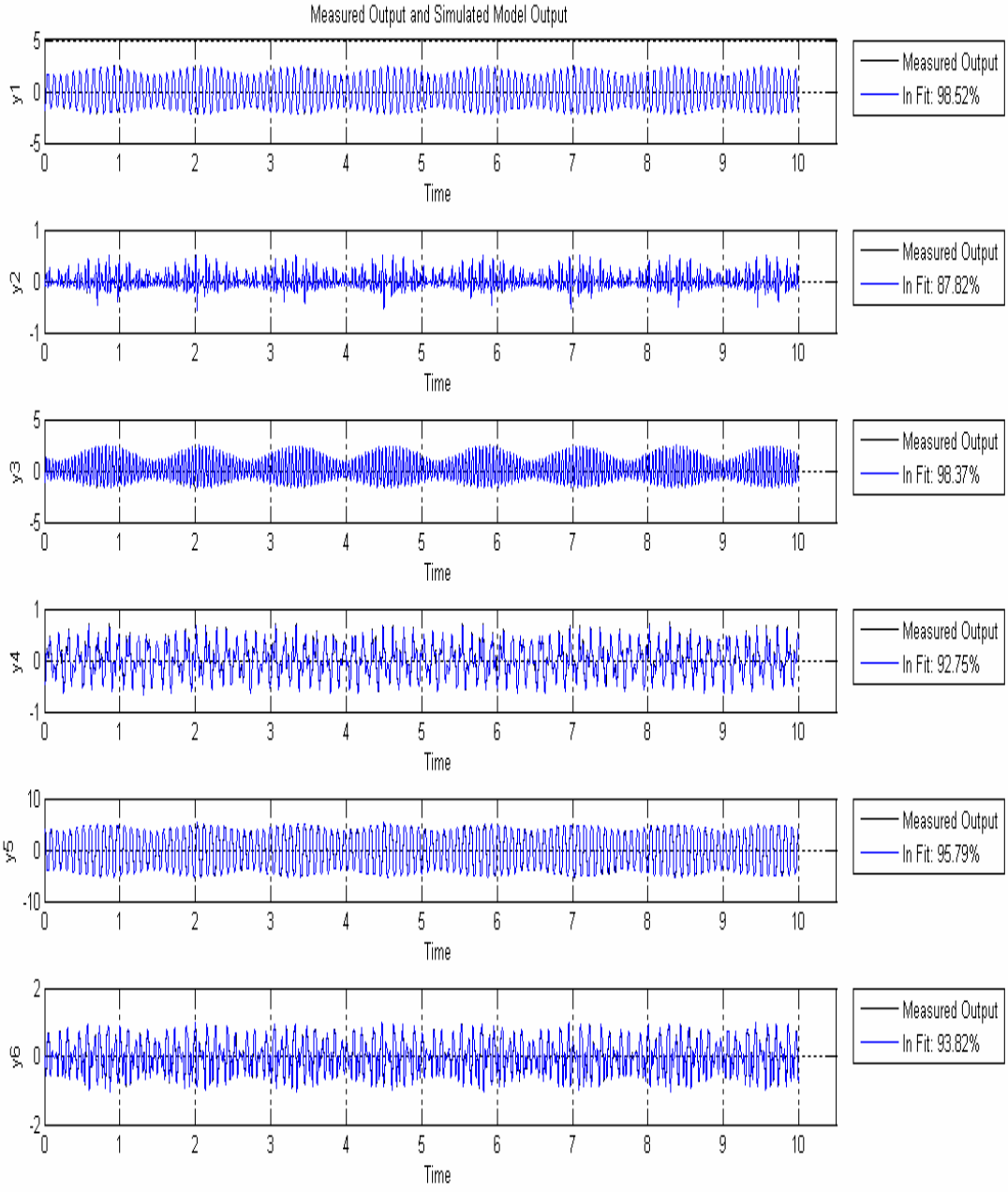

Figure 4.105 Comparison of the Identified System and the Measured System

4.18 Case Study 18

In this case study, the data of Honda Civic is used and is the same data set used in case studies 14 and 15. However the forcing is applied in yz and xz planes to investigate the effects of different excitations.

The error obtained for harmonic excitation of 200 N at 1.05 Hz in xz plane is:

$$\%Error = \begin{bmatrix} 5.78 & \pm 1.78 & \pm 3.93 \\ \pm 1.78 & 0.14 & 10.47 \\ \pm 3.93 & 10.47 & 3.16 \end{bmatrix}$$

The error obtained for harmonic excitation of 200 N at 1.05 Hz in yz plane is:

$$\%Error = \begin{bmatrix} 4.02 & \pm 2.64 & \pm 2.0 \\ \pm 2.64 & 0.03 & 11.86 \\ \pm 2.0 & 11.86 & 3.31 \end{bmatrix}$$

When compared to case study 14 (200 N forcing in xy plane at 1.05 Hz) there is no considerable improvement in accuracy.

The error obtained for harmonic excitation of 200 N at 2.1 Hz in xz plane is:

$$\%Error = \begin{bmatrix} 1.76 & \pm 3.87 & \pm 11.01 \\ \pm 3.87 & 1.15 & 20.15 \\ \pm 11.01 & 20.15 & 4.87 \end{bmatrix}$$

The error obtained for harmonic excitation of 200 N at 1.05 Hz in yz plane is:

$$\%Error = \begin{bmatrix} 3.20 & \pm 2.92 & \pm 10.03 \\ \pm 2.92 & 1.22 & 22.47 \\ \pm 10.03 & 22.47 & 7.13 \end{bmatrix}$$

When compared to case study 14 (200 N forcing in xy plane at 2.1 Hz) the same can be said for the 1.05 Hz case.

It is concluded that changing the direction of the forcing does not effect the accuracy of the results considerably.

4.19 Discussion of Case Study Results

Seventeen case studies were studied in total. The first nine case studies demonstrate the evolution of the development stage of the experimental set up, whereas the last eight cases are run with data of commercially available vehicles.

In general, it is seen that the measurement of external forces have direct effect on the convergence. For the linear forcing cases, the best results were obtained in the first two cases, where the applied forces were measured. However applying a translational force is not practical when compared to the application of a harmonic forcing using an unbalanced mass – motor assembly.

All 6 elements of the inertia matrix are identified with good accuracy when the applied forces are measured as in cases 1 and 2. The highest error was 8 % in roll/yaw product of inertia value.

In the third case, where applied forces were not measured, all the elements of the inertia tensor except J_{yz} and J_{zz} are measured up to an acceptable error interval. However the error came out to be 12.6 % for J_{yz} and 30 % for J_{zz}. Although 12.6 % error can be considered to be reasonable, 30 % error in a diagonal element of the inertia tensor is unacceptable, since diagonal elements can be measured using other simpler tehniques with very high accuracy.

It is concluded that; these errors can be decreased to an acceptable level by estimating the forces; instead of measuring them. In this case, the accuracy of the estimation will have a direct effect on the error. However, it is seen that even without measuring the forces and without estimating them, four of the six elements of the tensor are identified with high accuracy.

In case 4; only the data points after the application of the forces were considered, i.e. no forces were applied in the part of the data used for the identification. In this case only J_{zz} was measured with good accuracy. Error in the other diagonal elements came out to be less than 13.5 %. As mentioned above, this amount of error is considered high for diagonal elements.

The technique used in case 4 can be considered to be used in conjunction with case 3, which gives good accuracy for J_{xx} and J_{yy} (with maximum error 0.37 %) in order to measure diagonal elements.

In case 5; a convergence map was plotted. According to this plot; it can be seen that a reasonable degree of convergence can even be achieved by measuring only the second applied force; and running

the identification code with the data starting from a data point just after the first force. However vast regions of divergence can also be observed for certain intervals of starting data points.

In case 8; the experiment was started from another position according to the findings of the 7th case. No external force was applied. 10 seconds of motion was recorded with 0.01 s sampling. In this case, good level of accuracy was achieved in the diagonal terms, with a maximum error of 3.76%.

According to the results of the 8th case, it can be concluded that diagonal terms can be identified with good accuracy without using externally applied and measured forces, but starting with an initial displacement. However it must be noted that in this case unacceptably high errors are observed for the off-diagonal elements.

In case 9; a sinusoidal forcing is applied and measured. The error in results are less than 0.5% in diagonal terms; and in acceptable range for off-diagonal terms.

Interestingly, when case 1 was experimented with longer time range, it was observed that although convergence was achieved, the accuracy of the results decreased. Best results were obtained with a data set total of 7 seconds (i.e. only 1.9 seconds after the release of the second external force) whereas accuracy decreased regularly with 10, 15, 20 and 50 seconds time range. However, since the system has no damping, the motion is always the same, no matter how long the time range is. The only difference is that with longer time range; more oscillations are observed.

The increase in accuracy as the time range decreases and the end of the data set approaches to the release of the second external forcing is most probably because of the fact that the mathematical model used in the identification is a force based model. Although the cable forces are considered as external forces in the system model; the externally applied forces are the driving force of the experiment. Thus, as the collected data has less percentage information about the user applied force, worse results are obtained. The enforced motion of the body is more critical than the free motion of the body after the forcing is released.

This argument is supported by the 9th case as well. In this case the forces are applied continuously throughout the experiment. It is observed that as the length of the experiment increases; the accuracy, especially for the off-diagonal terms get better. It can be said that 9th case is the most applicable and probably the most feasible case for real life application.

In the cases 10-17; real data sets are used in order to verify the identification technique. The technique gives low percentage error for diagonal elements for every case. However the percentage error for the identified off-diagonal element is found to be higher than 15 % for certain cases. In these cases, the value of the off-diagonal element happens to be very low, which increases the percentage error despite the fact that absolute error between the identified and the real values of the parameter is acceptable.

In cases 10 and 11; the same vehicle was excited with an harmonic forcing of same frequency but different amplitudes to observe the effect of different forcings. In case 11, amplitude was doubled.

Although both of the identified tensors were found to be satisfactory, the results of the case 10 is slightly more accurate.

In cases 12,13 and 14, 15 the same vehicle was subjected to the forcings with same amplitudes but different frequencies, in order to observe if the frequency effects the identification process. In these cases accurcy of the identified tensor was better for the lower frequency cases. It is clear that the frequency of the forcing has a strong effect on the results.

In case 18, forcings in different directions are applied to investigate the effects of excitation in other planes. It is concluded that, although percentage error was decreased in certain elements of the tensor; there was no great improvement in overall accuracy.

CHAPTER 5

DISCUSSION AND CONCLUSION

5.1 Discussion

In this study, an simulink model of an experimental set up and a set of codes were developed in order to identify the mass properties of vehicles to be used in further vehicle dynamics research.

The simulink model simulates a certain experimental set up, which consists of a frame which is suspended by four steel cables from the ceiling of the laboratory. The body, the mass properties of which is to be measured is fixed into the frame.

The experimental set up in its statical equilibrium position is used to calculate the location of center of gravity of the vehicle. For this process, two experiments are made; one with a dummy mass with known center of gravity location, fixed to a known position on the frame.

In order to identify the inertia tensor of the vehicles, the experimental set up must be excited and the resulting motion must be recorded. After several case studies it is decided to use an unbalanced mass – motor assembly to excite the system. Translational accelerations and rotational velocities of the center of gravity are to be measured using accelerometers and gyroscopes. The tensions on the steel cables

and the harmonic forcing which is applied to a known position on the body must also be measured. Using the recorded motion data, the position and the orientation history of the body and the force vector histories are calculated in order to obtain the generalised force vector history.

The equation of motion of the system is derived using Newton's Second Law of Motion and a state space model is obtained using these equations. Elements of the mass moment of inertia matrix are introduced as free parameters of this model. Measured motion data and generalised force vector history are fed as input to the identification code.

In real life application instead of the experiment simulation, the actual experiment is going to be made. Thus the measured data must be transfered into MATLAB® workspace. Then the codes must be run in following order: Position tracking code, preprocessing code and identification code. Note that the user must have enough knowledge on the code and system dynamics to update the code according to possible changes in the experimental set up or measured data.

The case studies in Chapter 4 are presented in the order they were studied. They demonstrate the development of the study. In the first nine cases, the most feasible and applicable method is sought, whereas in the last ones, the decided method is further tested and verified.

The resulting identification code of this study has some limitations, one of which is that the code works only with one specific experimental configuration. The code must be modified in case of a change in number of suspending cables or a change in actuating

method. Also the successful identification of the inertia parameters and the convergence of the code is strongly dependent on the initial guess vector. Thus the user should use sensible figures for the initial guess vector for ensurence of the convergence. Different estimation methods can be found in the literature [18].

5.2 Conclusion

In conclusion, the major objective of this thesis, which is to develop a code and methodology that will identify the mass properties of vehicles using a specified test rig, for further vehicle dynamics studies, is achieved successfully. For this purpose, a methodology which provides a successful approach to the problem of modelling of the experimental system is derived. The center of mass is calculated using the equilibrium position of the set up. A Simulink model is developed to simulate the dynamic response of the experiment.

Final configuration of the experimental set up employs an unbalanced mass – motor assembly. This configuration is decided because of the better accuracy it offers and relatively easy application when compared to linear forcing case. The experimental set up consists of a carrying frame, four steel cables, three accelerometers, three gyroscopes, four load cells, and an unbalanced mass-motor assembly with two load cells to measure the forcing it exerts on the body.

Different cases were studied, six of which were taken from real life vehicles. The results of the experiment simulations were used as input for identification code. The results are found to be highly satisfactory both for diagonal elemnts and off-diagonal elements.

Although it has some limitations as stated above, designed identification code is a very useful tool and will satisfy the needs of the further vehicle dynamics studies. By using this code, the mass properties of vehicles will be obtained in shorter time when compared to conventional natural frequency methods.

5.3 Future Work

Some or all of the above mentioned limitations may be overcome in the future work, since the foundations of the design methodology is derived successfully in this thesis.

First limitation, need to use Matlab, can be removed by coding the identification code on a different development platform and making it a stand alone application. However, this would require development of the optimization routines instead of the MATLAB® functions used in this study. Other functions of the identification code can be directly used or modified depending on the selected development platform. The development platform can be a high level language such as Delphi or Visual Basic.

Detailed design and optimization of the test rig is another subject and may be examined in a future M.Sc. study.

The error introduced by the unbalanced mass – motor assembly is rather small and was neglected in this study. However since the position of the motor is fixed on the frame and the motion of the unbalanced mass is easy to track, its effect on the center of mass and inertia can be estimated, neglecting the change of inertia with time introduced by the rotating mass or remodelling the system with

a time dependent inertia model. The accuracy of the method would increase considerably in this case.

Another future work may be the addition of a module to estimate the natural frequencies of the experimental model and a study to investigate the optimum rotational speed for the unbalanced mass – motor assembly using the natural frequency data. According to the findings of this thesis; changing frequency of the loading leads to different results in terms of accuracy.

REFERENCES

[1] Erdogan, L, Guenther, D.A., “Suspension Parameter Measurement Using Side-Pull Test to Enhance Modeling of Vehicle Roll”, SAE 1999-01-1323

[2] Sharp, R.S., “Application of Multi-body Computer Codes to Road Vehicle Dynamics Modelling Problems”, Proc. of the Inst. of Mech. Eng., Part D: Journal of Automobile Eng. 208 (1), pp. 55-61, 1994

[3] Limebeer, D.J.N., Sharp, R.S., “Bicycles, Motorcycles, and Models”, IEEE Control Systems Magazine 26 (5), pp. 34-61, 2006

[4] Heydinger, G.J., Bixel, R.A., Durisek, N.J., Yu, E., Guenther, D.A., “Effects of Loading on Vehicle Handling”, SAE Special Publications 1361, pp. 87-95, 1998

[5] Almeida, R.A.B., Urgueria, A.P.V., Maia, N.M.M., “Identification of Rigid Body Properties from Vibration Measurements”, Journal of Sound and Vibration 299 (4-5), pp. 884-899, 2007

[6] Doniselli, C., Gobbi, M., Mastinu,G., “Measuring the Inertia Tensor of Vehicles”, Vehicle System Dynamics Supplement 37 pp. 301-313, 2002

[7]Mastinu, G., M. Gobbi, Miano, C.M., “The Influence of the Body Inertia Tensor on the Active Safety of Ride Comfort of Road Vehicles”, SAE-2002-01-2058

[8] Buyanov, E.V., “Method and Apparatus for Accurate Determination of the Inertia Tensor of a Solid Body”, Measurement Techniques 31 (12), pp. 1181-1184, 1989

[9] Buyanov, E.V., “Device for Measuring the Inertia Tensor of a Rigid Body”, Measurement Techniques 34 (6), pp. 585-589, 1991

[10] Chrstos, J.P., Heydinger, G.J., Guenther, D.A., “Error Analysis Techniques Applied to Inertial Parameter Measurement”, American Society of Mechanical Engineers, Dynamic Systems and Control Division (Publication) DSC 44, pp. 97-112, 1992

[11] Durisek, N.J., Heydinger, G.J., Chrstos, J.P., Guenther, D.A., “Non-Rigid Body Product of Inertia Measurement: Application to Land Vehicles”, American Society of Mechanical Engineers, Dynamic Systems and Control Division (Publication) DSC 54, pp. 375-386, 1994

[12] Da Lio, M., Doria, A., Lot, R., “A Spatial Mechanism for the Measurement of the Inertia Tensor: theory and Experimental Results”, Journal of Dynamic Systems, Measurement and Control, Transactions of the ASME 121 (1), pp. 111-116, 1999

[13] Pandit, S.M., Hu, Z.-Q., “Determination of Rigid Body Characteristics from Time Domain Modal Test Data”, Journal of Sound and Vibration 177 (1), pp. 31-41, 1994

[14] Conti, P., Bretl, J., “Mount Stiffnesses and Inertia Properties from Modal Test Data”, Journal of Vibration, Acoustics, Stress, and Reliablity in Design 111 (2), pp. 134-138, 1989

[15] Gentile, A., Mangialardi, L., Mantriota, G., Trentadue, A., “Measurement of the Inertia tensor: An Experimental Proposal”, Measurement: Journal of the International Measurement Confederation 14 (3-4), pp. 241-254, 1995

[16] Fregolent, A., Sestieri, A., “Identification of Rigid Body Inertia Properties from Experimental Data”, Mechanical Systems and Signal Processing 10 (6), pp. 697-709, 1996

[17] Serban,R., Freeman, J.S., Negrut, D., “Parameter Identification for Multibody Dynamic Systems”, Proceedings of ASME DETC’97, 1997

[18] MacInnis, D.D., Cliff, W.E., Ising, K.W., “A Comparison of Moment of Inertia Estimation Techniques for Vehicle Dynamics Simulation”, SAE-970951

[19] Stebbins, M., Blough, J., Shelley, S., Brown, D., “Estimation of a Structure’s Inertia Properties Using a Six-Axis Load Cell”, SAE 971957

[20] Metz, D., Akouris, C.K., Agney, C.S., Clark, M.C., “Moments of Inertia of Mounted and Unmounted Passenger Car and Motorcycle Tyres”, SAE 900760

[21] Huang, M., “Vehicle Crash Mechanics” pp.370-372, CRC Press, 2002

[22] Venture, g., Bodson, P., Gautier, M., Khalil, W., “Identification of the Dynamic Parameters of a Car”, SAE 2003-01-1283

[23] Andreatta, D.A., Heydinger, G.J., Bixel, R.A., Coovert, D.A., “Inertia Measurements of Large Military Vehicles”, SAE 2001-01-0792

[24] Allen, R.W., Klyde, D.H., Rosenthal, T.J., Smith, D.M., “Estimation of Passenger Vehicle Inertial Properties and Their Effect on Stability and Handling”, SAE 2003-01-0966

[25] Previati G., Mastinu, G., Gobbi, M., Piccardi, C., Bolzoni, L., Rinaldi, S., “A New Test Rig for Measuring the Inertia Properties of Vehicles and Their Subsystems”, IMECE2004-60903

[26] Bixel, R.A., Heydinger, G.J., Guenther, D.A., Novak, S.J., “Sprung/Unsprung Mass Properties Determination without Vehicle Disassembly”, SAE-960183

[27] Rizer, A.L., Albery, C.B., Anderson, B.A., “Comparison pf Measured and Predicted Human Whole-Body Inertial Properties”, SAE-973332

[28] Niebergall, M., Hahn, H., “Identification of the Ten Inertia Parameters of a Rigid Body”, Nonlinear Dynamics 13 (4), pp. 361-372, 1997

[29] Baruh, H., “Analytical Dynamics”,WCB/McGraw Hill, 1999

[30] Shabana, A.A., “Dynamics of Multibody Systems”, Cambridge University Press, 2nd Edition, 1998

[31] Garrott, W.R., “Measured Vehicle Inertial Parameters – NHTSA’s Data Through September 1992”, SAE-930897

[32] Bixel, R.A., Heydinger, G.J., Pyne, M., Garrott, W.R., Howe, J.G., Guenther, D.A., “Measured Vehicle Inertial Parameters – NHTSA’s Data Through November 1998”, SAE 1999-01-1336

[33] Niebergall, M., Hahn, H., Development of a Measurement Robot for Identifying all inertia parameters of a rigid body in a single experiment”, IEEE Transactions on Control Systems Technology 9 (2), pp. 416-423, 2001

[34] Ljung,L., “Prediction Error estimation Methods”, Rep. LITH-ISY-R-2365, Department of Electrical Engineering, Linköping University, Sweden, 2001

[35] Serban,R., Freeman, J.S., “Identification and Identifiability of Unknown Parameters in Multibody Dynamic Systems”, Multibody System Dynamics 5: 335-350, 2001

[36] Floret-Pontet, F, Lamnabhi-Lagarrigue, F, “Parameter Identification and State Estimation dor Continuous-time Nonlinear Systems”, Proceedings of the American Control Conference, Anchorage, AK May 8-10, 2002

[37] Moore, J.B., Weiss, H., “Recursive Prediction Error Methods for Adaptive Estimation”, IEEE Transactions on Systems, Man, and Cybernetics, Vol. Smc-9, No. 4, April 1979

[38] Zhang, Z., “Parameter Estimation Techniques: A Tutorial with Application to Conic Fitting”, INRIA, No 2676, October 1995

[39] Vahidi, A., Stefanopoulos, A.G., Wang, X., Tsao, T.C., “Experimental Verification of Discretely Variable Compression Braking for Heavy Duty Vehicles: Final Report”, California PATH Research Method, UCB-ITS-PRR-2004-33

[40] Pizarro, O., Sbarbaro, D., “Parameter Subset Identification by Recursive Least Square”, Proceedings of the American Control Conference, Volume 6, Issue, 31-26 June 1998, 2590-2591, vol. 6

[41] Schwanz, R.C., Wells, W.R., “Identification of Aeroelastic Parameters Using a Recursive Sequential Least Squares Method”, AIAA-1980-1634

[42] Ljung,L., “System Identification: Theory for the User”, Prentice Hall, 1987

[43] Ljung, L., “System Identification Toolbox 7 User’s Guide”, Mathworks, 2007

APPENDIX A

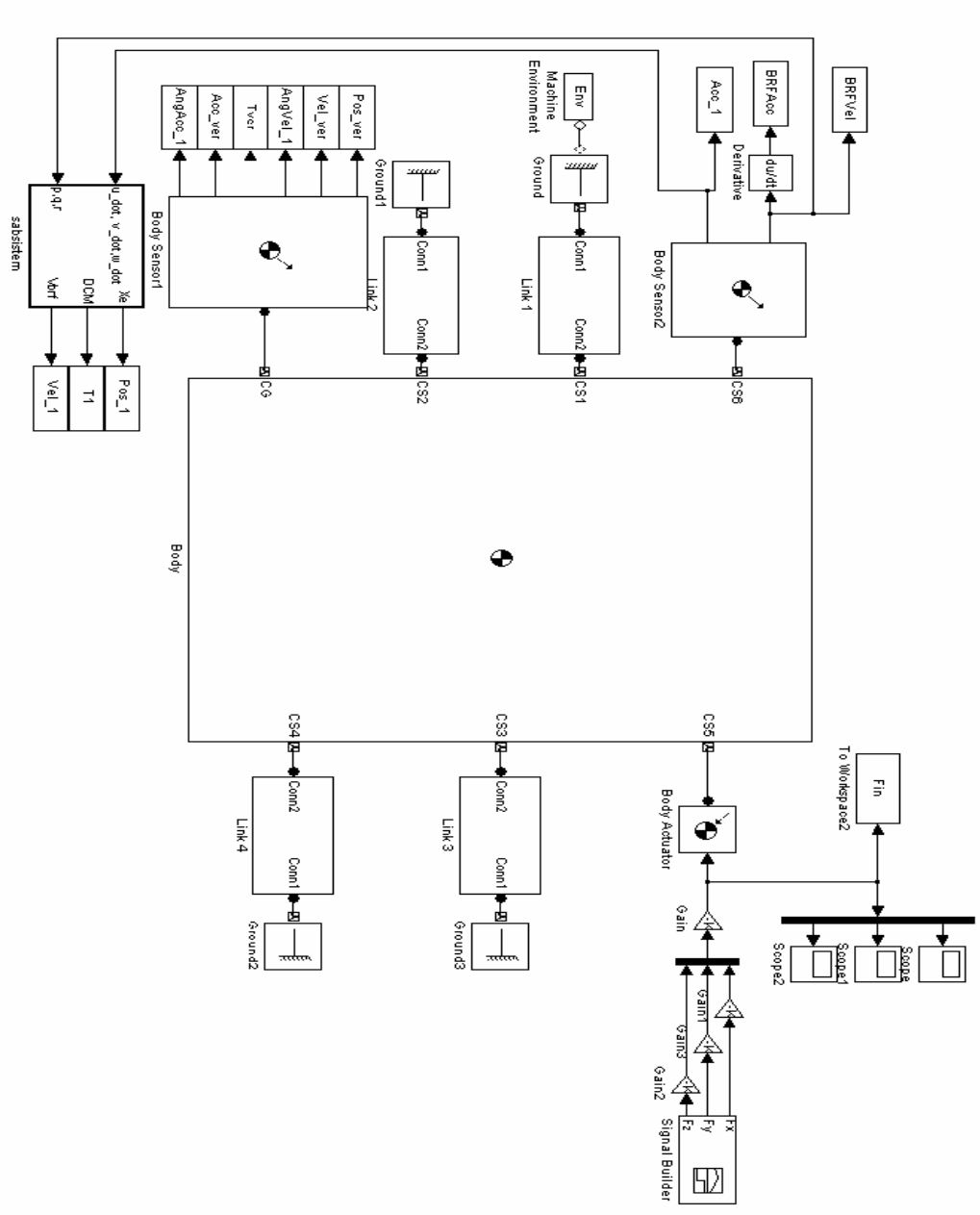

Figure A-1 Experiment Model

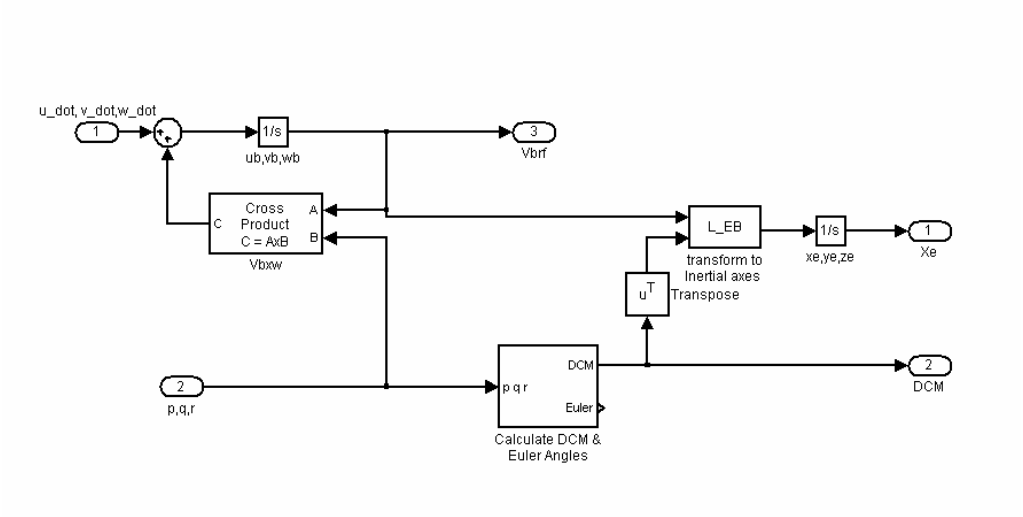

Figure A-2 Tracker Box

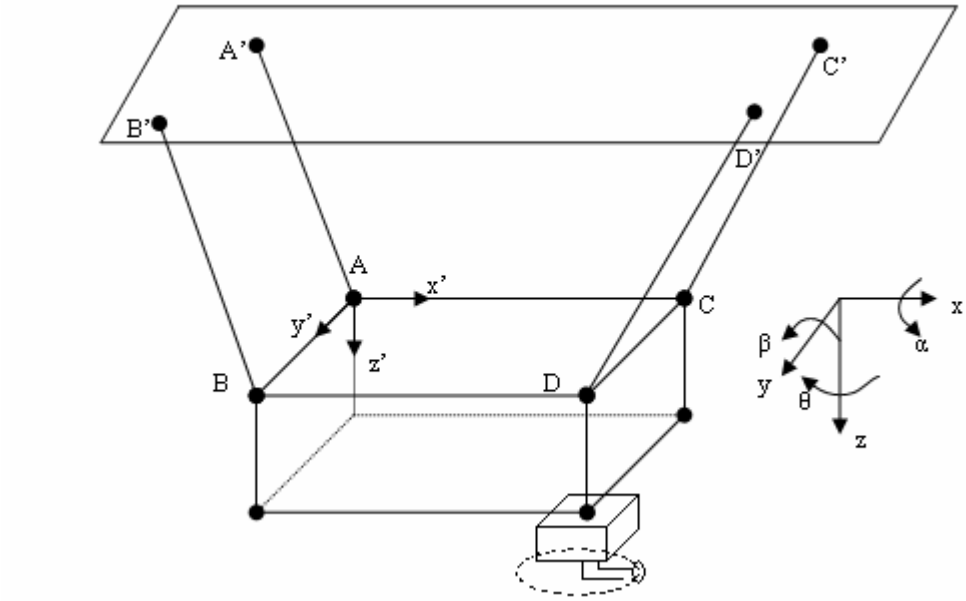

Figure A-3 Test Setup with Unbalanced Mass-Motor